Major- and minor-element analysis of Apollo 14 volcanic green glasses B, and petrogenic modeling of Apollo 14 green glasses A and B

A thesis presented to the Faculty
of the University at Albany, State University of New York
in partial fulfillment of the requirements
for the degree of

Master of Science
College of Arts and Sciences
Department of Earth and Atmospheric Sciences

Vera Assis Fernandes
1999

Major- and minor-element analysis of Apollo 14 volcanic green glasses B, and petrogenic modeling of Apollo 14 green glasses A and B

Abstract of
thesis presented to the Faculty
of the University at Albany, State University of New York
in partial fulfillment of the requirements
for the degree of

Master of Science
College of Arts and Sciences
Department of Earth and Atmospheric Sciences

Vera Assis Fernandes
1999

ABSTRACT

The lunar picritic volcanic glasses have been identified as being quenched samples of primary magmas extruded onto the lunar surface via fire-fountains. The study of the compositiom of these glasses is of extreme importance for the understanding of the Moon's mantle composition and petrogenetic processes.

Based on their chemical signature (low-Ti and high Mg#) and physical characteristics, the lunar picritic glasses are believed to represent primary magmas. Experimental data suggest that these melts formed at 360-500 km depth (18-25 kbar) in the lunar mantle, and were transported onto the lunar surface through a "channel" network (McKenzie, 1985b) that isolated these magmas and minimized fractionation. The aim of this work is to obtain high precision electron microprobe analysis in order to more confidently model melting processes that may have occurred deep within the lunar mantle.

For these study, Apollo 14 volcanic green glasses A and B were analyzed. These glasses (A and B) show large enrichments of incompatible elements (e.g. K, Na, Ti) and an intragroup trend that does not follow olivine (olivine is known to be the liquidus phase for all pressures less than about 20 kbar), low-Ca pyroxene, augite or plagioclase fractionation trends. Although batch melting, mantle source hybridization and/or assimilation of KREEP in the magma source region have been considered, these processes fail to explain the behavior of major elements.

More recently, it has been suggested (Delano, 1996; Delano and Fernandes, 1998) that the trends observed reflect deep-seated magmatic processes resulting from dynamic melting of an ascending mantle diapir (Delano and Fernandes, 1998). This model, the dynamic partial melting process, involves the differential flow of melt and

residual matrix (Eggins, 1992). In the melt region, the degree of melting will increase as a function of decompression, therefore of height above the adiabat and peridotite (source) solidus intersection. The amount of melt present (i.e. porosity) at a particular height, however will be less than the degree of melting due to the more rapid buoyancy-driven ascent of melt compared to the matrix. The magnitude of this melt-filled porosity (ϕ) will depend upon the velocity of the melt relative to the matrix and upon the rate of melting. The amount of melt created will dictate the abundance of elements in a specific melt fraction.

Based on dynamic melting modeling, the degree of partial melting involved in the origin of these melts (the glasses) is within the range of values (5 to 25%) expected for conventional petrogenetic processes (e.g. batch melting). The model results for Al, Ca, K, Na, and Ti show a wide range of porosity and distribution coefficients that may have been involved in the origin of these melts. The little sensitivity to the model shown by K and Na suggest that these two elements are important in the identification of the degree of partial melting undergone by the source mantle diapir. These two elements may provide important information that will allow all of the other elements, including Ti, to be better constrained in the model

DEDICATION

Dedico esta tese à minha Avó Virginia Monteiro

(I dedicate this thesis to my Grandmother Virginia Monteiro)

Table of Contents

List of Tables

List of Figures

CHAPTER I - Introduction

1.1 Picritic volcanic glasses and their importance in lunar geology

The understanding of the early solar system has been aided by the research done on the samples returned from the Moon. Other than meteorite impacts, no other major geologic events have occurred on the Moon for the past 3.16 billion years. The maria basalt of the dark lowlands are ~4.2 - 3.16 Ga., as old as the oldest rocks on Earth (Hess, 1989a). The bright highlands are even older (4.5 Ga.), dating back almost to the origin of the Earth, Moon, and solar system. Furthermore, with the realization that the picritic volcanic lunar glasses, found within breccias were excellent "windows" into the lunar interior, much development in lunar geochemistry and petrogenesis has been achieved.

The picritic volcanic glasses are spherules, 100-300 μm in diameter (Figure 4.1.1) and are commonly found in the breccias returned by the Apollo and Luna missions. The picritic glasses are samples of MgO-rich quenched liquids from the deep lunar interior (~ 400 ± 50 km; 18 -25 kbar; Delano, 1980) brought to the surface and widely dispersed by explosive fire-fountain eruptions (Figure 1.1.1). These glasses have a low-SiO_2 content (33 - 48 wt%; Delano, 1986) representing lavas with very low viscosity that were easily dispersed. The eruption of these mafic to ultramafic lavas was accompanied by the release of volatiles (e.g. S, Cl, Cu, Zn, McKay et al., 1974; Meyer et al., 1975 and Delano, 1986) that condensed on the glass surfaces. These basaltic lava eruptions formed the deposits of volcanic picritic glasses observed on the

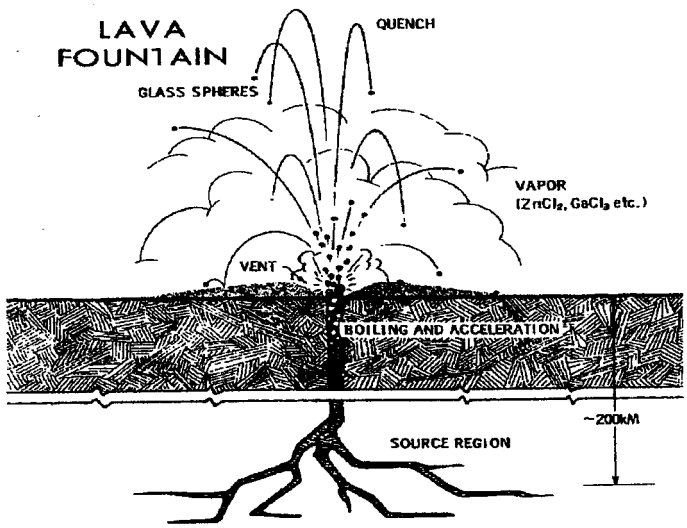

Figure 1.1.1 Schematic representation of a fire fountain as suggested by Meyer et al., 1975. The erupted lava quenches instantaneously when in contact with the lunar vacuum forming 100 - 300 um diameter spherules. The vapor composition indicated is based on Meyer et al., 1975 ion microprobe analyses of the surface-correlated volatiles.

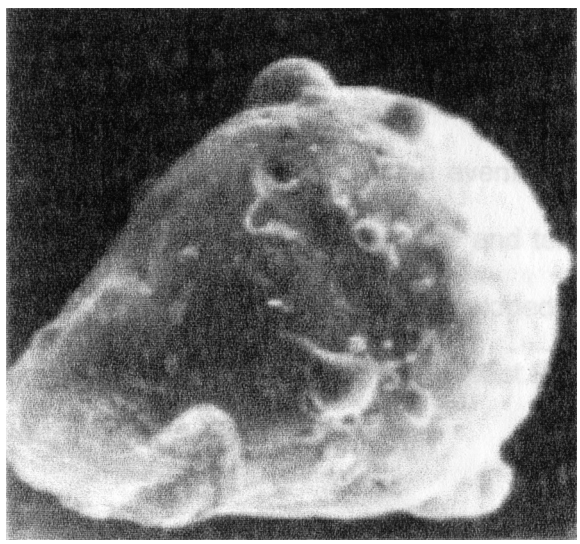

Figure 1.1.2 Composite green glass droplet, ~ 950 um long. Composite spherules form due to the impact of multiple droplets during flight in the lunar vacuum. After the magma is erupted and quenched, small spherules of similar chemical composition impact at low velocity to form these large spherules (Taylor, 1975).

lunar surface. During fire-fountaining, not only did individual spherules form, but also multiple droplets (McKay et al., 1974). These composite spherules were built up by low-velocity impacts of material with the same composition (Figure 1.1.2).

Lunar picritic volcanic glasses have high MgO concentrations in the range of 11.6 - 19.1 wt % (Delano, 1980; Delano and Livi, 1981; Delano, 1986). The range of MgO/(MgO+FeO)x100 = Mg# (weight %) - of 44 to 66, is higher than that observed in bulk analyses of fine-grained mare basalts. These two parameters, MgO wt% and Mg#, are indicative of high liquidus temperatures (1300-1450°C at 0 bar, Delano, 1990a) and suggest primitive magmas. Another distinctive feature of these glasses is the wide range in the TiO_2 concentration. The TiO_2 concentration varies from 0.26 to 16.4 wt% (Table 1.1.1). These glasses are considered by some scientists (Delano et al., 1980) to be better candidates for primary lunar magmas than the majority of crystalline mare basalts, and thus excellent probes of the lunar interior. In general, the most primitive glasses have low-Ti and high Mg# (Delano, 1986).

A preliminary problem for the study of these picritic volcanic glasses is to initially distinguish them from impact glasses, also found within lunar breccias. Following this separation based on glass formation, there is the eventual division of volcanic glasses into groups based on common origins. A chemical and textural criteria to differentiate volcanic glasses from impact glasses has been developed (Delano, 1979; Delano and Livi, 1981; Delano, 1986) and indicates there are at least 25 different groups of volcanic picritic glasses on the lunar surface (Table 1.1.1).

	1	2	3	4	5	6	7	8	9	10	11	12	13
SiO_2	48.0	45.5	43.9	46.0	45.1	45.2	44.8	46.0	43.7	45.3	44.3	44.1	42.9
TiO_2	0.26	0.38	0.39	0.40	0.41	0.43	0.45	0.55	0.57	0.66	0.91	0.97	3.48
Al_2O_3	7.74	7.75	7.83	7.92	7.43	7.44	7.14	8.30	7.96	9.60	6.89	6.71	8.30
Cr_2O_3	0.57	0.56	0.39	0.55	0.55	0.54	0.54	0.58	0.46	0.40	n.a.	0.56	0.59
FeO	16.5	19.7	21.9	19.1	20.3	19.8	19.8	18.2	21.5	19.6	20.2	23.1	22.1
MnO	0.19	0.22	0.24	n.a.	0.22	0.22	0.24	0.21	n.a.	0.26	0.23	0.28	0.27
MgO	18.2	17.2	16.9	17.2	17.6	18.3	19.1	15.9	17.0	15.0	19.5	16.6	13.5
CaO	8.57	8.65	8.44	8.75	8.43	8.15	8.03	9.24	8.44	9.40	7.40	7.94	8.50
Na_2O	n.d.	n.d.	n.d.	n.d.	n.d.	n.d.	0.06	0.11	n.d.	0.27	0.10	n.d.	0.45
K_2O	n.d.	n.d.	n.d.	n.d.	n.d.	n.d.	0.03	0.07	n.d.	0.04	n.d.	n.d.	n.d.

	14	15	16	17	18	19	20	21	22	23	24	25
SiO_2	40.8	40.5	39.4	38.5	37.9	38.8	37.3	37.2	35.6	35.6	34.0	33.4
TiO_2	4.58	6.90	8.63	9.12	9.12	9.30	10.0	12.5	13.8	15.3	16.4	16.4
Al_2O_3	6.16	8.05	6.21	5.79	5.63	7.62	5.68	5.69	7.15	4.81	4.6	4.6
Cr_2O_3	0.41	0.63	0.67	0.69	0.65	0.66	0.63	0.86	0.77	n.a.	0.92	0.84
FeO	24.7	22.3	22.2	22.9	23.7	22.9	23.7	22.2	21.9	23.7	24.5	23.9
MnO	0.30	0.25	0.28	n.a.	n.a.	0.29	n.a.	0.31	0.25	n.a.	0.31	0.30
MgO	14.8	12.6	14.7	14.9	14.9	11.6	14.3	14.5	12.1	13.0	13.3	13.0
CaO	7.74	8.64	7.53	7.40	7.41	8.55	7.62	7.04	7.89	6.49	6.9	6.27
Na_2O	0.42	0.39	0.41	0.38	0.36	0.39	0.31	0.28	0.49	0.50	0.23	0.05
K_2O	0.10	n.d.	0.04	n.d.	n.d.	n.d.	n.d.	0.29	0.12	n.d.	0.16	0.12

Table 1.1.1 Delano (1986) compiled the 25 varieties of pristine lunar glass known. The data are shown in increasing TiO2 (wt%) concentration. Each variety is represented by the most primitive composition (highest MgO wt%). (1) Apollo 15 green C; (2) Apollo 15 green A; (3) Apollo 16 green; (4) Apollo 15 green B; (5) Apollo 15 green D; (6) Apollo 15 green E; (7) Apollo 14 green B; (8) Apollo 14 VLT; (9) Apollo 11 green; (10) Apollo 17 VLT; (11) Apollo 17 green; (12) Apollo 14 green A; (13) Apollo 15 yellow; (14) Apollo 14 yellow; (15) Apollo 17 yellow; (16) Apollo 17 orange; (17) Apollo orange 17 (74220-type); (18) Apollo 15 orange; (19) Apollo 17 orange; (20) Apollo 11 orange; (21) Apollo 14 orange; (22) Apollo 15 red; (23) Apollo 14 red; (24) Apollo 14 red (preliminary); (25) Apollo 12 red (Delano, 1986 and references therein).

1.2 Previous work

By studying the chemical composition of volcanic glasses, it is possible, in general, to develop petrogenetic and chemical models that give insight into lunar mantle chemistry and processes responsible for the origin of the magmas represented by the glass spheres. Despite the chemical composition of the lunar glasses has allowed much speculation regarding the origin of these glasses, no model used until the present has satisfactory cover all aspects of the chemistry of these glasses. The high-MgO contents together with high contents of incompatible elements are properties difficult to reconcile with anyone of the known models.

Crystallization experiments on these glasses have identified points in P-T phase space where liquids become multisaturated (Chen et al., 1982; Delano, 1979 and 1980; Longhi, 1987 and 1992; Stolper et al., 1974; Figure 5.4.1). Experiments undertaken with synthetic mixes of Apollo 15 green and red glasses, Apollo 14 VLT and Apollo 17 VLT (Chen et al., 1982; Delano, 1979, 1980; Longhi, 1987, 1992; Stolper et al., 1974), have demonstrated that olivine is the liquidus phase in the pressure range from 0 to 18-24 kbar (0 to 400±50 km) (Figure 4.4.1). Somewhere between 18 to 24 kbar (400 to 480 km), the liquidus is multisaturated with both olivine and orthopyroxene. At pressures greater than 18 kbar for Apollo 14 VLT and Apollo 17 VLT, and greater than 20 kbar for Apollo 15 green glass and greater than 24 kbar ($\geq$ 400±50 km) for Apollo 15 red glass, orthopyroxene has been identified as the liquidus phase. Theoretical results also suggest that if olivine were the liquidus phase controlling the chemical variations within each group of glasses, then this variation should coincide with the line of olivine fractionation as it will be suggested in Chapter IV. Moreover, in the cases of Ca, Na, Ti and K, the enrichments levels in these elements are significantly elevated (8.4-13%, 99-108%, 117-192%, 158-187%, respectively) in the case if the Apollo 14 volcanic green glasses. For these enrichment levels, mixing models have been suggested as the process to originate these enrichment levels in which the mantle magma source and a KREEP-like material were the end-members. However, for these models to be satisfactory, the chemical variation between the two end-members should be linear on diagrams of one oxide versus another (Figure 4.5.1).

Delano (1980) suggested that the observed Apollo 15 red glass intergroup chemical changes were due to a rising mantle diapir (Figure 5.1.1). This ascending diapir would have episodic magma segregations each at a different pressure (polybaric melt segregation). At each stage of melt segregation, partial melting would

systematically decrease as the ascending diapir reached shallower depths resulting in the increase of the more incompatible elements (i.e. Na, K, Ti and Ca). At any one pressure, the observed wide range in element concentration may be due to dynamic melting. The dynamic melting process will be discussed later in Chapter V, but the view presented is of a process within a rising, homogeneous mantle diapir undergoing increasing partial melting from the periphery to the center.

1.3 Purpose of this study

The purpose of this study is three-fold: (a) to produce data that better characterize the chemical composition of the lunar picritic A14-B using recently developed high-precision microprobe methods (Hanson et al., 1996); (b) to model mantle processes (Delano and Fernandes, 1998) that occur deep within the lunar mantle using data from the reanalyzes of A14-A (Delano, 1996) and the reanalyzes of A14-B (Delano and Fernandes, 1998) and (c) to model the observed wide range of Ti, K and Na in the Apollo 14 volcanic green glasses using the dynamic melting process. This wide range is not explained by olivine fractionation and mixing of KREEP-like material in the magma source region.

CHAPTER II - Breccia Sample

2.1 Lunar stratigraphy

The purpose of lunar stratigraphy (Figure 2.1.1), like the terrestrial is to integrate geologic units into a stratigraphic column applicable over the entire planet and to correlate this column with absolute ages as they become available. The basis for construction of this stratigraphic column is the principle of superposition. In the lunar case of crater superposition (Wilhelms, 1987) of younger over older, the craters overlying a certain stratigraphic unit have size-frequency distributions and morphologies typical of stratigraphic intervals of the unit. Pairs of adjacent crater, basin, or mare units can normally be dated by direct observations of superposition and transections based on the simple concept that the younger units modify the older (Wilhelms, 1987). In some cases, the correlation can be extended over larger areas by secondary-impact craters.

Presently, the lunar stratigraphic column is divided into four major sequences as seen in Figure 2.1.1: pre-Nectarian (oldest), Nectarian, Lower Imbrium, and Upper Imbrium through Copernican (youngest) (Wilhelms, 1987). These sequences are defined based on laterally extensive deposits of the Nectaris, Imbrium and Oriental basins. This sequence is then subdivided into six units - from younger to older: (1) Copernican units are dated by the frequencies and morphologies of very small craters that are only visible on the best photographs; (2) Eratosthenian craters units are also identified by size-frequency distribution. On the other hand, the Eratosthenian mare units and some of the impact-melt pools are dated by the D_L method based on the

theoretical method of crater erosion operating in the steady state (Wilhelms, 1987); (3) Late Imbrium mare units are easy to identify using the D_L method; (4) only a few crater units of Late or Early Imbrium craters are large enough for statistic valid size-frequency identification. These craters are usually dated based on the degradation of their subunits; (5) the Early Imbrium Orientale and Imbrium basin materials are extensive enough, young enough, and photographed well enough to be dated by craters over a large diameter range; (6) the steady state increases for older units and craters larger than 20 km in diameter are thought be valid as counters for the whole Nectarian and pre-Nectarian periods (the two oldest lunar stratigraphic units). Craters larger than about 20 km in diameter are supplemented by size-frequency identification.

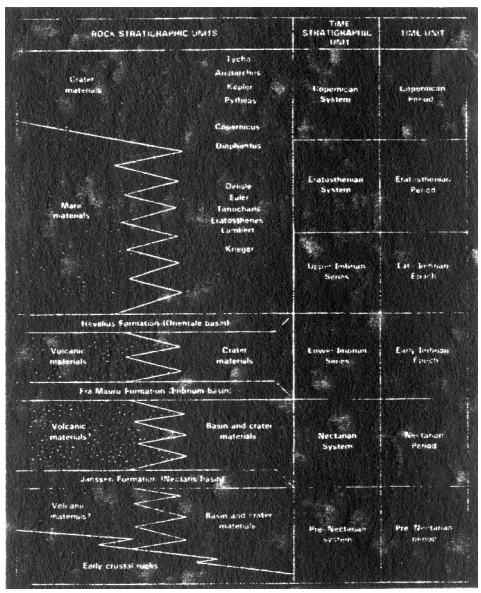

Figure 2.1.1 Schematic lunar stratigraphic column showing the relations among four stratigraphic units. These rock-stratigraphic units are based on three major craters (basins) materials: Nectaris, Imbrium, and Orientale. Individual lunar rock-stratigraphic units (mare and crater materials) formed within very brief time intervals, but groups of rock-stratigraphic units may cross time-stratigraphic boundaries (Wilhelms, 1987).

The stratigraphic system most relevant for the work presented here is the Imbrium system. The Imbrium System is divided into two series: (1) the Lower Imbrium Series that contains all the material from the bottom of the Fra Mauro formation to the top of Hevelius formation (ejecta from the Orientale basin, Figure 2.1.1); (2) the Upper Imbrium Series that contains all the materials above the Hevelius formation (younger than the Orientale basin) to the top of the Imbrium System (Wilhelms, 1987).

The Apollo 14 breccias appear to have been formed due to multiple cycles of pre-Imbrium cratering. During these events, impact melts and different rock clasts mixed several times (Stöffler, 1989). The material most important for the understanding of Fra Mauro formation and the evolution of the pre-Imbrium crust, are those of fragmental and impact melt breccias (i.e. polymict continuous ejecta deposits and the coherent melt deposit - melt sheet - respectively).

The Fra Mauro formation is considered to be the most distinctive Imbrium-basin unit within the Lower Imbrian Series (Wilhelms, 1987). The lower age limit for Fra Mauro formation is 3.75 Ga. (Stadermann et al., 1991) or 3.85 Ga. (Turner et a., 1971). Breccias found near Cone Crater rim (depicting a discrete older stratigraphic age subunit within the Fra Mauro formation) represents an older impact melt > 3.9 Ga. (Stöffler, 1989). The extensively exposed and relatively well sampled Lower Imbrian Series (Figure 2.1.1) is the key to the ages and origins of most materials of the lunar terrae. Deposits of the Lower Imbrium Orientale and Imbrium basins establish the Moon's most extensive laterally continuous stratigraphic horizons (the Imbrium basin is older that the Orientale basin). The Imbrium basin is the largest visible feature on the Moon's surface from the Earth, and it was the first basin to be treated stratigraphically. Deposits of the Orientale basin dominate the terrae on both sides of longitude 90 W and serve as models for other basin materials (Wilhelms, 1987). Therefore, the Lower

Imbrium Series dominates a large part of the lunar surface. Both of these basin groups are excellent stratigraphic markers for dividing the lunar stratigraphy (Figure 2.1.1).

2.2 Sampling locations

Cone crater, located 1,100 m from the LM (Figure 2.2.1), is Copernican in age, and the impactor that formed it excavated approximately 90 m into the Fra Mauro formation (Swann et al., 1971 and 1977). Therefore, between the LM and the crater there is an increase in boulder density and size as well as an increase in the source depth of the boulders from within the crater (Swann et al., 1971 and 1977). The two stations that are of most interest for the present work are Station G and Station G1 (Figure 2.2.1).

2.3 Sample descriptions

The surface of the Moon is covered mostly by a thin layer (a few meters) of fine material, the regolith. The regolith forms due to the repeated comminution of the Moon's early formed anorthositic crust resulting from the impact of meteorites (Wilhelms, 1987). The process that lithifies the lunar surface regolith fragments into a breccia is the same type of event that initially broke them apart, a meteorite impact. Beneath the point of impact, particles and fragments are instantaneously packed

Apollo 14 landing site and traverses

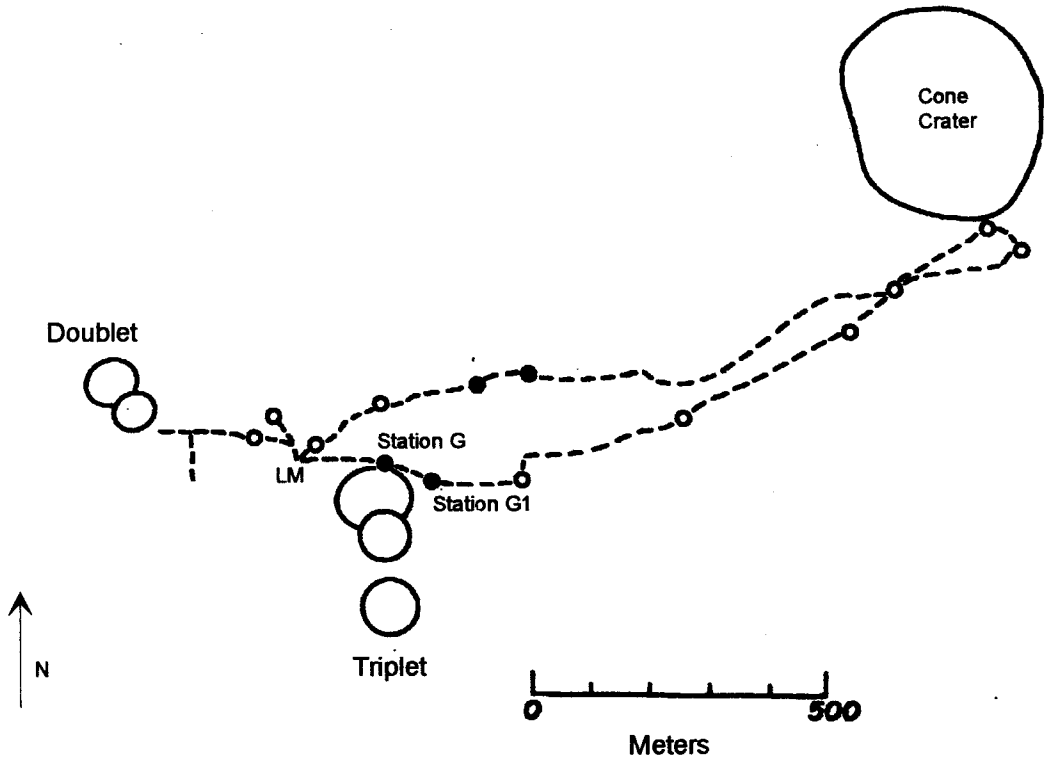

Figure 2.2.1 Apollo 14 landing site and traverses taken by the astronauts Shepard and Mitchell (modified after Sutton et al., 1972). Breccia sample 14307 was collected at Station G. Breccia sample 14313 was collected at Station G1. LM-Lunar Module.

together. The stresses may cause some melting along fragment surfaces, and this fluid acts as a glue when it solidifies.

The breccias are commonly composed of angular fragments, minerals, and glass in a groundmass of comminuted material and glass (Swann et al., 1971 and Carlson et al., 1978). The presence of both igneous and fragmental rock fragments in most breccias indicates a history of repeated fragmentation and consolidation. Breccias may exhibit shock deformation as a result of the continuous bombardment of the lunar surface after their formation. These shock features may include shock induced twinning, fracturing, vitrification, melting and recrystallization (Chao et al., 1970). Thus, a breccia sample represents the agglumeration of bedrock material and overlying regolith and the recycling of pre-existing breccias before the impact.

The complexity offered by the samples returned by the Apollo 14 mission, shows that the Fra Mauro formation is a good example of the accumulation of debris from a large number of impacts and other phenomena resulting from an impact.

The volcanic glasses analyzed were found within breccia grab-samples 14307 and 14313 (Figure 2.3.1.1 and Figure 2.3.2.1, respectively) collected during the second Extra Vehicular Activity (EVA) of the Apollo 14 mission. These samples were then cut and prepared for petrographic thin-section mounting by NASA curators. Specific numbers were given per cut forming a "genealogy" that eases in the determination of the thin-section orientation with respect to the parent sample (Carlson et al., 1978) as well as for historical interest.

Sample 14307 (Figure 2.3.1.1) was collected in station G (Figure 2.2.1) that was located 230 m ESE of LM and 50 m E of North Triplet Crater rim crest. Sample 14313

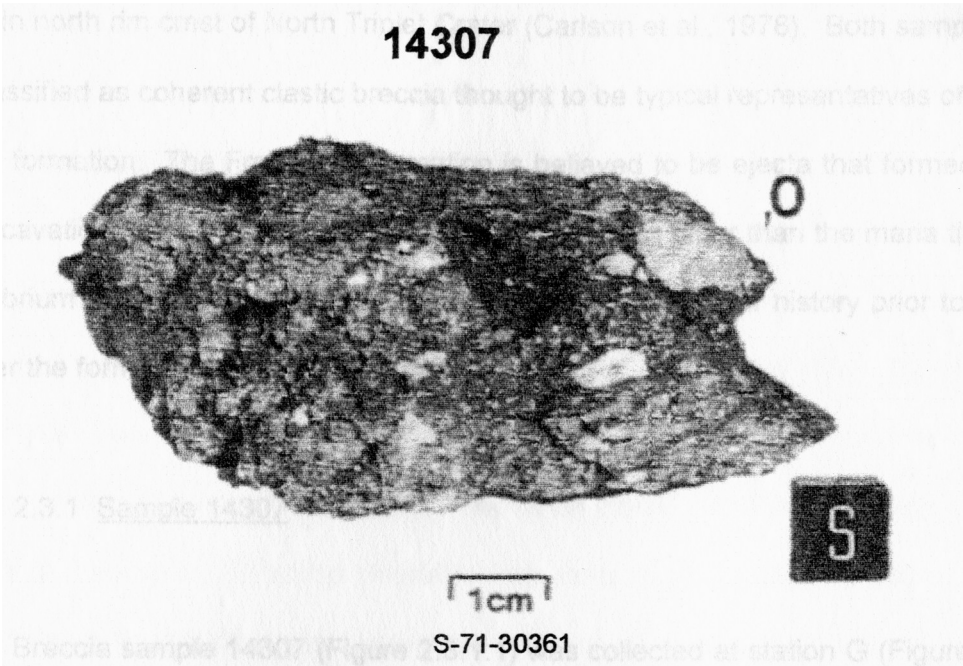

Figure 2.3.1.1 Apollo 14 breccia sample 14307 collected during the second EVA at station G. The mass of the sample is 155.0 g; the dimensions 5.0 x 2.5 x 8.0 cm (Carlson et al., 1978).

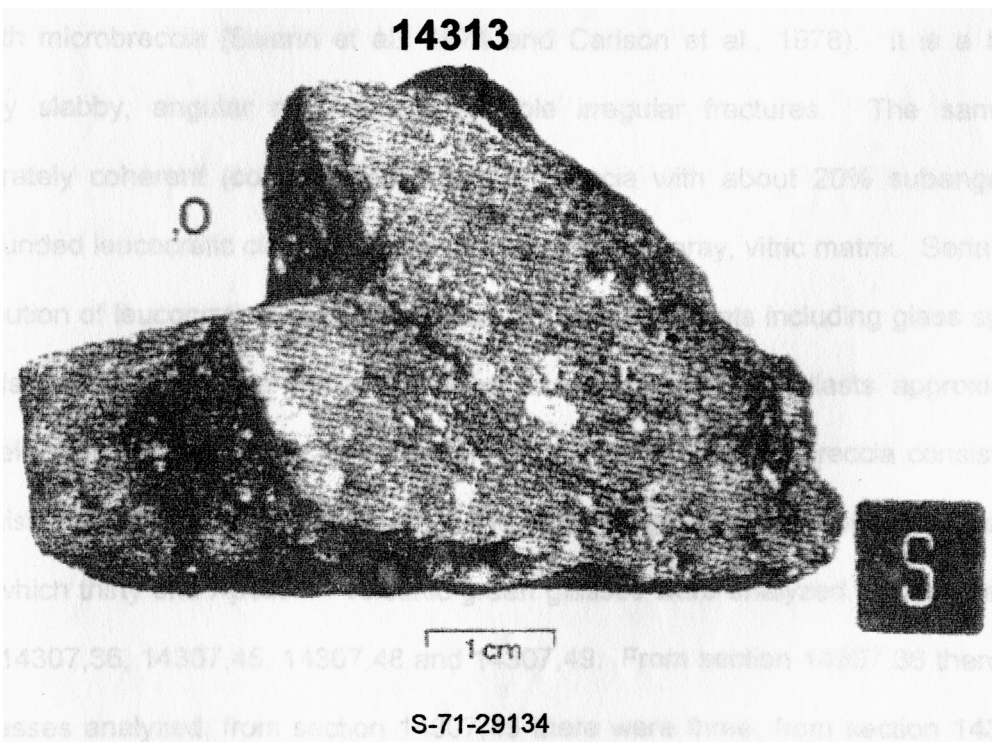

Figure 2.3.2.1 Apollo 14 breccia sample 14313 collected during the second EVA at station G1. The mass of the sample is 144 g; the dimensions 6.0 x 6.0 x 4.0 cm (Carlson et al., 1978).

(Figure 2.3.2.1) was collected in station **G1** (Figure 2.2.1) that was located 150 m E of LM in north rim crest of North Triplet Crater (Carlson et al., 1978). Both samples are classified as coherent clastic breccia thought to be typical representatives of the Fra Mauro formation. The Fra Mauro formation is believed to be ejecta that formed during the excavation of the Imbrium Basin. Thus, this ejecta is older than the maria that filled the Imbrium Basin and is suspected to reveal much of the lunar history prior to as well as after the formation of the large basins.

2.3.1 Sample 14307

Breccia sample 14307 (Figure 2.3.1.1) was collected at station G (Figure 2.2.1). Station G was located 230 m ESE of the Lunar Module (LM) and 50 m E of North Triplet rim crest, SW of Cone Crater. The sample is considered to be a shocked regolith microbreccia (Swann et al., 1971 and Carlson et al., 1978). It is a blocky, slightly slabby, angular rock cut by multiple irregular fractures. The sample is moderately coherent (consolidated) polymict breccia with about 20% subangular to subrounded leucocratic clasts in a fine-grained, medium-gray, vitric matrix. Seriate-size distribution of leucocratic clasts is apparent. Glassy fragments including glass spheres are also present. There appeared to be a weak foliation of clasts approximately parallel to the flat side of the rock (Station G). The matrix of this breccia consists of a brownish-yellow glass. Four thin-sections were investigated in the work presented and from which thirty one Apollo 14 volcanic green glasses were analyzed. These sections were 14307,36, 14307,45, 14307,48 and 14307,49. From section 14307,36 there were six glasses analyzed; from section 14307,45 there were three; from section 14307,48

there were five glasses analyzed; from section 14307,49 there were eleven glasses analyzed.

2.3.2 Sample 14313

Breccia sample 14313 (Figure 2.3.2.1) was collected at Station G1 (Figure 2.2.1). Station G1 was located 150 m E of LM on north rim crest of North Triplet Crater. The sample is a coherent, polymict breccia with a complex history of comminution and reagglumeration (Carlson et al., 1978). The main clasts found in this sample are (1) noritic rock fragments, (2) monomineralitic fragments, (3) microbreccia clasts, and (4) glassy fragments including glass spherules. Clasts of mare basalt are not common. The matrix of this breccia is constituted of fine grains of brownish yellow glass. Evidence for damage due to shock is not present in all clasts. Carlson et al. (1978) suggested that the presence of noritic fragments indicate that they were an important part of the pre-Imbrium (pre-Fra Mauro formation) rock type within the Imbrium basin area. From this sample six Apollo 14 volcanic glasses were analyzed solely from section 14313,41.

When observed under low-power in transmitted light, the color of the thin sections is a blotched brown with abundant white clasts (Figure 3.1.2). Many of these clasts are themselves lithic microclasts of breccia material.

CHAPTER III - Glass spherules

3.1 Volcanic glass

The Apollo 14 green, mafic to ultramafic volcanic glass spherules analyzed in the present work (Figures 3.1.1 and 3.1.2) have a range in diameter between 50 to 300 μm. These glasses were found within the Apollo 14 breccias 14307 and 14313. Some believe that these glasses originated by the impact of a meteorite with the lunar surface (Chao et a., 1972; Stolper et al., 1974; Wood and Ryder, 1977; Dence et al., 1974; Rhodes, 1978). The arguments in favor of this hypothesis focused on the compositional homogeneity, lack of phenocrysts, and the non-existence of complimentary fine-grained phaneritic samples. Furthermore, Rhodes (1978) suggested that green glasses were derived from a major meteorite impact that caused the melting of olivine cumulate in the lunar mantle. Work by Stolper et al. (1974) and Wood and Ryder (1977), suggested that olivine crystals found within vitrophyres were not in equilibrium with bulk melt compositions (~Fo_{74} of olivine compared with Fo_{82} predicted for the bulk melt). The concept of melt rising from a depth of ~ 300 km, with enough strength to form a lava fountain at the surface was hard to accept (Dence et al., 1974). Chao et al. (1970 and 1972), suggested that the wide range in chemical composition of glasses is representative of specific rock target. Experimental work of Green and Ringwood (1973) suggests that the formation of the green glass liquid required pressures and temperatures in the order of 15 kb and 1450°C, respectively. Trace element analysis by Cavarretta et al. (1972), showed that the glass spherules had very large trace element variations that differ with the major-element homogeneities. They suggested, instead, that this discrepancy could only result from variable degrees of condensation from a

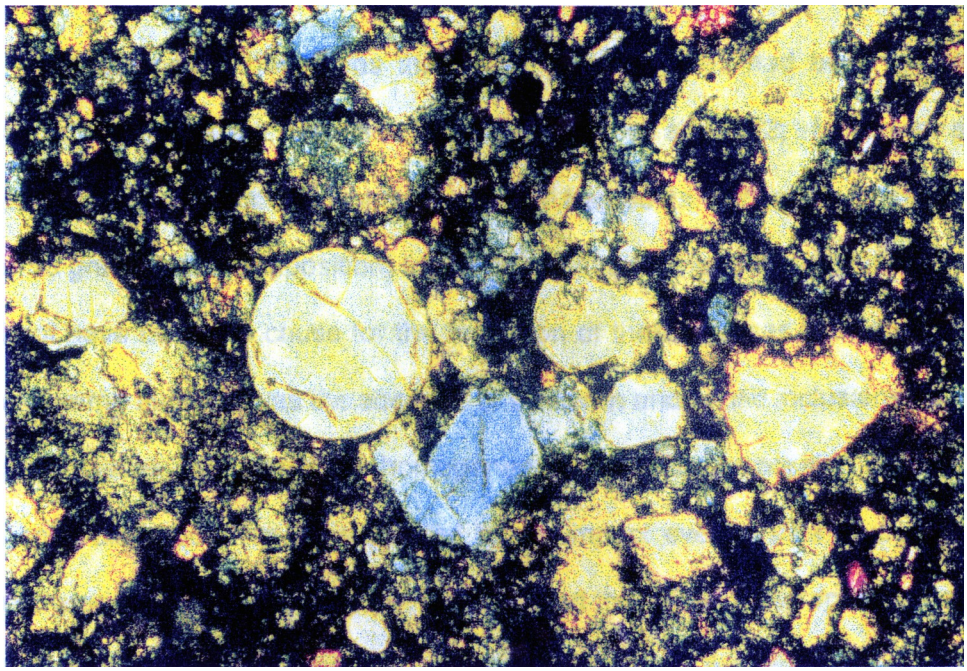

Figure 3.1.1 Lunar volcanic glass from the Apollo 14 from breccia sample 14307 obtained at Station G. The glass is ~100 um in diameter; the non-true colors displayed were obtained by using a filter.

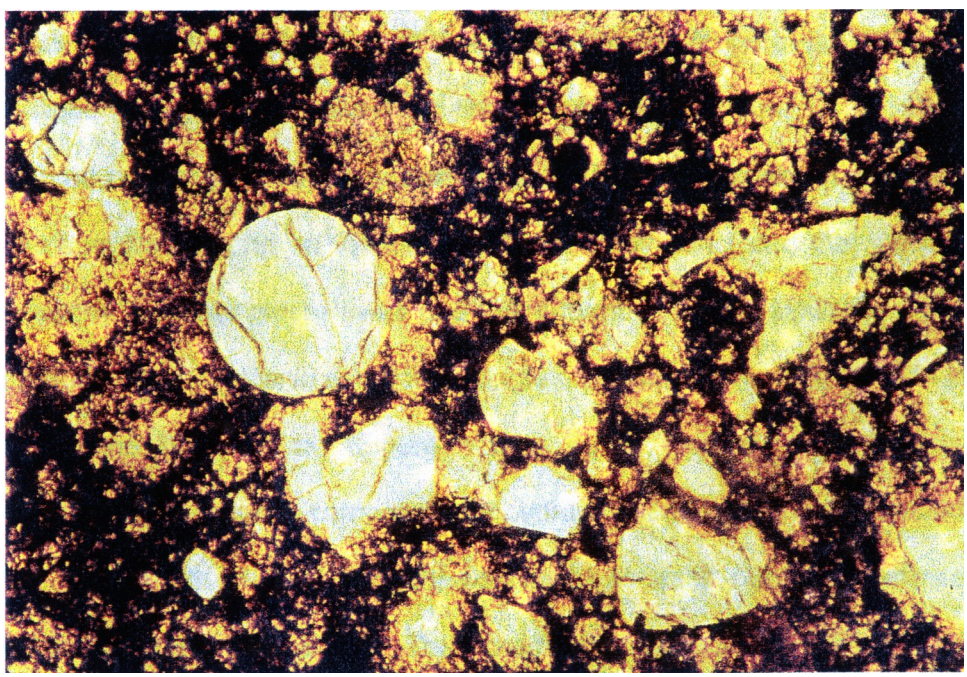

Figure 3.1.2 Lunar volcanic glass from the Apollo 14 from breccia sample 14307 obtained at Station G. The glass is ~100 um in diameter; the colors represented are real and obtained at low-power in transmitted light.

Vapor phase that had been produced due to a large impact.

The competing belief was that these glass spheres had been formed due to endogenic processes (i.e. volcanic origin, Cameron et al., 1972; McKay et al., 1974). The authors argued that the absence of rock fragments with glass composition (e.g. Apollo 15 green glass composition) found on the lunar surface suggested that an impact could not have been the cause for the formation of these glasses. Another observation by these same authors, was the absence of schlieren and exotic inclusions usually found in impact glasses. Moreover, the homogeneous chemical composition presented by the glass spherules could not be explained by an impact event. In a study of Apollo 15 volcanic green glasses, McKay et al. (1974) found that these glass spheres had surface-correlated volatiles. This was also recognized by other authors (Meyer et al., 1975; Delano et ., 1979; Delano and Livi, 1981; Delano, 1986).

Heiken et al. (1974) compared lunar homogeneous, vitric glasses with analogous terrestrial glasses and proposed that the orange glasses found in the Apollo 11, 15 and 17 missions were derived from a mafic fire-fountain event (Figure 1.1.1). These authors commented on the great similarity that exists between the spherules found in Hawaiian droplets and those found on the lunar surface. They concluded that the homogeneity presented by the lunar glasses was due to fire-fountain events similar to those on Earth that produced vitric, volcanic ash from a single eruption. Meyer et al. (1975) proposed a model for the fire fountain (Figure 1.1.1). This type of volcanic eruption was accompanied by a gaseous component (anhydrous fluoride, chloride and sulfide carrying Zn, Ga, Pb, Cu, Tl). This component was found as a thin-film of micromounds of the surface on lunar glass spherules. The schematic representation shown in Figure 1.1.1 suggests that the decrease in pressure caused boiling and acceleration of the rising magma. When erupted onto the lunar surface, glass spherules were formed and dispersed.

These glasses are presently widely accepted by scientists as picritic volcanic glasses following the criteria developed by Delano (1979, 1980, and 1986) and Delano and Livi, 1981; Delano, 1986). The primary tool of these criteria is the chemical signature of the mafic glasses, but physical parameters such as schlieren and exotic inclusions are also important.

3.2 Volcanic Character

Soon after the Apollo missions' returned samples were examined, and the homogeneous glass spheres were observed, Heiken et al. (1974) found that glasses from the Apollo 11, 15 and 17 sites showed a very homogeneous petrography and chemical composition. In particular, orange glasses showed high Ti, Fe, Mg and low Si, Al, Na and K (Table 1.1.1). The initial proposition for the origin of these glasses was impact derived melt. If this were the case, the unusual characteristics of the glasses could disclose important information relative to impact processes and possibly to the composition of the impactor. Conversely, a volcanic origin for these glasses can provide invaluable information on the deep source region and history of lunar volcanism. Already, in the Apollo 15 Preliminary Science report, it was suggested that the green glass droplets found had originated by the eruption of lava during a fire-fountain event. This phenomenon is envisioned as being a jet of lava (Figure 1.1.1) that when in contact with the lunar vacuum, cooled rapidly and formed the glass droplets that preserve a pristine chemistry.

The controversy regarding impact versus volcanic origin of these ubiquitously distributed spheres led to the need for and development of a criteria (Delano, 1979; Delano and Livi, 1980; Delano, 1986) that is believed to enable differentiation between

volcanic glasses and impact glasses. These criteria include: (1) absence of schlieren or exotic mineral or lithic clasts; (2) intrasample compositional homogeneity; (3) intersample compositional homogeneity (compositional clustering or crystal/liquid fractionation trends; (4) higher Mg/Al ratio when compared with multicomponent lunar regoliths; (5) uniform, Mg-correlated abundances of Ni; (6) the presence of surface-correlated volatiles; and (7) distinctive ferromagnetic resonance intensity. No criteria can be used alone as a sole scrutiny parameter.

3.3 Pyroclastic deposits and their sources

The lunar volcanic glasses are usually associated with lunar dark-mantle deposits. These lunar dark-mantle deposits were commonly observed in uplands surrounding areas of mare deposition and were associated with lunar mare lavas (Head, 1974; Heiken et al., 1974). These deposits may represent a pyroclastic component of the lava extrusions that were deposited close to their source because the age relationship between basalts and these pyroclastic materials shows a great overlap as suggested by Podosek and Huneke, (1973) for the Apollo 15 site. The Apollo 15 green glasses' age appears to be the same as that of the mare plains found at the site. However, the origin of this pyroclastic material was suggested (Rhodes et al., 1976) to have probably originated from a different magma than that of the sampled basalt. This suggests that the magma source is heterogeneous in composition implying that within a single eruptive event, heterogeneous, multiple-source materials are involved in the magma generating process.

The existence of vents has been suggested by Heiken et al. (1974). These vents are low rimmed craters with a broad, low profile shape similar to those predicted by

McGetchin and Head (1973) for lunar cinder cones located near the basin rim of Apollo 11, 15 and 17 sites. Furthermore, numerous rilles can be observed on mare surfaces near the basin rims. A recent study by Weitz and Head (1998) detailed spectral data analyzed over Marius Hills. The authors observed an area showing a complex variety of volcanic features. This complexity is related to both the accumulation rate and the temperature of the pyroclastic materials. In cases where accumulation rates and temperatures are believed to be high, clasts when landing may be hot enough to coalesce and form lava flows, forming in some cases sinuous rilles. On the other hand, domes form when slow, eruptive rates construct a low shield volcano and have some coeval pyroclastic activity. Moreover, cooler clasts and lower accumulation rates result in cone volcanoes and cinder cones, respectively.

Large dark-mantle deposits have been identified along the rim of the Mare Serenitatis (SE and SW regions surrounding the basin), Mare Vaporum region, Sinus Aestenuum region, Alphonsos crater floor (several dark-haloed craters), southern Mare Humorum (a small area near the crater Dopplemayer), and Aristarchus Plateau (Head, 1974). As mentioned in Chapter I, many of the glass samples found in some of these dark-mantle areas are composite glasses (Heiken et al., 1974 and McKay et al., 1974). The composite glasses indicate low-velocity impact of molten glass and solid particles of same (or similar) chemical composition. The authors believe that most particles present in these pyroclastic "fields" were solid before reaching the lunar surface.

Two genetically distinct types of pyroclastic deposits [suggested by Coombs (1990) and Coombs and McKay (1991)], are ubiquitously distributed over the nearside of the Moon. Based on geologic and remote sensing data, these authors differentiated between regional and localized deposits. Regional dark mantling deposits (RDMD) refer to those that occupy a larger area and are usually found in lunar highland areas juxtaposed to most of the large lunar maria. Localized dark mantling deposits (LDMD)

are smaller than the RDMD and are usually found on the floors of pre-Imbrium and Imbrium craters.

As realized from the early Apollo era, these small, mafic to ultramafic spherules are of extreme importance for the study of the lunar physical and chemical characteristics, as well as the understanding of the processes involved in their extrusion. The ubiquitous distribution of the pyroclastic material (glass spheres) is of great relevance for lunar stratigraphy and selenochronology as well as for geochemistry and petrology of the planet.

CHAPTER IV - Apollo 14 green glass A and B electron-microprobe data

High-precision, electron microprobe analyses of the lunar volcanic glasses indicate that the melts were not compositionally uniform as they were transported onto the lunar surface, as shown in the following sections. The intragroup trends show a chemical continuum in some cases suggesting a chemical evolution of the mantle source. In other cases, this continuum is substituted by a clustering of melts belonging to the previously designated group. This behavioral dichotomy shown by the lunar volcanic glasses will be kept in mind in the model presented in the following Chapter (V). With the high-precision data presented in the following sections, the intent is to use these results to better constrain the physical and chemical characteristics of the processes that originated these melts in Chapter V.

4.1 Analytical Methods

Apollo 14 volcanic green glasses were analyzed by electron-microprobe using a JEOL 733 superprobe equipped with five wavelength-dispersive spectrometers at Rensselaer Polytechnic Institute, Troy, New York, USA. The analytical method used in these high-precision analyses was modified after Hanson et al. (1996) to accommodate the chemical differences of the anhydrous, mafic-ultramafic lunar volcanic glasses. Operating conditions were at 15 keV, ~70 nA beam-current and a ~10 μm beam diameter. The analyses comprised the measurement of major- (Si, Al, Fe, Mg, Ca) and minor-elements (Ti, Cr, Mn, K, Na).

Every analytical session was divided into three different packages each containing five elements. The first package of elements included Na_2O, K_2O, Al_2O_3, Cr_2O_3, TiO_2. For this set, each element was analyzed by one spectrometer for 550 seconds. The second package of elements included MgO, CaO, Al_2O_3, Cr_2O_3, TiO_2. For this package the analysis time was 300 seconds, and, as above, each element was analyzed by one spectrometer. The third package of elements was comprised of MgO, SiO_2, Al_2O_3, MnO, FeO, with 300 seconds analyzing time per element, per spectrometer. Background counts were done during machine calibration for 40 seconds per element measured.

Minimum Detection Limits (MDL) and standard deviation were calculated and are presented in the table below (Table 4.1.1). The low MDL and standard deviation values ($\pm 1\sigma$) are a result of the high exposure time of these samples to the electron beam permitted.

Table 4.1.1 List of the ten oxides analyzed using the electron-microprobe, the standard used to calibrate the device, the crystal for each oxide measured, Minimum Detection Limit (ppm), and Standard deviation (1σ, $\pm$ wt%).

Oxide	**Standard**	**Crystal**	**MDL** (ppm)	1σ ($\pm$wt%)
SiO_2	Kyanite	TAP	49	0.0189
TiO_2	Rutile	LIF	74	0.0067
Al_2O_3	Kyanite	LIF	61	0.0080
Cr_2O_3	Chromite	LIF	22	0.0051
FeO	Synfayalite	LIF	73	0.0253
MnO	Tephroite	LIF	68	0.0043
MgO	Synfosterite	TAP	31	0.0106
CaO	Diopside	PET	51	0.0135
Na_2O	Jadeite	TAP	28	0.0019
K_2O	Orthoclase-1	PET	49	0.0013

4.1.1 Working standards

The working standards are glasses from within the group of the Apollo 14 volcanic green glasses being analyzed and are analyzed several times per analytical session. A set of two working-standards was analyzed twice per element package at each analytical session with a total of six analyzes per session. Background counts were made after machine standard calibration and before analysis of the reminder of the lunar volcanic glasses. In this fashion, precision and accuracy ($\pm 1\sigma$, Table 4.1.1) of analyses from one session to another could be better monitored.

Precision of the analyzes was determined using calibration-factors to correct daily-errors were determined and applied to all glass analyses of that analytical session. The calibration factors were obtained by using all the working-standard analyses, and a "true-composition" (an average composition) for that glass was calculated. After every session, the working-standard analyses for that day were compared with the values of the "true-composition" of this working-standard glass. The difference in percentage ($\pm$1-2%) was then used as a correction factor for all the glass data obtained that day. The other working-standard glass was also corrected, and its data is used to demonstrate the precision of the electron-microprobe method (Figure 4.1.1.1).

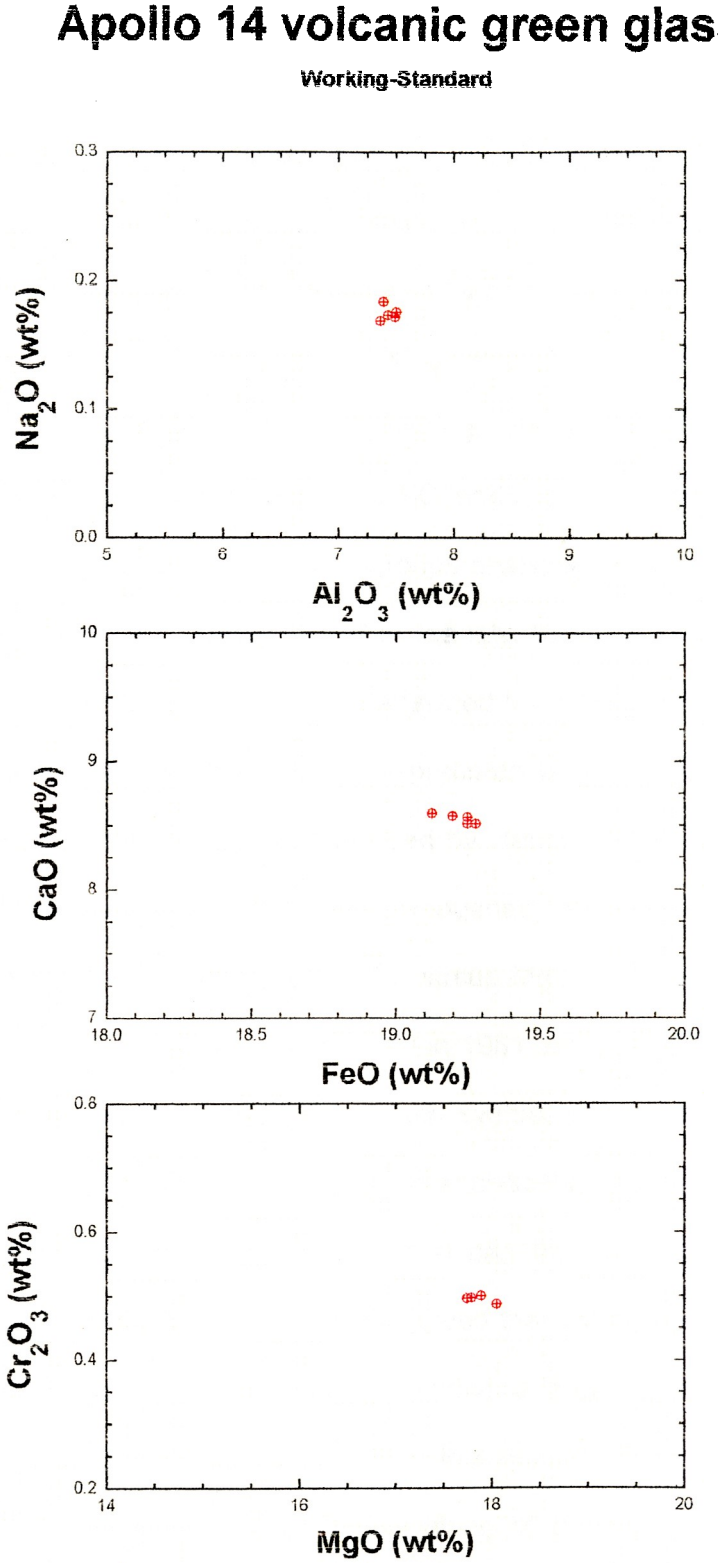

Figure 4.1.1.1 Results of 5 "compound" data points (see text for explanation) of Apollo 14 volcanic green glass working-standard.

4.2 Purpose of reanalyzing

The Apollo 14 volcanic green glasses are an important part of the geology of this landing site. These glasses were found within the same Fra Mauro formation breccias that were exposed due to the impact that created Cone Crater (Figure 2.2.1). The three groups observed in the Apollo 14 volcanic green glasses were first analyzed and recognized by (Chao et al., 1970). These groups are identified as A14-A, A14-B and A14-C based mainly on their MgO and TiO (wt%) content. These groups were later confirmed by Delano (1981). The glass groups analyzed in this study are A14-A and A14-B only (Appendix A). Delano (1996a) reanalyzed the A14-A glasses, and more recently, Delano and Fernandes (1998) reanalyzed the A14-B glasses. The purpose of reanalyzing these glasses was to improve precision and accuracy of glass analyses using a modified version of the method used by Hanson et al. (1996). Furthermore, this method has reinforced the intragroup homogeneity observed earlier (Delano, 1981; Delano, 1986). In Figures 4.2.1 a,b, TiO_2 versus MgO and CaO versus MnO plots, show data for both A and B groups obtained in 1981 analyses (filled symbols) and the 1996-1998 reanalyzes (open-symbols). Each symbol corresponds to the data for a single analysis of a single glass. The present analytical precision is represented by the red-box along one of the graph corners and can be compared with that of 1981 represented by the black-box. It can be observed that the data quality obtained in the most recent microprobe method analyses shows a great improvement in precision (shown by the red-box) when compared with the 1981 data set (shown by the black-box), as indicated by the reduction in scattering of the data points. For the TiO_2 content, the range in 1981 was between 0.83 and 2.48 wt% for group A and between 0.39 and 0.91 wt% for group B. Conversely, the TiO_2 range obtained more recently in

Apollo 14 volcanic green glass

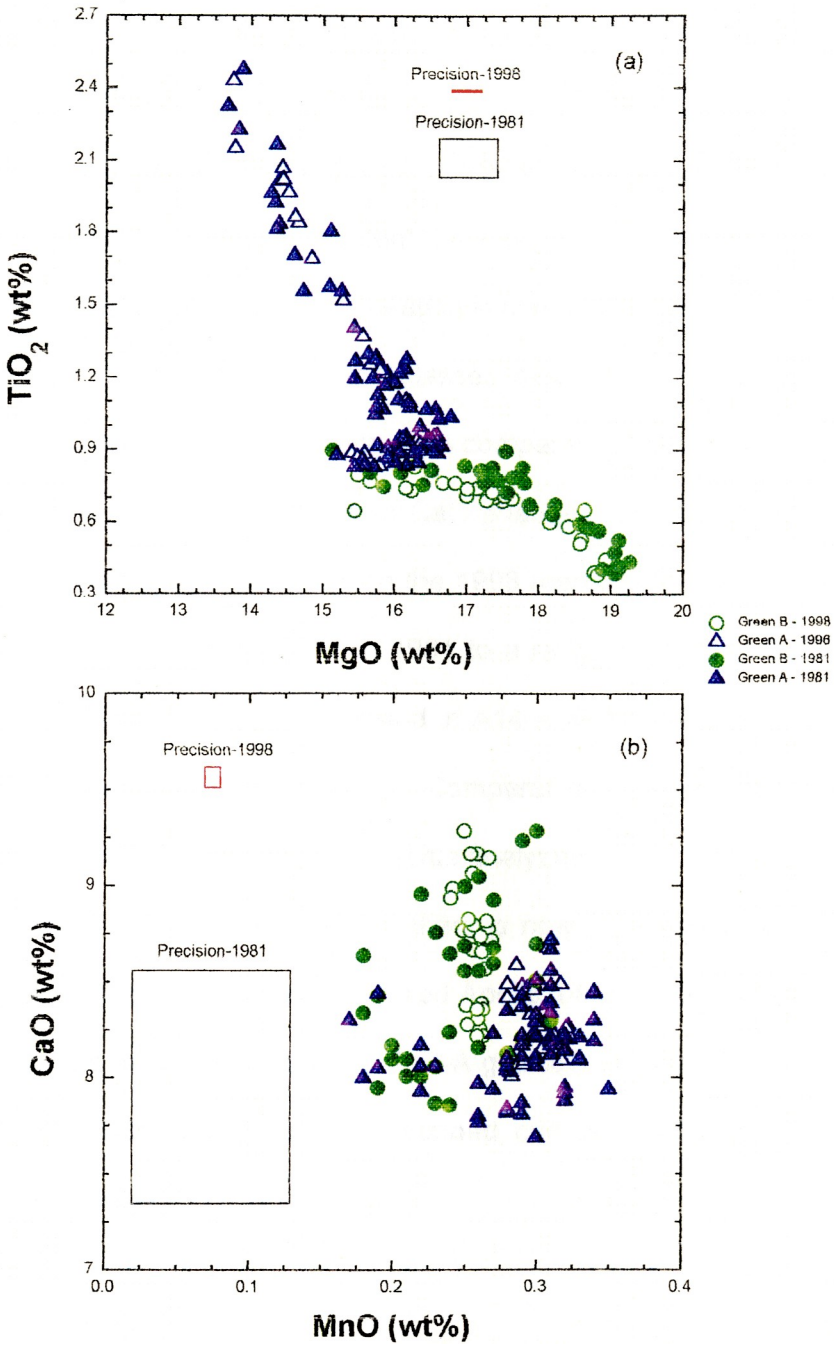

Figure 4.2.1 Apollo 14 green glass A and B from 1981 and 1996-98 data for single analysis per single glass. (a) TiO_2 (wt%) vs. MgO (wt%), and (b) CaO (wt%) vs. MnO (wt%). Green open-circles - green B 1998; green filled-circles - green B 1981. Blue open-triangles - green A 1996; blue filled-triangles - green A 198. 1998 precision indicated by the red-box and 1981 precision indicated by the black-box (Delano, 1981; Delano, 1996; Delano and Fernandes, 1998).

1996 for group A was between 0.84 and 2.44 wt% while group B was between 0.38 and 0.83 wt% in 1998. A14-A and A14-B groups have low to very-low TiO_2 wt%, respectively (Table 1.1.1). The MgO range for group A changed from a 13.69-16.79 wt%, to a 13.76-16.60 wt%. The MgO range for group B changed from 15.15-19.27 wt% in 1981 to a range of 15.46-19.12 wt% in 1998. However, in Figure 4.2.1a, the subtrend observable in the low-Ti content in A14-A shows a positive correlation between TiO_2 and MgO. This positive correlation is contrary to the general trend shown by both A14-A and A14-B. Moreover, the glasses included in this subtrend of A14-A show narrower MgO and TiO_2 content ranges as compared to the main trends observed for A14-A and A14-B. Lastly, the range of CaO changed for group A from 7.69-8.72 wt% in 1981 to a range of 8.01-8.68 wt% in the 1998 reanalyzes. The range observed for group B went from a 7.86 to 9.29% in 1981 to a range of 8.22 to 9.29 wt%. The more recent analyzes show that the subtrend in A14-A with concomitant decreases in TiO_2 and MgO is more clearly indicated. Comparatively, improvement and better defined trends were observed for other elements analyzed.

As a result of the data improvement there is now (1) a clearer definition of the intrasample homogeneity of the two reanalyzed Apollo 14 volcanic green glass groups (A and B); (2) the subtrend observed in the A14-A glasses, at lower TiO_2 levels is better defined, and (3) the high-precision data obtained can be used more confidently in future petrogenetic models.

4.3 Data description

Thirty-seven A14-A and thirty-one A14-B glasses were reanalyzed for 10 different elements using the method mentioned above (see Appendix A for full data

set). All glasses were devoid of crystals, so that undesirable effects caused by crystallization (devitrification) could be minimized (Delano, 1980). The glasses found within Fra Mauro breccia samples have a mafic to ultramafic composition as can be observed in Figures 4.3.1 a,b, SiO_2 versus Mg# (wt%) and Al_2O_3 versus Mg# are plotted, respectively. A14-A have Mg# ranging from 37.71 to 41.74. A14-B have a Mg# range from 44.48 to 50.0. It can be observed that with decreasing MgO (wt%) there is an increasing SiO_2 content reflecting the progressive differentiation of the magma. The same inverse proportionality can be observed in the plot Al_2O_3 versus Mg#. These two distinct ranges define clearly the two different groups previously described (Chao et al., 1970; Delano, 1981; Delano, 1986). Moreover, the higher Mg# of glass B (Figures 4.3.1 a,b) and lower TiO_2 content (Appendix A) suggest that the glass B group is more primitive than group A. The low-Ti and high-Mg content of the lunar volcanic glasses are important "markers" for consideration of these melts as primary magmas (Delano, 1986; Longhi, 1987; Longhi, 1992).

The data trends for both glass types behave similarly when two oxides are plotted against each other. This behavior is illustrated in Figures 4.3.2 a,b where K_2O versus MgO and CaO versus Al_2O_3 are plotted, respectively. In other cases (Figures 4.3.2 c,d - SiO_2 versus Al_2O_3 and FeO versus MgO), the two glass groups show very discrete trends with no data continuum. However, the slope is approximately the same. There is a positive proportionality between CaO and Al_2O_3 (Figure 4.3.2b) as the melts represented become increasingly differentiated. The CaO and Al_2O_3 increases are similar varying from 6 to 11% (A and B, respectively) for CaO, and varying from 17 to 23% (A and B, respectively) for Al_2O_3. Furthermore, in Figure 4.3.2a, it can be observed that as the melts become increasingly differentiated (decrease in MgO wt%

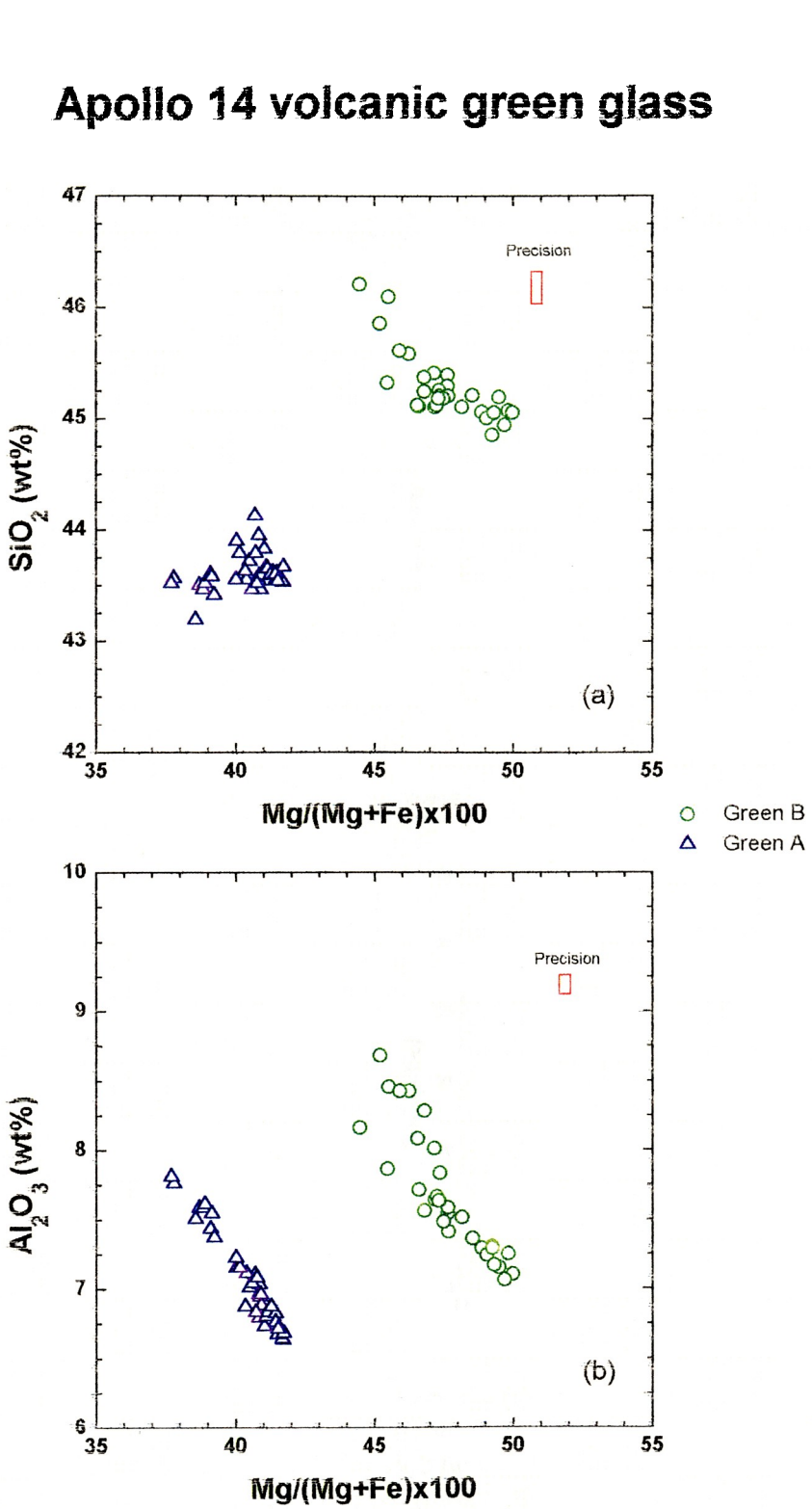

Figure 4.3.1 Apollo 14 green glass A (blue-triangles) and B (green-circles). (a) SiO_2 (wt%) vs. Mg#. (b) Al_2O_3 (wt%) vs. Mg# (Delano, 1996; Delano and Fernandes, 1998). Each data point represents a single analyses for a single volcanic green glass. Analytical precision is represented by the red-box along one of the corners of the graph.

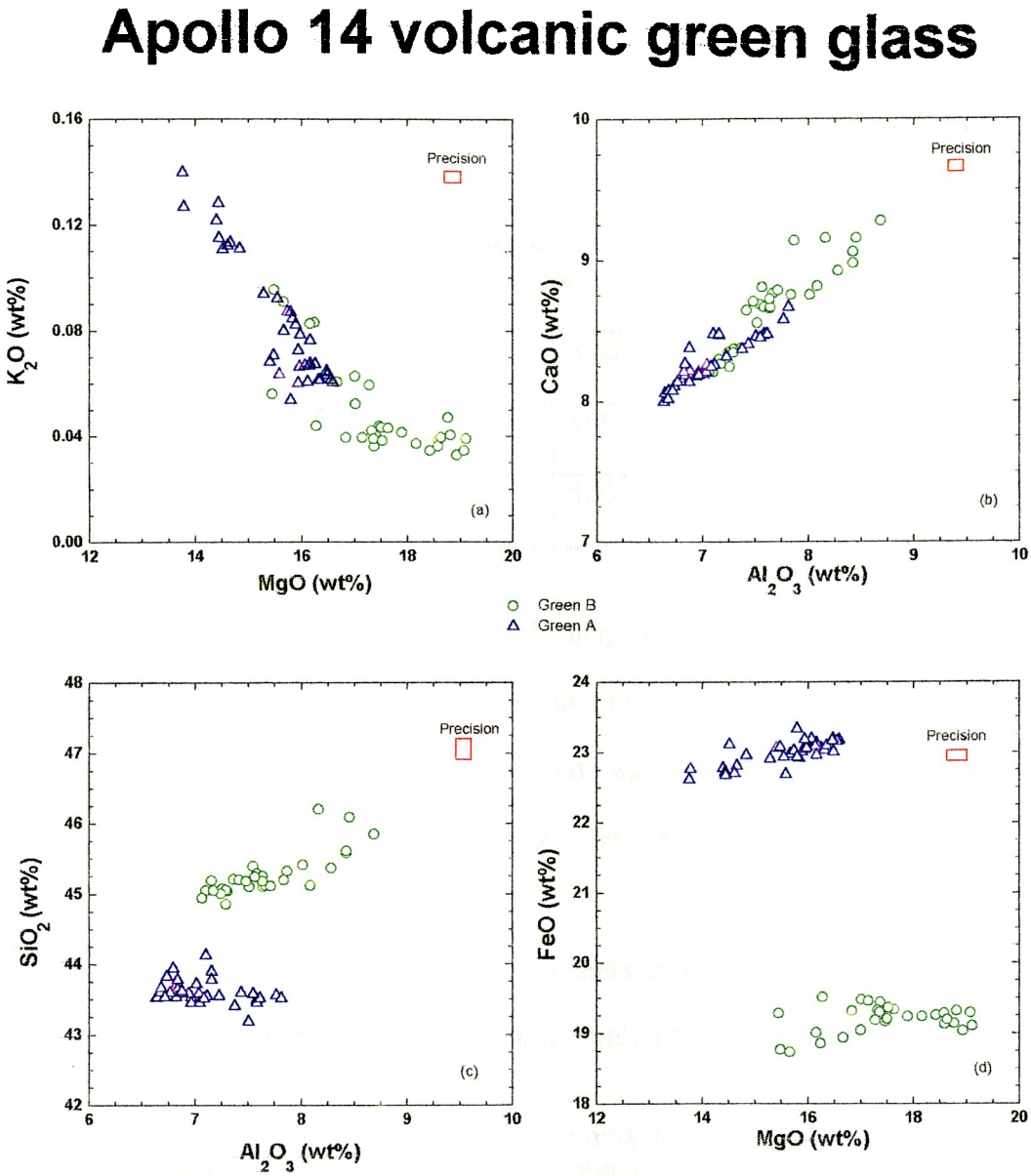

Figure 4.3.2 Apollo 14 green glass A and B data for single analyses per single glass. (a) K_2O(wt%) vs. MgO (wt%). (b) CaO vs. Al_2O_3 (wt%). (c) Na_2O (wt%) vs. MnO (wt%). (d) FeO (wt%) vs. MgO (wt%). Blue open-triangle - A14 green A; green open-circle - A14 green B glass (Delano, 1996; Delano and Fernandes, 1998). Analytical precision represented by the red-box along one of the corners of the graph.

up to 17% for A and 19% for B) there is a 1 to 2 fold increase in K_2O wt% (similar increase is also observed in Na_2O). This increase is quite large from ~160% to ~190% (A and B, respectively). This enrichment is also observed in other elements (Table 4.3.1) and will be discussed in the section below.

Table 4.3.1 Relative enrichment of Al_2O_3, CaO, K_2O, Na_2O and TiO_2 for Apollo 14 volcanic green glass A and B. These enrichments were calculated as a function of decreasing MgO wt% and are in percent (%).

	Al_2O_3	CaO	K_2O	Na_2O	TiO_2
Apollo 14 A	17.8	8.4	158.1	108.0	191.5
Apollo 14 B	22.9	13.0	186.6	99.3	116.9

These enrichment values are obtained by dividing the wt% of the glass with highest concentration of the incompatible element by that of the glass with lowest concentration of the same incompatible element, corresponding approximately to the glass with the lowest and highest MgO contents, respectively. The enrichment values were calculated separately for A14-A and A14-B.

The normalization of these enrichment values by the total MgO wt% variation of each group is shown in Table 4.3.2. This normalization shows that Al_2O_3, CaO and K_2O

Table 4.3.2 Normalization of the relative enrichments shown on Table 4.3.1 by the MgO wt% variation from the glass with highest- to the lowest-MgO content within each glass group.

	Al_2O_3	CaO	K_2O	Na_2O	TiO_2
Apollo 14 A	6.3	2.9	55.7	38.0	67.4
Apollo 14 B	6.3	3.6	51.0	27.1	31.9

behaved similarly during the petrogenetic process that originated either glass group. This reinforces the suggestion of a similar deep-seated magmatic process that originated the two glass groups. Conversely, the Na_2O and TiO_2 results suggest that these two elements behaved differently during the formation of A14-A and A14-B. The A14-A show greater enrichment in Na_2O and TiO_2 than A14-B.

A14-A and A14-B plots show the possible existence of 2 to 3 subgroups within these major groups. Figures 4.3.3 a,b show the plots for K_2O versus Cr_2O_3 and CaO versus Cr_2O_3, respectively. Each green glass type has been divided into two subgroups distinguishable by the open versus solid symbol correspondent to the glass group. The cause for these subdivisions is not well understood, however, (1) similar subdivisions have been observed for Apollo 15 volcanic green glasses A and B (Steele et al., 1992). These authors suggested that the glass subdivisions were the result of different melting events from a common source and from a similar petrologic process. (2) As an alternative approach, the "gaps" observed in the data set presented here may result from a sampling problem which does not allow the representation of a data continuum. For case (1) dynamic partial melting of an ascending mantle diapir (Figure 5.1.1) is proposed (Chapter V) as the petrogenetic model for the petrologic process that originated these liquids in light of the polybaric partial melting model suggested by Longhi (1992). Additionally, in other plots showing Cr_2O_3 data (Figures 4.3.4 a,b), this phenomena of subdivisions can be observed. The high Cr_2O_3 content (~4350 to 5500 ppm - terrestrial is < 700 ppm) and possibly the changes in concentrations within a group to have been suggested by Delano (1990b) to be caused by changes in f_{O2} as the mantle diapir rises (Cr becomes more soluble at spinel saturation in a mafic melt as oxygen fugacity decreases). Thus, mare magmas with a Cr_2O_3 wt% between 4350 and 5500 ppm were possibly derived from mantle source-regions having a low-redox state

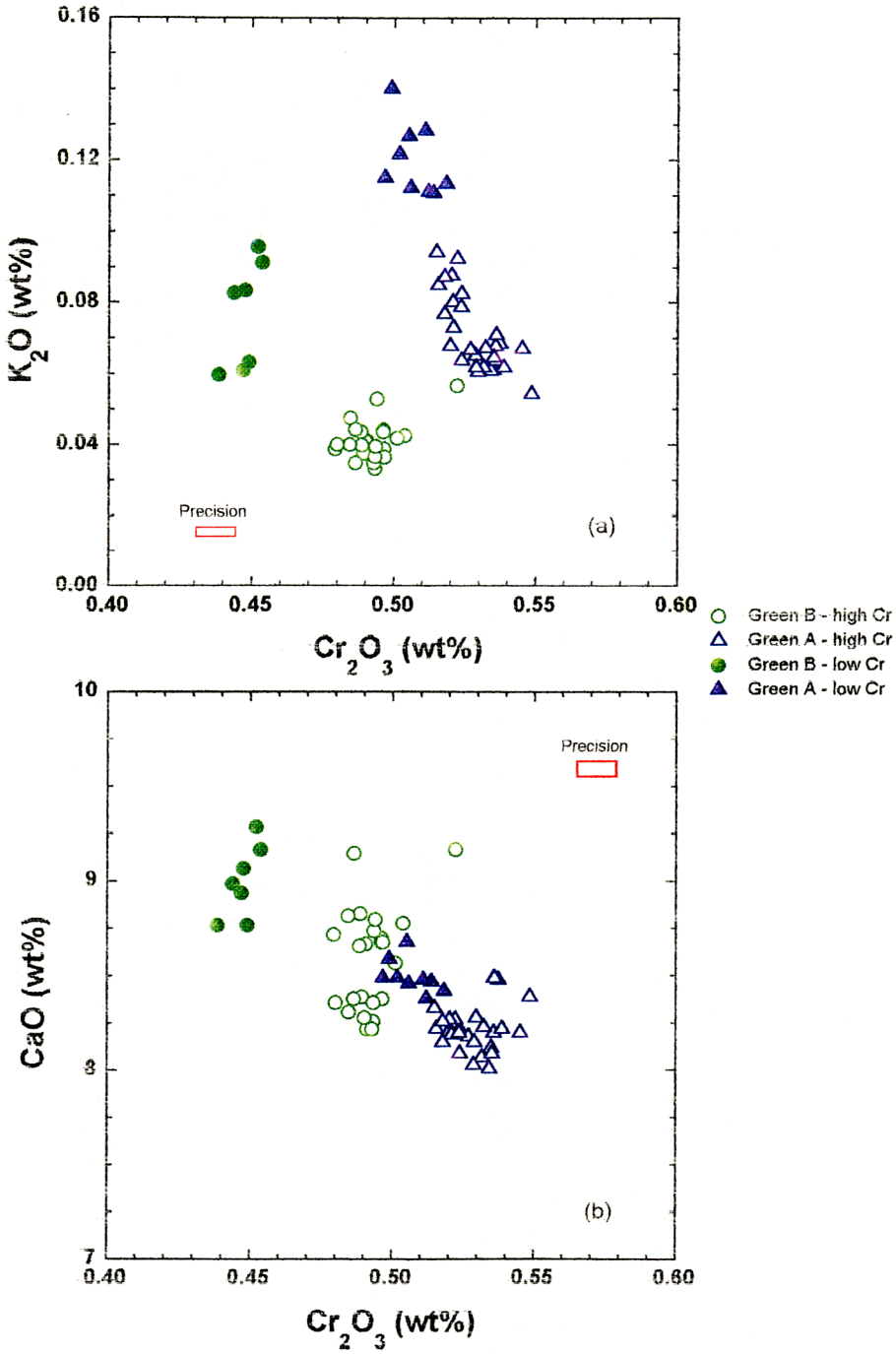

Figure 4.3.3 Apollo 14 green A and B. (a) K_2O (wt%) vs.Cr_2O_3 (wt%). (b)CaO (wt%) vs. Cr_2O_3 (wt%). Blue open-triangles - high-Cr A14-A; blue filled-triangles - low-Cr A14-A; green open-circles - high-Cr A14-B; green filled-circles - low-Cr A14-B (Delano, 1996; Delano and Fernandes, 1998).

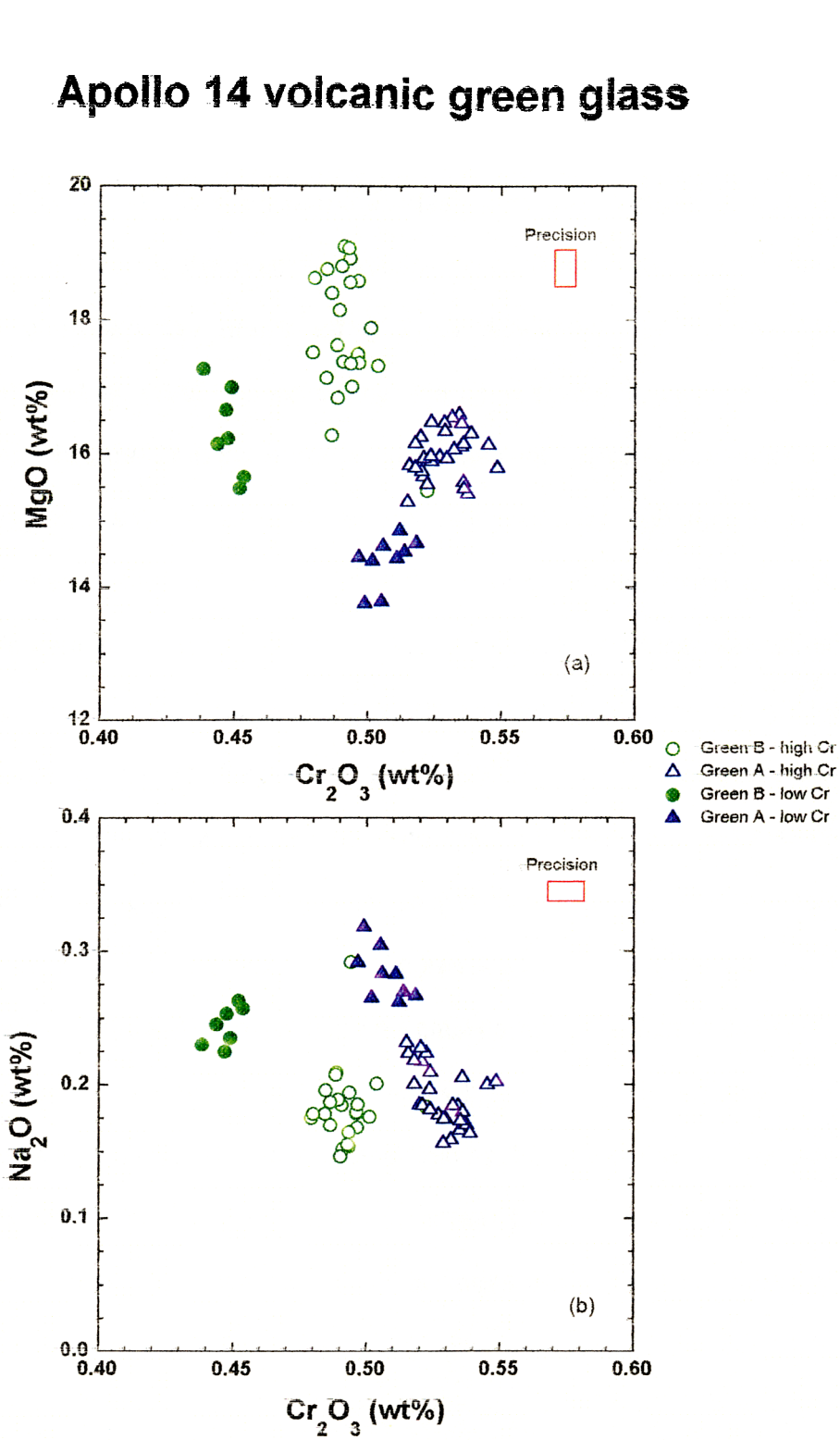

Figure 4.3.4 Apollo 14 green A and B. (a)Cr_2O_3 (wt%) vs. MgO (wt%). (b)Na_2O (wt%) vs. Cr_2O_3 (wt%). Blue open-triangles - high-Cr A14-A; blue filled-triangles - low-Cr A14-A; green open-circles - high-Cr A14-B; blue filled-circles - low-Cr A14-B (Delano, 1996; Delano and Fernandes, 1998).

(Delano, 1990b). Also, auto-reduction of lunar melts has been suggested to be a consequence of shallow carbon-reduction at shallow depths (Sato, 1976). If so, then the high-Cr content observed in these picritic glasses (A and B) could be considered a "late-stage" event - during the eruptive process. In a study of reduced chromium in lunar olivine and pyroxene grains using X-ray Absorption Near Edge Structure (XANES), Sutton et al. (1993) observed that the Cr in olivine is predominantly, if not totally, divalent while the Cr in pyroxene is mainly trivalent. These observations led the authors to suggest that Cr^{2+} in lunar olivine probably occurs through substitution for Mg in octahedral sites. This preference by the Cr^{2+} may be a consequence of the low-siderophile element levels in the Moon. Under very-low oxygen fugacities, siderophile elements (e.g. Ni, Fe) might be reduced to the metallic state, however, Cr became divalent and entered olivine (Steele and Smith, 1975). In a more recent study on metallic-blebs found in or between olivine phenocrysts within volcanic glasses (Weitz et al., 1997), CO was suggested to be the main gas phase produced in the reduction process. For case (2) the "gaps" shown in Figures 4.3.3 a,b and 4.3.4 a,b can be due to sampling error. Presently, no other green glasses from the Apollo 14 landing site have been identified as either A and/or B (and C). Considering that only three thin-sections have been considered, perhaps other thin-sections of the same breccias could possibly show more glasses of these two (or three) groups. It is hoped that future human or robotic missions to the Apollo 14 site might return samples that may "fill-in this gap".

4.4 Chemical trends

The low-TiO_2 wt% and high-Mg# places the Apollo 14 green glasses in the category of primitive magmas. The preliminary approach to model or understand the wide range of chemical content observed for some elements in the lunar volcanic glasses is by low-pressure olivine/liquid fractionation. Olivine is used as a criterion to determine primitive melts because the olivine/liquid distribution coefficient for Fe-Mg (K_D^{Fe-Mg}) between olivine and melt is not strongly affected by changes in temperature and pressure. This approach is used based on different experimental work done on these lunar volcanic glasses. It has been determined experimentally that olivine is the liquidus phase for these low-Ti melt compositions (Delano, 1980; Delano, 1982) at pressure up to 18-20 kbars (Figures 4.4.1 a,b) - corresponding to depths of 300 to 400±50 km. At greater pressures, there are two liquidus phases, olivine and low-Ca pyroxene. As Figures 4.4.1 a,b indicate, experimental work by Delano (1980, 1982) and suggestion by Hughes et al. (1990), the low-Ti magmas appear to be derived from multiple saturation regions at great depth where olivine and low-Ca orthopyroxene are the liquidus phase. This result can be explored further when fractionation trends for olivine, low-Ca pyroxene, augite and plagioclase are determined for both A14-A and A14-B compositions (Figures 4.4.2 a,b). These vectors were determined following a series of iterations having as starting composition that of the most primitive (highest MgO wt%) melt (glass) of each group. The olivine trend shown by the black-arrow represents a total of 25% crystallization (calculated at 1% removal of olivine per step). Similarly, for low-Ca pyroxene (blue-arrow) with a total 15% crystallization, augite (green-arrow) a total crystallization of 15% is represented, and plagioclase (red-arrow) with a one-step, 10% crystallization. These vectors show clearly that there is no direct

relation between the compositional trends of A14-A and A14-B and the fractional crystallization of the minerals considered.

The most striking characteristic for both group A and B glasses is the wide chemical compositional range. However, as observed previously by Delano (1981), the chemical trends displayed by A14-A and A14-B cannot simply be explained by olivine/liquid fractionation (Figures 4.4.2 a,b), or any other mineral determined experimentally. In these K_2O versus SiO_2 and TiO_2 versus MgO plots (Figures 4.4.2 a,b), A14-A and A14-B are plotted, and the expected olivine/liquid fractionation vector is also shown. The lack of correspondence between the trends of the Apollo 14 volcanic green glasses (A and B) and the expected vector for olivine/liquid fractionation is evident. Furthermore, the large enrichments observed in these glasses for TiO_2, Na_2O and K_2O as a function of MgO decrease (Tables 4.3.1 and 4.3.2) are not accounted for by low-pressure, olivine/liquid fractionation or crystallization of low-Ca pyroxene, augite and plagioclase. The enrichment observed in these elements will be discussed below.

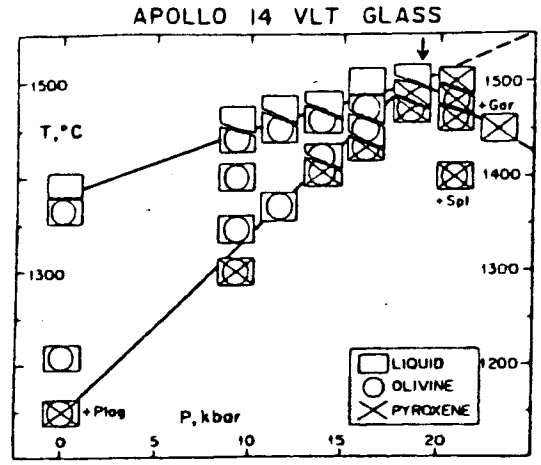

(a)

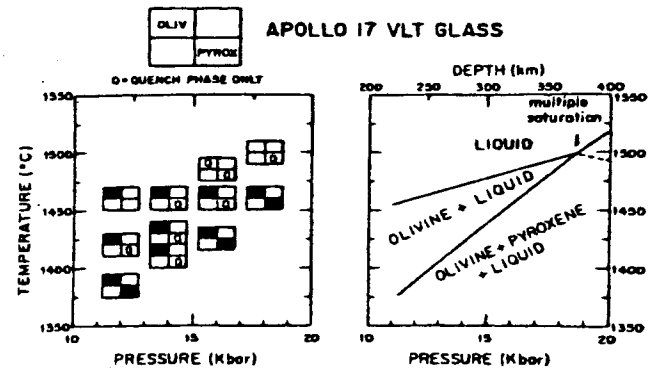

(b)

Figure 4.4.1 High pressure phase relations of (a) Apollo 14 VLT glass and (b) Apollo 17 VLT glass (Chen et al., 1982). Olivine is the sole liquidus phase at pressures up to 18-20 kbars for (a) and (b). The uncertainty in temperature and pressure for these high-pressure experiments are indicated by the size of the boxes shown.

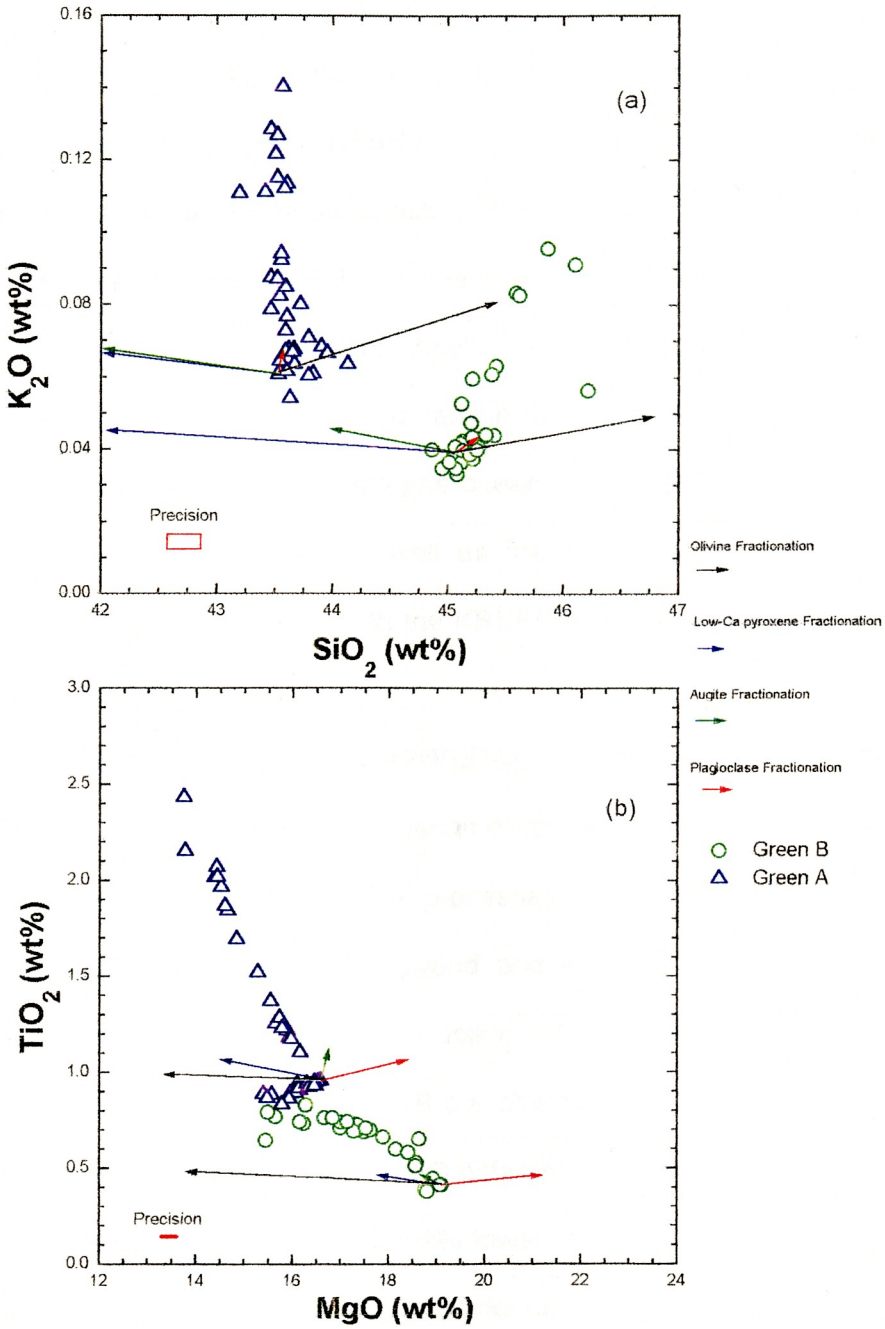

Figure 4.4.2 Apollo 14 green glass A and B volcanic green glass data for single analysis per single glass (blue-triangle) and B (green-circle) data and calculated olivine fractional crystallization (25%, black-arrows), plagioclase fractional crystallization (10%, red-arrows), augite fractional crystallization (15%, green-arrows) and orthopyroxene fractional (15%, blue-arrows) . Arrows show calculated trends for (a) K_2O (wt%) vs. SiO_2 (wt%) and (b) TiO_2 (wt%) vs. MgO (wt%) (Delano, 1996; Delano and Fernandes, 1998).

4.5 KREEP assimilation

KREEP (lunar basalt rich in potassium, rare earth elements, phosphorus and other incompatible elements) bulk assimilation has often been used to be the explanation for the incompatible element enrichment observed in the Apollo 14 volcanic green glasses (Tables 4.3.1 and 4.3.2). KREEP was first discovered in Apollo 12 samples, but it is more abundant in the Apollo 14 samples, namely the breccia samples. KREEP is believed to have formed early in the history of the Moon during the solidification of the planet following the magma ocean event. KREEP volcanism may have begun as early as ~4.1 Ga., as well as the earliest high-Ti mare basaltic volcanism, and was contemporaneous with the KREEP basaltic volcanism and appear to extend in age to 3.6 Ga.

KREEP hybridized source region (KREEP-like liquid obtained during the late stages of lunar magma ocean (LMO) that became trapped in the source region) and KREEP material assimilation have been processes highly suggested by several workers (Hubbard and Minear, 1975; Ringwood and Kesson, 1976; Hughes et al., 1990; Shearer et al., 1991; Shearer and Papike, 1993) to be the source for the enrichment observed. The A14-A and A14-B are characterized by an enriched LREE signature with a slight Eu-anomaly due to LMO differentiation early in the lunar history. The green B REE abundances are substantially lower than those of group A (Shearer and Papike, 1993). A14-A also appears to be enriched with incompatible elements Ba, Sr and Zr. This enrichment was viewed by Shearer et al. (1991) as the result of a KREEP component residing at the Apollo 14 glass source region. The REE-enrichment observed in the A14-A and A14-B was suggested by Shearer et al. (1989) to be caused by a 20 - 30% incorporation of KREEP into the melt. However, this recommended

amount would not only affect the trace elements behavior, but would also affect the major element characteristics of the melts in a manner not observed. Furthermore, it was suggested that the incorporation of KREEP into the source region by hybridization was a more thermally efficient mechanism, rather than assimilation or magma mixing. Conversely, Hughes et al. (1990) viewed this KREEP-like component not so much as a compositional characteristic, but the result of a process that may have enhanced that composition. Moreover, when bulk-KREEP data (Warren and Wasson, 1979) are plotted together with A14-A and A14-B (Figure 4.5.1 a,b), it can be clearly observed that there are no glass data along the mixing lines between the most primitive melt of A14-A and A14-B and the bulk-KREEP composition. Thus, the incorporation of KREEP-like material into the source of the Apollo 14 volcanic green glasses by bulk assimilation is not believed to be the process responsible for the enrichments observed in the incompatible elements.

Fractional assimilation is also considered presently as another approach for the possible integration of KREEP-like material into the melt and eventual enrichment of incompatible elements. This consideration has in mind the possible reaction of the ascending melt with the wallrock. The incorporation of the KREEP-like material would occur due to partial melting of the bulk KREEP wallrock caused by the heat transfer from the rising melt. The partial melts produced would intrude into the picritic magma by fractional assimilation and cause the observed enrichments of the incompatible elements. Shown in Figures 4.5.2 a,b are the results from crystallization experiments starting with bulk low-K Fra Mauro basalt (LKFM, Hess et al., 1977) compared with A14-A and A14-B chemical data. In Figures 4.5.2a are shown Na_2O vs. SiO_2 concentrations for three residual melts obtained by Hess et al. (1977) and A14-A and A14-B data from this study. Departing from the bulk LKFM an equilibrium line of descent, determined

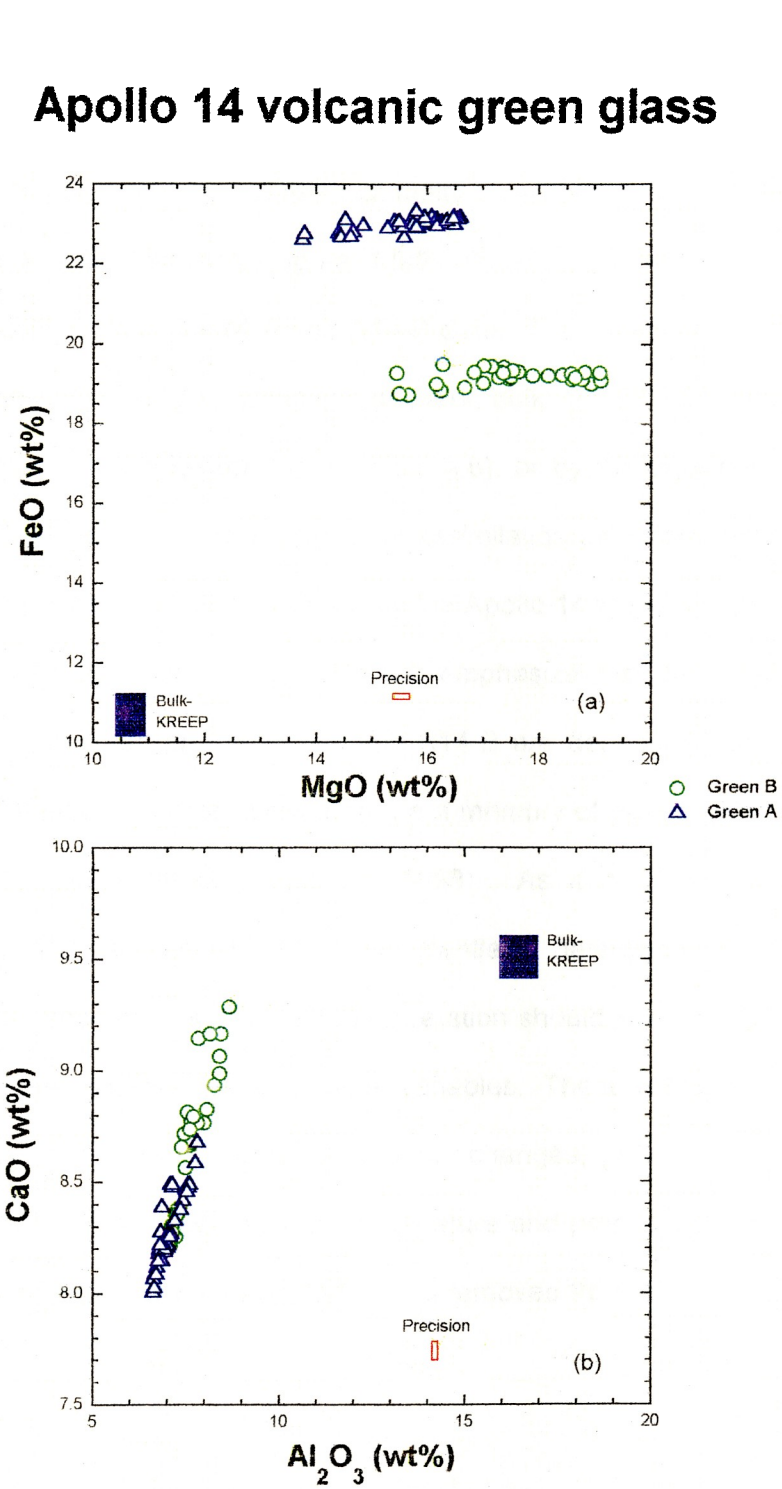

Figure 4.5.1 Apollo 14 green glass A (blue-triangle) and B (green-circles) data per sinlge analysis per glass (Delano, 1996; Delano and Fernandes, 1998) compared with KREEP (filled blue-box Warren and Wasson, 1979). (a) MgO(wt%) vs. FeO (wt%). (b) Al_2O_3 (wt%) vs. CaO (wt%). In both plots the two Apollo 14 glass types occupy well defined chemical composition ranges. These chemical compositions do not appear to form any mixing lines between the most primitive glass of each group and the KREEP composition.

by the composition of representative residual melts, is shown together with the three temperatures where melts were held. The steady increase in SiO_2 and the small changes in Na_2O shown by the residual melts do not encompass the trends shown by A14-A and A14-B. Similarly, Figure 4.5.2b shows CaO vs. FeO concentrations for three residual liquids and A14-A and A14-B data. The trends of the glass data are not encompassed by either the mixing line between bulk-KREEP composition and the most primitive glass of each group (Figure 4.5.1 a,b), or by the equilibrium line of descent (Figures 4.5.2 a,b). Therefore, fractional assimilation also does not appear to be the cause for the enrichment trends shown by the Apollo 14 volcanic glasses.

Later in this work, the author will emphasize that the chemical trends and enrichments observed on the A14-A and A14-B are dependent upon many variables (including the source composition), and are a memory of deep-seated processes in the lunar mantle (Delano and Fernandes, 1998). As it is largely accepted by selen petrologists and geochemists, the lunar mantle is heterogeneous at many different levels. Thus, new models and their interpretation should keep in mind the interference a change in one variable has on all other variables. These variables include the source composition, temperature and pressures changes, change in the distribution coefficients of different elements as temperature and pressure change, porosity of the source region, and how the melt produced is removed from its source.

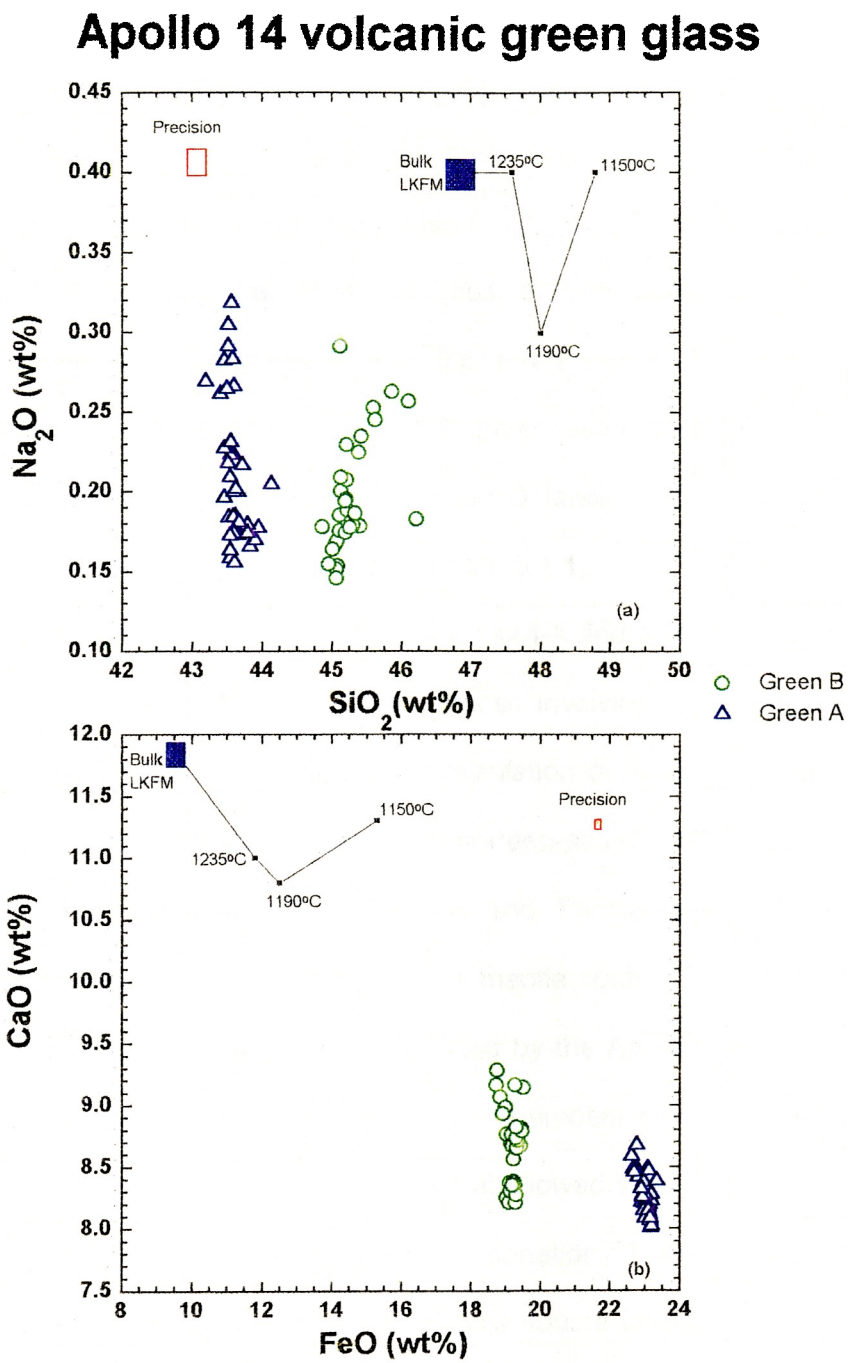

Figure 4.5.2 Apollo 14 green glass A (blue-triangle) and B (green-circles) data per sinlge analysis per glass (Delano, 1996; Delano and Fernandes, 1998) compared with KREEP bulk composition (bulk-LKFM, filled blue-box) and partial melting (black line) with specific hold temperatures of which composition was determined (Hess et al., 1977). (a) MgO(wt%) vs. FeO (wt%). (b) Al_2O_3 (wt%) vs. CaO (wt%). In both plots the two Apollo 14 glass types occupy well defined chemical composition ranges. These chemical compositions do not appear to form any mixing lines between the most primitive glass of each group and the KREEP composition.

4.6 Conclusion

A14-A and A14-B differ primarily in the TiO_2 and MgO content (Figure 4.2.1a). In general, it is believed that those glasses containing low-Ti and high-Mg# represent primitive magmas (least fractionated). Thus, those glasses represented by group B represent more primitive magmas than those represented by group A. It should be noted, that in this study, A14-A and A14-B are considered as glasses originated by the same petrogenetic process (Delano, 1981; Delano, 1996; Delano and Fernandes, 1998), e.g. an ascending mantle diapir (Figure 5.1.1).

The observed fractionation trends for A14-A and A14-B do not result from a low-pressure (<18-20 kbars) fractionation process involving the liquidus phase (olivine), mixing of KREEP-like material by bulk assimilation or fractional assimilation. Instead, the trends appear to be the consequence of deep-seated magmatic processes (Delano and Livi, 1981; Delano, 1996a; Delano and Fernandes, 1998) that have been preserved during the melt ascent from the mantle source. Furthermore, these trends suggest that the picritic magmas represented by the Apollo 14 volcanic green glasses did not aggregate and homogenize in larger chambers after their generation. Instead, there must have been some mechanism that allowed these melts to erupt shortly after their formation, but did not promote melt fractionation. These trends appear to reflect a continuous chemical "evolution" of the magma source over the duration of the eruptive event (Delano and Fernandes, 1998).

CHAPTER V - Dynamic melting model

5.1 Dynamic melt inversion (DMI)

The origin of the highly-incompatible to compatible elements chemical variations observed within the A14-A and A14-B was suggested by Shearer and Papike (1993) to be the result of partial melting of a heterogeneous mantle source consisting of intermediate stage LMO cumulates composed mainly of olivine and orthopyroxene. More recently, Delano (1996a) suggested that the intragroup chemical variation categorized volcanic glasses into *enriched* and *depleted* glasses. These variations may have resulted from different degrees of partial melting in a rising mantle diapir (Figure 5.1.1) as follows: the lower-Mg, high-Na, -K and -Ti from *enriched* areas of the source regions (periphery of the diapir), and the higher-Mg, low-Na, -K and -Ti melts from *depleted* areas of the source region (center of the diapir) (Delano, 1996a). The process by which this variation is thought to be possible is polybaric dynamic partial melting of a homogeneous mantle source region (Delano and Fernandes, 1998). This process includes varying degrees of partial melting of an uprising mantle source with continuous but incomplete removal of melt as melting proceeds (Langmuir et al., 1977; Longhi, 1992).

In low viscosity melts, such as those represented by the mafic to ultramafic A14-A and A14-B, the incompatible minor and trace element signatures of melts derived from peridotites can result from extraction of these elements from large volumes of the mantle that do not undergo extensive melting (McKenzie, 1985b; O'Hara, 1985; and Zou and Zindler, 1996). This initial melt (first stage) is produced in the peripheral

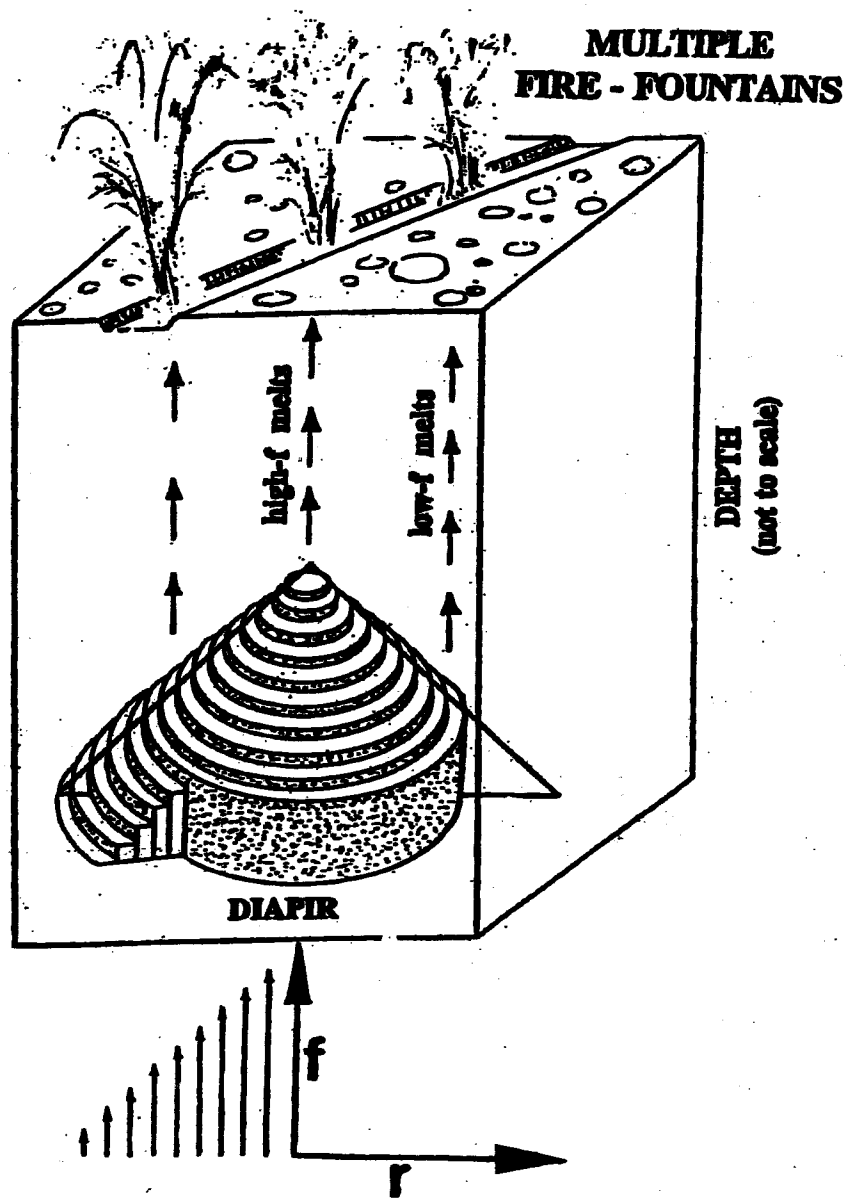

Figure 5.1.1 An hypothesized mantle diapir (Delano and Fernandes, 1998) that could have originated the lunar picritic magmas. These picritic magmas are here assumed to have formed at different regions of an ascending mantle diapir characterized by a lateral temperature gradient. The compositional ranges shown within individual magmatic suites (Figures 4.3.1, 4.3.2, 4.3.3, and 4.3.4) are perceived as having originated from different regions of the diapir (different degrees of partial melting - f), and being erupted onto the lunar surface without having mixed with magmas generated at other regions of the same diapir.

regions of the melting region. Eventually, this melt separates from the source region and occupies the overlying mantle region to produce a second stage source region (polybaric melting model, Longhi, 1992). This second source is affected by large extents of melt. The melting of the peridotitic source occurs at deep regions because at shallower depths larger fractions of melt would be produced, thus the enriched incompatible-element signatures would not be produced.

Apollo 14 picritic green glasses are, in general, suggested to require magma transport without fractionation over hundreds of kilometers (~400 km, Longhi, 1992) from the source to the lunar surface. It has been demonstrated in Chapter IV, Figures 4.5.1 and 4.5.2 that the enrichment in incompatible elements is not a result of either bulk assimilation of KREEP material or partial melting of KREEP-like wallrock. Transport of magma through the lunar lithosphere via a connected "channel" network (melt isolation) prevents green glass magmas from undergoing significant fractionation on the way to the lunar surface (Spera, 1992). Although, low-Ti picritic magmas (e.g. Apollo 14 volcanic green glasses) tend to have lower density, higher liquidus temperature, lower viscosity, higher density contrast with residuum and higher velocity of melt segregation per fraction of partial melting (Delano, 1990), the mean ascent rate and crack width calculated by Spera (1992) are 10 m/s and >40 m, respectively. In this context, near the surface and aided by the vapor fraction (CO, CO_2, COS), the melt expands greatly and the internal vapor energy is converted to mixture, kinetic energy with accompanying high speed ejection of vapor and pyroclastics to form lunar fire-fountain deposits (Spera, 1992). This suggestion appears to be unlikely.

Longhi (1992) has proposed an alternative to overcome some of the problems relative to temperature loss that may occur during the transport of these magmas from the source to the point of extrusion as well as the pressure/depth memory carried by

these melts. Longhi (1992) polybaric generation of mare basalt magmas suggests that melts might pool at the base of a thermal lithosphere. This thermal lithosphere would extend below an outer, elastic lithosphere with thickness of ~50-100 km. In such a physical regime, mare basalt magmas would pool at the base of a lithosphere thinned by the thermal erosion and rise afterwards to the surface along fractures caused by impacts. The result would be melts with an average depth memory of ~400 km (melt pool), however the melt contributions originated at depths $\leq$ 1000 km.

The process used in this work to model polybaric dynamic partial melting of cogenetic magmas (e.g. the Apollo 14 volcanic green glasses) was proposed by Zou and Zindler (1996). This method is based on dynamic melting inversion (DMI) that permits calculation of the Degree of Partial Melting (DPM) for cogenetic magmas in the context of a dynamic model proposed by Langmuir et al. (1977). For partial melting to occur, the rate of melt production needs to equal the rate of melt extraction. Also, for melt extraction to occur, it is necessary that the melt portion exceeds porosity (ϕ). Actually, in dynamic melting, the extraction rate is greater than the melting rate after the porosity requirement is fulfilled. In this study, mass of melt extracted and DPM data will be the focus. In this method, dynamic partial melting occurs on the surface of a homogeneous mantle source region (mantle diapir, Figure 5.1.1).

The amount of melt formed in individual stream lines of upper mantle rocks passing through a partial melting regime is suggested by O'Hara (1985) to increase from zero at the edge to a maximum at the central axis (Figure 5.1.1) with a maximum value of ~25 to 35 vol%. The different melt compositions that result from this melting regime represent different partial melts. This mantle diapir model with a stream line of increasing melt from the periphery to the center of the diapir (Figure 5.1.1) assumes (1)

that incompatible elements geochemistry, which appear to point to very small fractions of partial melt, formed at the periphery of this mantle diapir, and (2) the compatible elements geochemistry dominates the regions where melting approximates its maximum (McKenzie, 1985; O'Hara, 1985) - at the center of the diapir. Moreover, the increase in the DPM can be interpreted as a result of the gradational increase in temperature from the edge to the center of the ascending mantle diapir. Also, it is important to note that adiabatic decompression is the driving force for this melting event.

The Zou and Zindler method allows calculation of the DPM by using the concentration ratio of an incompatible or highly-incompatible element in two magmas presumed to be originated from the same source and event, but from a different region (different parcel). This method does not require assumptions regarding source incompatible element concentrations or ratios. However, there are a few assumptions to be noted: (1) the rate of melting and porosity are constant and finite while the system of matrix and interstitial fluid are moving (McKenzie, 1985a); (2) the mantle is composed of only one phase: olivine - a peridotitic source; (3) pressure and temperature regime remain constant throughout the diapir; and (4) each element distribution coefficient is constant along the mantle diapir during the melting event. To overcome the constraints forced by these assumptions, the model has been applied for a wide range of porosity values (0.01 and 0.05), and a wide range of distribution coefficients for each element considered presently: Al, Ca, K, Na and Ti (see Table 5.1.1).

Zou and Zindler (1996) applied their method to terrestrial rocks, namely the nephelinitic Koloa suite of Kauai, Hawaii, the Honolulu volcanics of Oahu, Hawaii, and alkalic basalts from SE Australia. In this study, the Zou and Zindler method is used to

model dynamic partial melting of cogenetic lunar magmas within two groups of homogeneous glass spherules with a dry, ultramafic composition obtained at the Apollo 14 site (A14-A and A14-B). This method is thought to be more realistic in representing the production of basaltic magmas than the true batch melting model as proposed by Langmuir et al. (1977) and McKenzie (1985a) because it permits a wide range of possibilities to be tested, namely for porosity and distribution coefficients.

The method used here is termed the "concentration ratio". As the name indicates, the concentration ratios were determined for the five elements that show an enrichment as a function of decreasing MgO wt% (Table 4.3.1 and 4.3.2) for A14-A and A14-B. The three equations shown below are those most important for the model used. For further details, refer to Appendix B.

$$\frac{C_L^1}{C_L^2} = \frac{X2[1-(1-X1)^{G(1-D)+1}]}{X1[1-(1-X2)^{G(1-D)+1}]} \qquad \text{(eq. 1)}$$

$$f1 = \frac{X1.\rho_s.(1-\phi)}{\rho_f.\phi+\rho_s.(1-\phi)} + \frac{\rho_f.\phi}{\rho_f.\phi+\rho_s.(1-\phi)} \qquad \text{(eq. 2)}$$

and

$$f2 = \frac{X2.\rho_s.(1-\phi)}{\rho_f.\phi+\rho_s.(1-\phi)} + \frac{\rho_f.\phi}{\rho_f.\phi+\rho_s.(1-\phi)} \qquad \text{(eq. 3)}$$

Where C_L is the incompatible element concentration in the glass, **f** is the degree of partial melting which increases form Stage 1 (Low) to Stage 2 (High), **X** is the mass fraction of the liquid extracted, ρ_f melt density (2.882 g/cm^3; Delano, 1990), ρ_s residue density (3.3 g/cm^3, Zou and Zindler, 1996), ϕ porosity (amount of melt present), **G** is a parameter that includes porosity, density and **D** (distribution coefficient; see Appendix B for details).

The elements chosen for modeling were Al, Ca, K, Na and Ti (see Table 4.3.1 and 4.3.2 for overall enrichments observed per Apollo 14 volcanic green glass group

considered in this study). For the model per se, Ti was chosen as the base-element for calculation of the concentration ratios (eq. 1, C_L^1 is the highest TiO_2 or corresponding Al_2O_3, CaO, K_2O, Na_2O; and C_L^2 is the lowest TiO_2 or corresponding Al_2O_3, CaO, K_2O, Na_2O). The same procedure was used for either A14-A and A14-B. This choice was based on the large enrichment observed for Ti in the Apollo 14 volcanic green glasses as well as that shown by the different glass groups known (Table 1.1.1). The Al, Ca, K and Na concentration values used in the model were those corresponding to the highest and lowest TiO_2-containing volcanic glasses of each glass group. In summary, the enrichment values used per element per glass-group are approximately the same as those shown in Table 4.3.1.

Mass fraction of liquid extracted (MFEM, X1 and X2, eq. 1), DPM (f1 and f2, eq. 2) shown in Figures 5.2.1 and Figures 5.2.2, and source concentration (Co1 and Co2, equation not shown) for each element were calculated separately per glass type (A14-A and A14-B refer to Appendices B and C for complete details of the results). The calculations of each glass type were divided into two sets: (1) for ϕ = 0.01 (McKenzie, 1985b) and (2) for ϕ = 0.05. Each set consisted of five subsets each represented by one of the elements used in the model (i.e. Al, Ca, K, Na, and Ti). The range of D values chosen for each element used in this model, and used for both glass types, were based, in part, on a review by Irving (1978), and were derived from olivine/liquid partitioning experiments with exception of Al and Ca. The values are listed below:

D	Values considered
D_{Al}	0.05, 0.10, 0.15, 0.20 and 0.40
D_{Ca}	0.02, 0.05, 0.10, 0.20 and 0.40
D_{K}	0.0001, 0.001, 0.005 and 0.01
D_{Na}	0.0001, 001, 005 and 0.01
D_{Ti}	0.02, 05 and 0.10.

Table 5.1.1 The distribution coefficient values (D) used in the model for Al, Ca, K, Na and Ti. Each value was used for calculations when ϕ = 0.01 and 0.05.

This choice for a wide range of distribution coefficients had in mind the simplification of the modeling as well as the uncertainty of the lunar mantle chemical composition and mineralogic phase(s) present (olivine is assumed) at the depths under consideration (~ 400 km). Similar to porosity, the wide ranges used for D values had in mind the coverage of all possibilities. Thus, the ranges used for both the D and ϕ attempted to take into account all the plausible values of these variables. The density of the picritic liquid (ρ_f) produced due to melting was assumed to be 2.882 g/cm^3 (Delano, 1990). The density of the source region (ρ_s) was assumed to have the value of 3.3 g/cm^3 (Zou and Zindler, 1996).

Partial melting is assumed to be a result of the decompression of hot mantle ascending along an adiabat intersecting the solidus curve (O'Hara, 1985). During this ascent, the same author suggested that auto-reduction of some elements could occur (i.e. Cr, Fe, Ni) due to the carbon-reduction model. This model appears to explain many other observed facts, including the liquidus precipitation of Fe° as metallic-blebs (Sato, 1976; and Weitz et al., 1997), and perhaps the high Cr_2O_3 concentration in the green glasses (Figures 4.3.3 a,b and Figures 4.3.4 a,b). This partial melting regime

affects individual parcels of mantle and produces a continuous partial melt; a process in which some mass fraction of the residue is trapped liquid, but in which further liquid is drained continuously from the parcel as melting proceeds (O'Hara, 1985). However, contrary to the suggestion of O'Hara (1985), the melts produced do not eventually aggregate and mix as it can be observed in Figures 4.3.1, 4.3.2, 4.3.3 and 4.3.4. Instead, the glass data show a progressive chemical continuum. The melts preserve a range of melt compositions that existed within the plumbing system of the ascending diapir undergoing dynamic melting (Delano, 1996a). The varied melts represented by the different spherules were produced in different regions of the mantle diapir (Eggins, 1992) and were erupted onto the lunar surface without having mixed with any other magmas (Figure 5.1.1, Delano and Fernandes, 1998). Furthermore, data in Figures 4.3.1, 4.3.2, 4.3.3 and 4.3.4 suggest that the two Apollo 14 volcanic green glass groups (A and B) are genetically related, meaning that these melts were originated via similar process not meaning that they had the same source.

In summary, the DMI model allows the determination of the DPM by simply using the chemical composition of cogenetic melts. The dynamic partial melting process involves the differential flow of melt and residual matrix (Eggins, 1992). In the interval of melting, the degree of melting will increase as a function of decompression, and of height above the adiabat and peridotite (source) solidus intersection. The amount of melt present (i.e. porosity) at a particular height, however, will be less than the degree of melting due to the more rapid buoyancy-driven ascent compared to the matrix. The magnitude of this melt-filled porosity (ϕ) will depend upon the velocity of the melt relative to the matrix and the rate of melting. The increase in ϕ from 0.01 to 0.05 may take into consideration a possible increase in temperature along the mantle diapir or as melting proceeds.

5.2 Model Results

The plots on Figures 5.2.1 a,b,c,d and Figures 5.2.2 a,b,c,d show the model results for A14-A and A14-B green glasses, respectively, for the different ϕ and D values used. It should be noted that only *the range of results* are represented in this chapter. All the data and plots for the model results can be found in Appendices B and C. Figures 5.2.1 a,c and 5.2.2 a,c correspond to the model results for DPM and (MFEM) for A14-A and A14-B, respectively, when $\phi = 0.01$. Figures 5.2.1 b,d and 5.2.2 b,d correspond to the model results for DPM and MFEM for A14-A and A14-B, respectively, when $\phi = 0.05$. The abscissa of Figures 5.2.1 a,b and 5.2.2 a,b must be interpreted as the lowest possible DPM (f1, Low-MgO) and the ordinate as the maximum DPM (f2, High-MgO) observed along the mantle diapir (Figure 5.1.1). Similarly for Figures 5.2.1 c,d and 5.2.2 c,d, the abscissa must be interpreted as the lowest possible MFEM (X1, Low-MgO) at the periphery of the mantle diapir, and the ordinate must be interpreted as the maximum possible of MFEM (X2, High-MgO) from the center of the mantle diapir (Figure 5.1.1). The ideal situation for the model results would be the identification of a single-point common to all the elements used currently. The two coordinates would inform on the lowest (f1) and highest (f2) possible DPM, and also the lowest (X1) and highest (X2) possible mass of extracted melt along the rising mantle diapir (Figure 5.1.1) that produced these glasses. However, the ideal situation is not that encountered here.

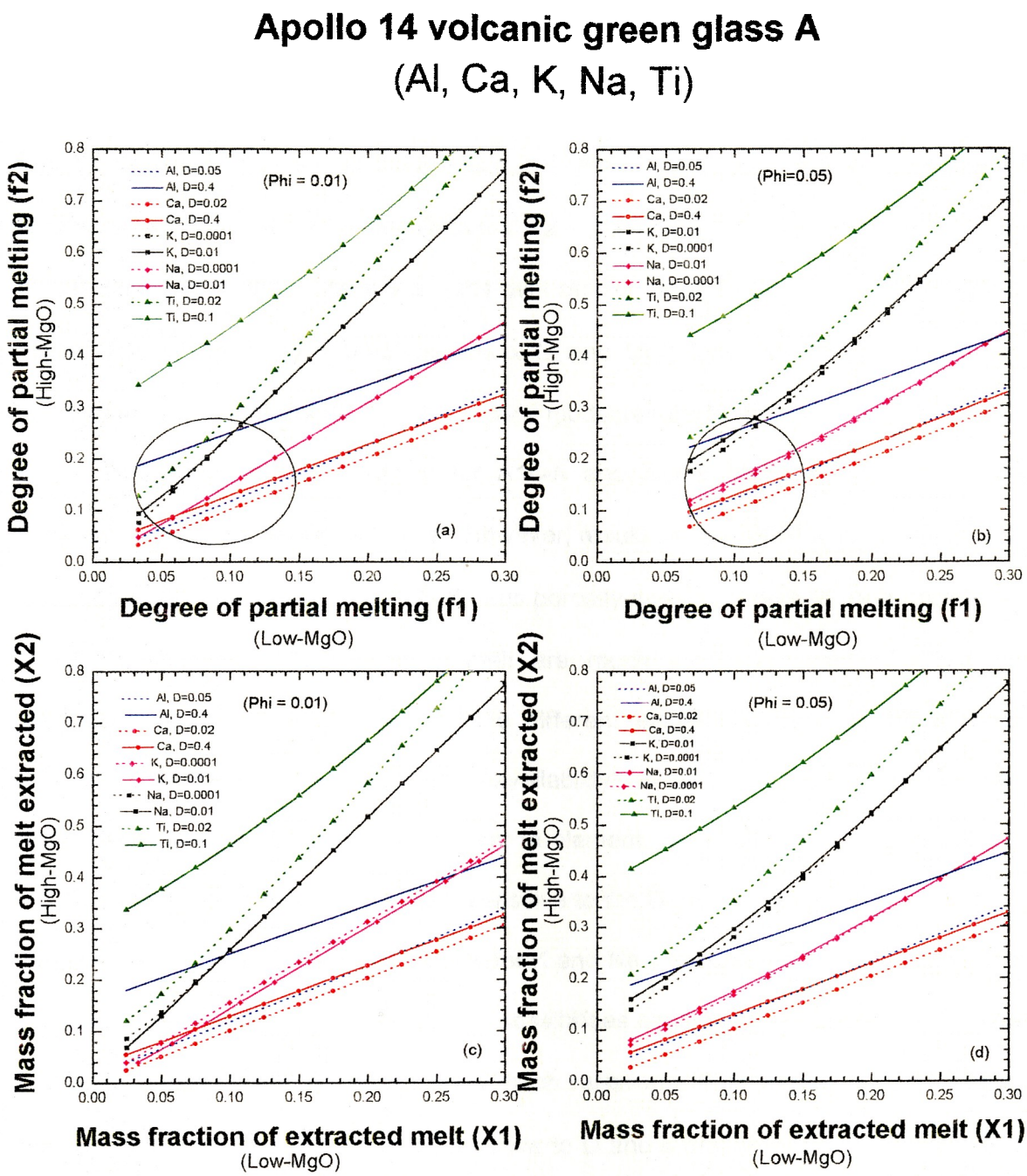

Figure 5.2.1 Apollo 14 volcanic green glass A model results for Degree of partial melting and Mass fraction of extracted melt for Phi = 0.01 and 0.05. The model calculations are based on element content of two cogenetic glasses of A14-A.

It can be observed that for both A14-A and A14-B, the MFEM results obtained for ϕ = 0.01 for the different values of D_{Al}, D_{Ca}, D_K, D_{Na} and D_{Ti} are, in general, lower than those obtained for ϕ = 0.05 (Figures 5.2.1 c,d and 5.2.2 c,d). The same generality is true for the DPM at low values (Figures 5.2.1 a,b and 5.2.2 a,b). However, at the higher values of f1 and f2 there is a cross-over resulting in the values for ϕ = 0.01 being higher than those for ϕ = 0.05 (Appendix C and D). There is an overall positive correlation between f1 and f2, and X1 and X2 model results for both A14-A and A14-B.

The model results obtained for A14-A and A14-B show that the elements behaved similarly for either melt type. However, results for the DPM when ϕ = 0.01 are generally lower than those for ϕ = 0.05, thus porosity does not seem to be a parameter to which elements entering into a melt are much dependent on. Conversely, distribution coefficient values (D) for the different elements appear to be a more important parameter in terms of the "availability" of an element. However, this dependency appears to vary from element to element. In Figures 5.2.1 a,b and 5.2.2 a,b, Ti appears to be the element most sensitive to the D_{Ti} value - the broadest range of values obtained. Conversely, the results for K and Na show the least sensitivity for the D value. The broad range of D_K and D_{Na} possibilities considered (including a 10^2 value increase) for both K and Na do not show much variation with change of ϕ or D. These two elements appear to be the least sensitive to D and ϕ and likely the most indicative of the partial melting range along the mantle diapir. This suggestion is most evident in Figures 5.2.2 a,b (A14-B) where K and Na model results for A14-B are nearly converging. The K DPM and MFEM results for A14-A are less constraining than in A14-B. The values for a14-A appear to reflect higher DPM than the values for a14-B, and perhaps resulting in the lower-K enrichment for A14-A. Also, the plots showing the

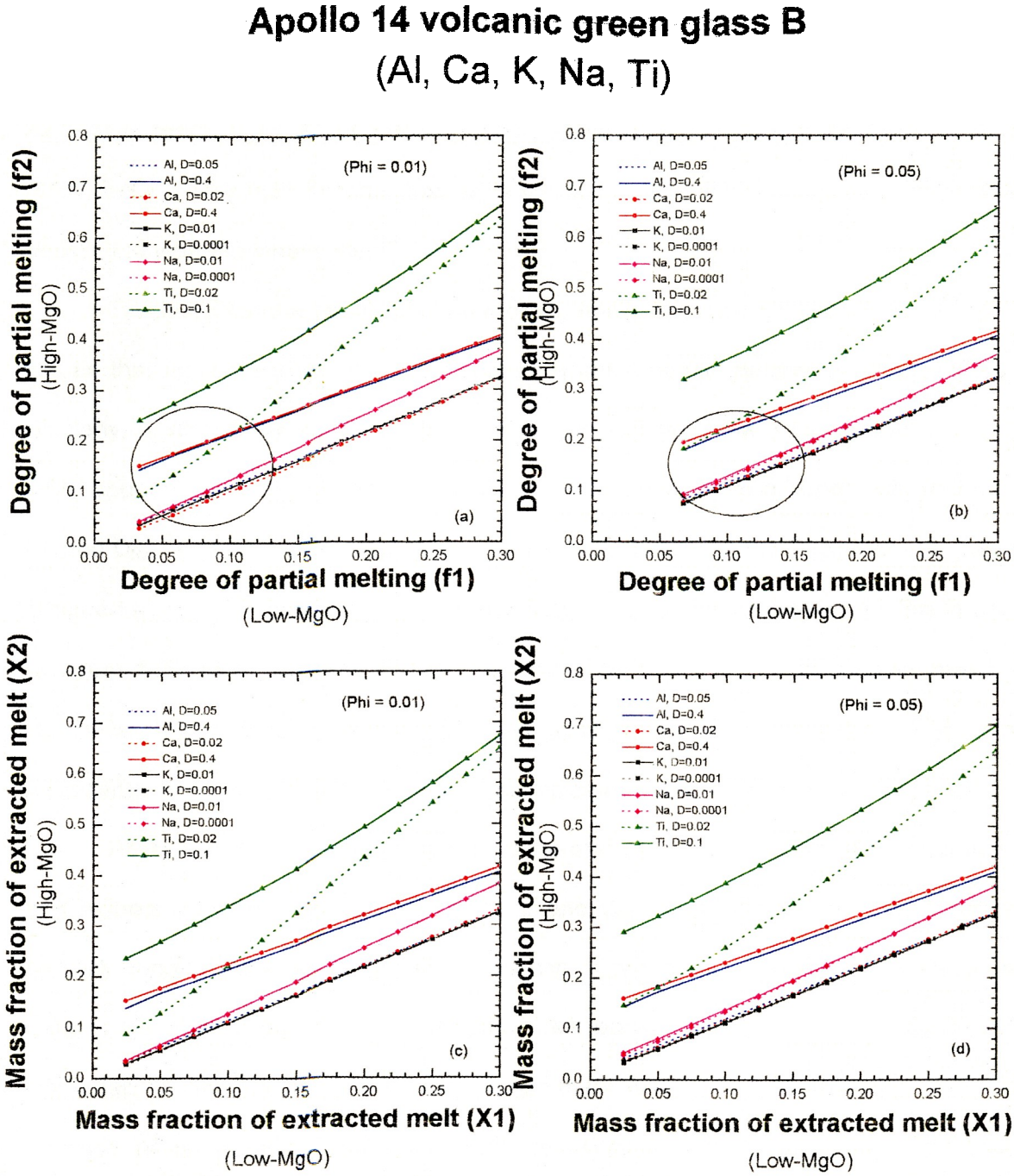

Figure 5.2.2 Apollo 14 volcanic green glass B model results for Degree of partial melting and Mass fraction of extracted melt for Phi = 0.01 and 0.05. The model calculations are based on element content of two cogenetic glasses of A14-B.

model results for A14-A and A14-B with the different ϕ and D ranges used for each element (Figure 5.2.2) are similar (Appendix C and D for details). The model values for X2 and f2 are usually larger when ϕ = 0.05 than when ϕ = 0.01 (Figures 5.2.2 a,b, respectively). This may indicate that at larger DPM (and MFEM) there is a greater dependency on the ϕ parameter.

Ti results are the least conclusive of all, however it can be speculated that D_{Ti} values that most likely satisfy the polybaric, dynamic partial melting event are <0.02. Similarly, Al also shows to be sensitive to D. Nonetheless, lower D_{Al} values, such as 0.05, appears to be a good estimate for a plausible value to be grouped with those of D_K and D_{Na}. A tentative range of values to plausibly constraint the DPM that may have occurred along the mantle diapir is 10±2 (Low-MgO) to 24±2% (High-MgO). The f1 and f2 values for A14-A are slightly higher than those for A14-B. This dissimilarity may be indicative of the difference between the two glass groups on the extent of DPM each represents, and perhaps this difference also indicates some relative chronology.

Potassium and sodium appear to be the elements better constraining the lowest and highest degrees of partial melting. D_K and D_{Na} values used, and the range of porosity considered suggest that K and Na can participate in the melt production at a wide range of both parameters. However, their participation in the melt extracted is dissimilar. K and Na removal occurs preferentially when ϕ = 0.05 (possibly showing increase of temperature). This behavior for K and Na may be a result of their incompatible character and their preference to remain in the liquid. In the case of Ca, the range of D_{Ca} values used in DPM modeling has targeted the "shared region" constrained by K and Na. This is specially for A14-A. For the A14-B results, this observation cannot be totally applied. The D_{Ca} value(s) that most likely will satisfy the DPM will be those in the range of 0.02 - 0.2. These observations are consistent for

both porosity values used. The DPM results for Al show that the D_{Al} values most suitable for either glass-group and both porosities are within the range 0.05 - 0.2.

Comparing the lowest and highest values for the DPM with those for MFEM (Figures 5.2.1 c,d and 5.2.2 c,d), one can observe that there are larger differences when $\phi = 0.05$ than when $\phi = 0.01$. In other words, the difference between melt formed and melt removed from the source is greater when $\phi = 0.05$ than when $\phi = 0.01$. This difference may be a direct consequence of the need this model for melt extraction to occur, it is necessary for melt production to exceed porosity (ϕ).

The most intriguing observation one can make concerning Figures 5.2.1 a,c is that at high degrees of partial melting (f2), those results obtained for $\phi = 0.01$ are higher than those obtained for $\phi = 0.05$ (an inversion, Appendix C and D). The cross-over can be observed for K, Na, and Ti, the three elements that show the largest enrichments (Table 4.3.1 and 4.3.2). The elements Ca and Al maintain the parallel trend of both ϕ values throughout the plot - the cross-over is not observed. These two elements also are the least enriched of those used in the model (Table 4.3.1) for both green glass types considered here. The cross-over observed for the elements showing the largest enrichments (K, Na, Ti) may show some dependency on porosity by the element to participate in the melt and greater DPM.

As suggested earlier, the A14-A and A14-B groups are originated via a similar process, and those glasses belonging to group B are believed to be more primitive than those of group A (higher MgO and lower TiO_2, Appendix A). The A14-A have a smaller Ca-enrichment = 8.36% than A14-B Ca-enrichment = 13.02%. Also, comparing the mass fraction of melt extracted for the two melt types, it can be observed that in the

"shared region", the X2 values for the elements Al and Ti are higher for A14-A than the X2 values for A14-B. This further indicates that the extent of melting during the A14-A melts formation was higher than that for A14-B melts. A14-A melts show a higher enrichment than A14-B for K, Na and Ti (Tables 4.3.1 and 4.3.2). This may have resulted from either (1) the difference in the extent of DPM between the event that originated A-melts and that that originated B-melts or/and (2) the composition of the source. The DPM difference inferred may be due to either (a) two different magmatic events within the same diapir that originated these glasses and/or (b) the melts for A14-A and A14-B were formed during the same magmatic event, however they represent different areas of the same mantle diapir. In the case of (a) the chemical composition of the source was modified from the first to the second event. In case (b), the two melt groups show the effects along a mantle diapir as the DPM increases from the periphery to the center of the diapir (possibly as the result of an increase in temperature from the periphery to the center of the diapir).

Lastly, above the region defined by Na and K, there is a region common to D_{Ti} = 0.02, D_{Ca} = 0.4 and D_{Al} = 0.4 for both porosities modeled. Can this second "shared region" represent a change of residuum phase or perhaps a change in pressure? It has been experimentally demonstrated by Delano (1980) and Chen et al. (1982) that D_{ti} = 0.1 and D_{Al} = 0.4 are close to those determined experimentally by for residual pyroxene and melt at pressure ≤25 kbars (≤ 500 km). For a residuum consisting not only of low-Ca pyroxene, but also of olivine (the assumed composition of the mantle source for the dynamic model), Delano (1986) suggested that the D for Ti and Al during melt would be <0.15 and <0.4, respectively.

5.3 Questions

1. What does the inability to constrain Ti mean in relation to the preferential distribution coefficients and the influence of porosity upon it? The Ti results for DPM show that this element has the highest sensitivity to the parameters used in the model (e.g., D). Although a wide range of D values were used, none of the results obtained could reproduce values that coexisted with those of Na and K. Ti appears to be behaving as an incompatible element despite the wide range of concentrations observed on the lunar volcanic glasses (Table 1.1.1).
2. What interpretations are suggested by the differences in D_{Ca} values between A14-A and A14-B regarding ϕ and D preferences resulting from the application of the model?

(a) Are these differences a result of the chemical evolution of the mantle diapir?

(b) Are the differences a result of the source initial composition and phases that may have been present (olivine $\pm$ low-Ca pyroxene $\pm$ ilmenite)?

3. How is it possible to have individual, microscopic magmas (the glass spherules) occupying one definite chemical composition in some graphs and part of a cluster of glasses in other? Are they the result of the amount of melt produced at each melting-parcel? In Figure 4.2.2 b, MgO vs. TiO_2 (wt%), are plotted both glass groups. For each group, at lower TiO_2 and high MgO levels, the individual glasses form clusters. As the TiO_2 increases and MgO decreases there is a decrease in the number of glasses, clustering is reduced, and actually glasses can be observed as individual melts. Does this change in the number of glasses as well as chemical composition mirrors the gradational DPM along the mantle diapir (Figure 5.1.1); i.e.

the clustering of glasses with higher MgO and lower TiO_2 formed closer to the center of the mantle diapir (high DPM), and those individual glasses with lower MgO and higher TiO_2 represent melts formed at lower DPM, near or at the periphery of the mantle diapir. A similar plot can be seen in Figure 4.3.2 a (K_2O vs. MgO).

4. How is it possible for the melts to travel from the source region to the lunar surface and not react with wall-rock, and only represent chemical variations within the mantle source diapir? As shown in Figures 4.5.1 and 4.5.2 in the case of the high enrichment of the incompatible elements
5. Every petrogenetic parameter in the magma source appears to be heterogeneous: phi, D, T, P and composition. Were the volcanic eruptions the result of a magma source needing to reestablish, both chemical and physical order? This question develops from the idea of "relative chronographies" of melts derived from the same mantle diapir, however during two different events. The time between events would have been characterized by a dynamic re-establishment of both chemical and physical equilibrium.
6. Does the melt separation point from the mantle source cause a secondary episode of melting similar to that of the main diapir? This secondary partial melting event would occur after the first main one, but before the actual separation of the melt from the source. Figure 5.3.1 shows a schematic representation of this concept.

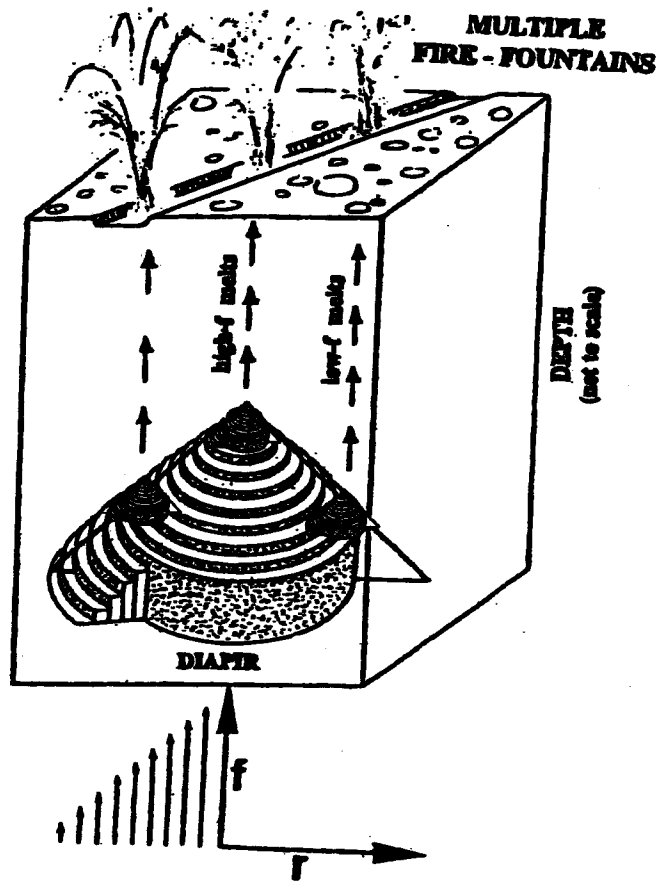

Figure 5.3.1 Modified (Figure 5.1.1) to emphasize the "stress" that may occur at the exiting of the melt from its source at the diapir surface (mini-diapirs are suggestive of final "stress" undergone by the green melts).

CHAPTER VI – Summary

The main observations and conclusions of this analytical and modeling study of the Apollo 14 volcanic green glasses A and B are as follows:

1. Apollo 14 volcanic green glasses A and B were found in the same impact breccias, however, they reveal different chemical compositions. These differences may have resulted from deep-seated processes in the lunar mantle within the same diapir during different magmatic events - not coeval.
2. The chemical trends shown by Apollo 14 volcanic green glasses have been suggested to have originated due to olivine/liquid fractionation and/or mixing of the source magma with a KREEP-like component which explains the large enrichments of incompatible elements. In Chapter IV, it was demonstrated that neither of these processes was the cause for the chemical trends shown.
3. As the mantle diapir rises through the mantle, it may pass through areas with varying chemical compositions. Therefore, the chemical evolution of the mantle diapir may be due to two factors: (1) degree of partial melting and (2) inherited heterogeneities within the mantle source.
4. The dynamic partial melting model results for the degree of partial melting are within those ranges expected (5-25%) for more conventional melting processes (e.g. batch melting).
5. The intragroup chemical variation from *enriched* to *depleted* glasses possibly resulted as follows: the lower-MgO, high-Na, -K and -Ti from *enriched* areas of the source regions (periphery of the diapir), and the higher-MgO, low-Na, -K and -Ti

melts were formed in *depleted* areas of the source region (center of the diapir) (Delano, 1996a).

6. The high contents of MgO and the large enrichment observed for some elements (Na, K and Ti) may have resulted from melts produced at high pressure and by low degrees of partial melting (O'Hara, 1985).
7. Ti appears to be the element that least constrains the dynamic partial melting model. Conversely, K and Na appear to be the best constraining elements since their participation into the melt with varying D does not seem to be sensitive to porosity or DPM. The results all appear to indicate similar DPM from 10±2 to 24±2%.
8. Porosity (ϕ) appears to be an important factor for Ca and Ti partitioning into the melt.

Bibliography

Carlson, I.C., Walton Jr., W.J.A. and Northrop Services, Inc. (1978): Apollo 14 Rock Samples. JSC-14240, NASA, Houston, 413 pp.

Chao, E.C.T., James, O.B., Minkin, J.A. and Boreman, J.A. (1970): Petrology of unshocked crystalline rocks and evidence of impact metamorphism in Apollo 11 returned lunar sample. Proc. Lunar and Plan. Sc. Conf., 1st, Geoch. et Cosmoch. Acta, vol. 1, supp., pp. 287-314.

Chao, E.C.T., Best, J.B. and Minkin, J.A. (1972): Apollo 14 glasses of impact origin and their parent rock types. Proc. Lunar and Plan. Sc. Conf., 3rd, Geoch. et Cosmoch. Acta, vol. 1, supp., pp. 907-925.

Chapman, P.K., Calio, A.J. and Simmons, M.G. (1971): Summary of Scientific Results. In Apollo 14: Preliminary Science Report, NASA SP-272, NASA, Washington, 309 pp.

Chen, H.K., Delano, J.W. and Lindsley, D.H. (1982): Chemistry and Phase relations of VLT Volcanic Glasses from Apollo 14 and Apllo 17. Proc. Lunar and Plan. Sc. Conf., 13th, Part I, J. Geoph. Res., supp., vol. 87, pp. A171-A181.

Coombs, C.R. (1990): Lunar explosive volcanism: The remote sensing perspective. In: Workshop on lunar volcanic glasses and resource potential, pp. 22-23. LPI Tech. Rep. 90-02.

Coombs, C.R. and McKay, D.S. (1991): The violent side of mare volcanism. In: Workshop on Mare Volcanism and Basalt Petrogenesis: "Astounding Fundamental Concepts (AFC)" Developed Over the Last Fifteen Years, pp. 9-10. LPI Tech. Rep. 91-03.

Delano, J.W. (1979): Apollo 15 green glass: Chemistry and possible orign. Proc. Lunar and Plan. Sc. Conf., 10th, pp. 275-300.

Delano, J.W. (1980): Chemistry and liquidus phase relations of Apollo 15 red glass: Implications for the deep lunar interior. Proc. Lunar and Plan. Sc. Conf., 11th, pp. 251-288.

Delano, J.W. (1981): Major-element composition of volcanic green glasses from Apollo 14 (abstract). In Lunar and Planetary Science XII, pp. 217-219. Lunar and Planetary Science Institute, Houston.

Delano, J.W. (1986): Pristine Lunar Glasses: Criteria, Data, and Implications. Proc. Lunar and Plan. Sc. Conf., 16th, Part 2 J. Geoph. Res, vol. 91, B4, pp. D201-D213.

Delano, J.W. (1988): Apollo 14 Regolith Breccias: Different Glass Populations and Their Potential for Charting Space/Time Variations. In Lunar and Planetary Science XVIII, pp. 59-65. Lunar and Planetary Science Institute, Houston.

Delano, J.W. (1990a): Buoyancy-driven Melt Segregation in the Earth's Moon, I. Numerical Results. Proc. Lunar and Plan. Sc. Conf., 20th, pp. 3-12.

Delano, J.W. (1990b): Pristine lunar glasses: A "window" into the Moon's mantle. In: Workshop on Lunar volcanic glasses: Scientific and resource potential. LPI Technical Report 90-02, pp. 28-29.

Delano, J.W. (1996a): Apollo14 green volcanic glasses with a compositional memory of melting processes in the lunar mantle. Proc. Lunar and Plan. Sc. Conf., 27th, pp. 301-302.

Delano, J.W. (1996b): Compositional range of primary magmas observed among the Apollo 17 orange volcanic glasses. Proc. Lunar and Plan. Sc. Conf., 27th, pp. 303-304.

Delano, J.W. and Livi, K. (1981): Lunar volcanic glasses and their constraints on mare petrogenesis. Geoch. et Cosmoch. Acta, vol. 45, pp. 2137-2149.

Delano, J.W. and Fernandes, V.A. (1998): Deep-seated magmatic processes reflected by compositional trends within Apollo 14 green glasses. Proc. Lunar and Plan. Sc. Conf. 29th, Abstract #1177.

Delano, J.W., Taylor, S.R. and Ringwood, A.E. (1980): Composition and Structure of the Deep Lunar Interior. Proc. Lunar and Planet. Sc. Conf. XI, pp. 225-227.

Delano, J.W., Hughes, S.S. and Schmitt, R.A. (1989): Apollo 14 Pristine Mare Glasses. In Workshop on Moon in transition: Apollo 14, KREEP, and Evolved Lunar Rocks, eds. Taylor, G.H. and Warren, P.H., pp.34-37. Lunar and Planetary Institute, Houston.

Eggins, S.M. (1992): Petrogenesis of Hawaiian tholeiites: 2, aspects of dynamic melt segregation. Contrib. Mineral. Petrol., vol. 110, pp. 398-410.

Glass, B.P., Storzer, D. and Wagner, G.A. (1972): Chemistry and particle rock track studies of Apollo 14 glasses. Proc. Lunar and Plan. Sc. Conf., 3rd, Geoch. et Cosmoch. Acta, vol. 1, supp., pp. 927-937.

Goins, N.R., Toksöz, M.N. and Dainty, A.M. (1978): Seismic structure of the lunar mantle: an overview. Proc. Lunar and Plan. Sc. Conf., 27th, pp. 301-302.

Gurenko, A.A. and Chaussidon, M. (1995): Enriched and depleted primitive melts included in olivine from Icelandic tholeiites: Origin by continuous melting of a single mantle column. Geoch. et Cosmoch. Acta, vol. 59, 14, pp. 2905-2917.

Hanson, B., Delano, J.W. and Lindstrom, D.J. (1996): High-precision analysis of hydrous rhyolitic glass inclusions in quartz phenocrysts using the electron microprobe and INAA. Am. Min., vol. 81, pp. 1249-1262.

Hawke, B.R. (1989): Geologic and bombardment history of the Apollo 14 region. In Workshop on Moon in transition: Apollo 14, KREEP, and Evolved Lunar Rocks, eds. Taylor, G.H. and Warren, P.H., pp.38-45. Lunar and Planetary Institute, Houston.

Head, J.W. (1974): Lunar dark-mantle deposits: possible clues to the distribution of early mare deposits. Proc. Lunar and Plan. Sc. Conf., 5th, Geoch. et Cosmoch. Acta, vol. 1, supp., pp. 207-222.

Heiken, G.H., McKay, D.S. and Brown, R.W. (1974): Lunar deposits of possible pyroclastic origin. Geoch. et Cosmoch. Acta, vol. 38, pp. 1703-1718.

Hess, P.C. (1989a): Origin of Igneous Rocks. Harvard University Press, 336 pp.

Hess, P.C. (1989b): Highly evolved liquids from the fractionation of mare and nonmare basalts. In LPI Technical Report 89-03, pp. 46-52: Workshop on Moon in transition: Apollo 14, KREEP, and evolved lunar rocks.

Hubbard, N.J. and Minear, J.W. (1975): A chemical and physical model for the genesis of lunar rocks: Part II. Mare basalts. Proc. Lunar and Plan. Sc. Conf., 6th, (abstracts), pp. 405-407.

Hess, P.C., Rutherford, M.J., and Campbell, H.W. (1977): Origin and evolution of LKFM basalt. Proc. Lunar and Plan. Sc. Conf., 8th, pp. 2357-2373.

Hughes, S.S., Delano, J.W. and Schmitt (1990): Chemistires of Individual Mare Volcanic Glasses: Evidence for Distinct Regions of Hybridized Mantle and a KREEP Component in Apollo 14 Magmatic Sources. Proc. Lunar and Plan. Sc. Conf., 20th, pp. 127-138.

Huneke, J.C., Jessberger, E.K., Podosek, F.A. and Wasserburg, G.J. (1974): The age of metamorphism of a highland breccia (65015) and a glimpse at the age of its protolith. Lunar Science V (abstract), pp. 375-377.

Irving, A.J. (1978): A Review of experimental studies of crystal/liquid trace element partitioning. Geoch. et Cosmoch. Acta, vol. 42, pp. 743-770.

Kinzler, R.J. and Grove, T. L. (1992): Primary Magmas of Mid-Ocean Ridge Basalts: 2. Applications. J. Geoph. Res., vol. 97, pp. 6907-6926.

Langmuir, C.H., Bender, J.F., Hanson, G.N. and Taylor, S.R. (1977): Petrogenesis of basalts from the FAMOUS area: Mid-Atlantic Ridge. Earth Planet. Sci. Lett., vol. 36, pp. 133-156.

Longhi, J. (1987): On the connection between mare basalts and picritic volcanic glasses. Proc. Lunar and Plan. Sci. Conf., Supp. J. Geoph. Res., vol. 92, No. B4, pp. E349- E360.

Longhi, J. (1992): Experimental petrology and petrogenesis of mare volcanics. Geoch. et Cosmoch. Acta, vol. 56, pp. 2235-2251.

McGetchin, T.R. and Head, J.W. (1973): Lunar cinder cones. Science, vol. 180, pp. 68-71.

McKay, D.S., Clanton, U.S. and Ladle, G. (1974): Scanning electron microscope study of Apollo 15 green glass. Proc. Lunar and Plan. Sc. Conf., 4th, supp. 4, Geoch. et Cosmoch. Acta, vol. 1, pp. 225-238.

McKenzie, D. (1985a): ^{230}Th-^{238}U disequilibrium and the melting processes beneath ridge axes. Earth and Planet. Sci. Let., vol. 72, pp. 149-157.

McKenzie, D. (1985b): The extraction of magma from the crust and mantle. Earth Plant. Sci. Lett. , vol. 74, pp. 81-91.

Meyer, C., McKay, D.S., Anderson, D.H. and Butler, P. (1975): The source of sublimates on the Apollo 15 green and Apollo 17 orange glass samples. Proc. Lunar and Plan. Sci. Conf., 6th, pp. 1673-1699.

Meyer, C., Williams, I.S. and Compston, W. (1989): Zircon-containing rock fragments within Apollo 14 breccia indicate serial magmatismfrom 4350 to 4000 million years. In Workshop on Moon in transition: Apollo 14, KREEP, and Evolved Lunar Rocks, eds. Taylor, G.H. and Warren, P.H., pp.75-78. Lunar and Planetary Institute, Houston.

O'Hara, M.J. (1985): Importance of the "shape" of the melting regime during partial melting of the mantle. Nature, vol. 314, pp. 58-62.

O'Keefe, J.A. (1980): Comments on "Chemical relationships among irghizites, zhamanshinites, Australian tektites and Henbury impact glass". Geoch. et Cosmoch. Acta, vol. 44, pp. 2151-2152.

Podosek, F.A. and Huneke, J.C. (1973): Argon in Apollo 15 green glass spherules (15426): ^{40}Ar-^{39}Ar age and trapped argon. Earth and Plan. Sc. Let., vol. 19, pp.413-421.

Rhodes, J.M. (1978): Primary mare basalts and green glass. Proc. Lunar and Plan. Sc. Conf. 9th, pp. 958-960.

Ringwood, A.E. and Kesson, S.E. (1976): A dynamic model for mare basalt petrogenesis. Proc. Lunar and Plan. Sc. Conf., 7th, pp. 1697-1722.

Sato, M.(1976): Oxygen fugacity and other thermochemical parameters of Apollo 17 high-Ti basalts and their implications on the reduction mechanism. Proc. Lunar and Plan. Sc. Conf., 7th, pp. 1323-1344.

Shearer, C.K. and Papike, J.J. (1993): Basaltic Magmatism on the Moon: A Perspective from Volcanic Picritic Glasses. Proc. Lunar and Plan. Sc. Conf., 24th, pp. 1285-1286.

Shearer, C.K., Papike, J.J. and Layne, G.D. (1996): Deciphering basaltic magmatism on the Moon from the compositonal variations in the Apollo 15 very low picritic magmas. Geoch. et Cosmoch. Acta, vol. 60, No. 3, pp. 509-528.

Shearer, C.K., Papike, J.J., Simon, S.B., Shimizu, N., Yurimoto, H. and Sueno, S. (1989): An Ion Microprobe study of trace elements in Apollo 14 "Volcanic" glass beads and comparisons to mare basalt. In Workshop on Moon in transition: Apollo 14, KREEP, and evolved lunar rocks (G.J. Taylor and P.H. Warren, eds.), pp. 113-117. LPI Technical Report 89-03.

Spera, F.J. (1989): Lunar Magma Transport Phenomena. In: Workshop on Mare Volcanism and Basalt Petrogenesis: "Astounding Fundamental Concepts (AFC)" Developed Over the Last Fifteen Years. LPI Tech. Rep. 91-03.

Spera, F.J. (1992): Lunar magma transport phenomena. Geoch. et Cosmoch. Acta, vol. 56, pp. 2253-2265.

Stadermann, F.J., Heusser, E., Jessberger, E.K. (1989): Fra Mauro formation, Apollo 14: II. ^{40}Ar-^{39}Ar ages of Apollo 14 rocks. In LPI Technical Report 89-03, pp. 137: Workshop on Moon in transition: Apollo 14, KREEP, and evolved lunar rocks.

Stadermann, F.J., Heusser, E., Jessberger, E.K., Linger, S. and Stöffler, Dieter (1991): The case for a younger Imbrium basin: New 40Ar-39Ar ages of Apollo 14. Geoch. et Cosmoch. Acta, vol. 55, pp. 2339-2349.

Steele, A.M. and Haskin, L.A. (1989): Apollo 15 Green Glass: The Range of Chemical Compositions in Individual Formational Events. Proc. Lunar and Plan. Sc. Conf., 20th, pp. 1050-1051.

Steele, A. M., Colson, R.O., Korotev, R. L. and Haskin, L. A. (1992): Apollo 15 green glass: Compositional distribution and petrogenesis. Geoch. et Cosmoch. Acta, vol. 56, pp. 4075-4090.

Steele, I.M. and Smith, J.V. (1975): Minor elements in lunar olivine as a petrologic indicator. Proc. Lunar and Plan. Sc. Conf. 6th, pp. 451-467.

Stöffler, D. (1989): Brecciated nature of the Apollo 14 lunar sample suite: A review. In: Workshop on Moon in transition: Apollo 14, KREEP, and evolved lunar rocks, LPI Technical Report 89-03, pp. 138-144.

Stolper, E., Walker, D., Longhi, J. and Hays, J.F. (1974): Compositional variation in lunar ultramafic glasses (abst.). In Lunar Science V, pp. 749-751. Lunar Science Institute.

Stone, C.D. and Taylor, L.A. (1982): Ferromagnetic resonance intensity: a rapid method for determining lunar glass bead origin. Proc. Lunar and Plan. Sc. Conf., 13th, Part I, J. Geoph. Res., supp., vol. 87, pp. A182-A196.

Sutton, R.L., Hait, M.H. and Swann, G.A. (1972): Geology of the Apollo 14 landing site. Proc. Lunar and Plan. Sc. Conf., 3rd, Supp. 3, Geoch. et Cosmoch. Acta, vol. 1, 27 - 38.

Sutton, S.R., Jones, K.W., Gordon, B., Rivers, M.L., Bajt, S. and Smith, J.V. (1993): Reduced chromium in olivine grains from lunar basalt 15555: X-ray Absorption Near Edge Structure (XANES). Geoch. et Cosmoch. Acta, vol. 57, pp. 461-468.

Swann, G.A., Bailey, N.G., Batson, R.M., Eggleton, R.E., Hait, M.H., Holt, H.E., Larson, K.B., McEwen, M.C., Mitchell, E.D., Schaber, G.G., Schafer, J.P., Shepard, A.B., Sutton, R.L., Trask, N.J., Ulrich, G.E., Wilshire, H.G. and Wolfe, E.W. (1971): Preliminary Geological Investigations of the Apollo 14 Landing Site. In Apollo 14: Preliminary Science Report, NASA SP-272, NASA, Washington, 309 pp.

Swann, G.A., Bailey, N.G., Batson, R.M., Eggleton, R.E., Hait, M.H., Holt, H.E., Larson, K.B., Reed, V.S., Schaber, G.G., Sutton, R.L., Trask, N.J., Ulrich, G.E. and Wilshire, H.G. (1977): Geology of the Apollo 14 Landing site in the Fra Mauro Highlands. U.S.G.S. Prof. Pap. 880, 103 pp.

Taylor, S.R. (1975): Lunar Science: A Post-Apollo View. Pergamon Press Inc., 361 pp.

Tera, F.and Wasserburg, G.J. (1974): U-Th-Pb systematics on lunar rocks and inferences about lunar evolution and the age of the moon. Proc. Lunar and Plan. Sc. Conf., 5th, supp. 5, Geoch. et Cosmoch. Acta, vol. 2, pp. 1571-1599.

Tera, F. and Wasserburg, G.J. (1976): Lunar ball games and other sports. Proc. Lunar and Plan. Sc. Conf., 7th, pp. 858-860.

Turner, G., Huneke, J.C., Podosek, F.A. and Wasserburg, G.J. (1971): ^{40}Ar-^{39}Ar ages and cosmic ray exposure ages of Apollo 14 samples. Earth and Planet. Sci. Let., vol. 12, pp. 19-35.

Wagner, T.P. and Grove, T.L. (1997): Experimental constraints on the origin of lunar high-Ti ultramafic glasses. Geoch. et Cosmoch. Acta, vol. 61, pp. 1315-1327.

Warren, P.H. and Wasson, J.T. (1979): The Origin of KREEP. Rev. Geophy. and Space Phys, vol. 17, pp. 73-88.

Weitz, C.M., Rutherford, M.J. and Head, J.W. (1997): Oxidation states and ascent history of the Apollo 17 volcanic beads as inferred from metal-glass equilibria. Geoch. et Cosmoch. Acta, vol. 61, pp. 2765-2775.

Weitz, C.M. and Head, J.W. (1998): Diversity of lunar volcanic eruptions at the Marius Hills complex. Proc. Lunar and Plan. Sc. Conf. 29th, Abstract # 1229.

Wilhelms, D.E. (1987): The geologic history of the Moon. U.S.G.S. Prof. Pap. 1348, 302 pp.

Wood, J.A. and Ryder, G. (1977): The Apollo 15 green clods and the green glass enigma. Proc. Lunar and Plan. Sc. Conf. 8th, pp. 1026-1028.

Zou, H., and Zindler, A. (1996): Constraints on the degree of dynamic melting and source composition using concentration ratios in magmas. Geoch. et Cosmoch. Acta, vol. 60, pp. 711-717.

Appendix A

Apollo 14 volcanic green glasses A and B

electron microprobe analyses

Appendix A

Electron microprobe analyses results for Apollo 14 volcanic green glasses group A. All data are in weight percent (wt%). See Chapter V for Minimum Detection Limit and Standard Deviation. Data obtained by J.W. Delano (1996).

Glass ID	SiO_2	TiO_2	Al_2O_3	Cr_2O_3	FeO	MnO	MgO	CaO	Na_2O	K_2O	Sum
14307,45#12	43.84	0.9408	6.74	0.5350	23.15	0.2820	16.12	8.12	0.1664	0.0611	99.96
14307,45#19	43.54	0.9610	6.64	0.5344	23.19	0.2830	16.60	8.01	0.1845	0.0609	100.00
14307,45#21	43.61	1.8469	7.44	0.5184	22.83	0.2800	14.67	8.42	0.2670	0.1137	99.99
14307,45#27	43.55	1.2211	6.97	0.5240	23.02	0.2974	15.90	8.22	0.2099	0.0827	99.99
14307,45#41	43.55	0.9577	6.65	0.5318	23.17	0.2910	16.56	8.07	0.1592	0.0618	100.00
14307,45#47	44.14	0.8876	7.11	0.5359	22.70	0.2800	15.59	8.49	0.2056	0.0639	100.01
14307,45#51	43.91	0.8890	7.16	0.5375	23.08	0.2900	15.41	8.48	0.1703	0.0687	100.00
14307,45#57	43.57	2.4360	7.77	0.4990	22.63	0.2860	13.76	8.59	0.3187	0.1404	100.00
14307,45#48	43.62	0.9533	6.68	0.5288	23.21	0.2820	16.48	8.03	0.1563	0.0653	100.00
14307,45#67	43.73	1.2569	7.02	0.5208	23.00	0.3010	15.67	8.21	0.2176	0.0803	100.00
14307,45#78	43.96	0.8930	6.80	0.5271	23.12	0.3080	15.97	8.18	0.1780	0.0668	100.00
14307,45#90	43.63	0.9260	6.81	0.5201	23.08	0.3090	16.27	8.20	0.1852	0.0679	100.00
14307,48#2	43.60	1.2371	7.04	0.5157	22.93	0.3130	15.84	8.22	0.2242	0.0851	100.00
14307,48#12	43.42	1.6969	7.38	0.5122	22.98	0.3070	14.85	8.38	0.2621	0.1115	99.90
14307,48#21	43.67	0.9085	6.81	0.5361	23.15	0.3110	16.17	8.20	0.1737	0.0680	100.00
14307,48#29	43.60	1.1817	6.95	0.5210	23.06	0.2910	15.95	8.19	0.1850	0.0731	100.00
14307,48#31	43.51	2.0203	7.59	0.5021	22.79	0.2970	14.40	8.49	0.2654	0.1220	99.99
1430748#33	43.60	0.8963	6.89	0.5324	23.21	0.3190	16.08	8.23	0.1849	0.0674	100.01
14307,48#44	43.66	0.9215	6.84	0.5454	23.10	0.3100	16.15	8.20	0.2005	0.0672	99.99
14307,48#49	43.47	1.1775	6.97	0.5237	23.08	0.3230	15.98	8.20	0.1971	0.0789	100.00
14307,48#50	43.56	1.3746	7.12	0.5224	22.95	0.3220	15.56	8.27	0.2238	0.0926	100.00
14307,48#54	43.80	0.8695	7.16	0.5362	23.09	0.3170	15.49	8.49	0.1800	0.0711	100.00

Appendix A (cont.)

Electron microprobe analyses results for Apollo 14 volcanic green glasses group A. All data are in weight percent (wt%). See Chapter V for Minimum Detection Limit and Standard Deviation. Data obtained by J.W. Delano (1996).

Glass ID	SiO_2	TiO_2	Al_2O_3	Cr_2O_3	FeO	MnO	MgO	CaO	Na_2O	K_2O	Sum
14307,48#55	43.55	0.9418	6.83	0.5389	23.05	0.3230	16.32	8.22	0.1640	0.0619	100.00
14307,48#59	43.68	0.9337	6.69	0.5239	23.02	0.3180	16.49	8.09	0.1816	0.0638	99.99
14307,48#60	43.80	0.8657	6.84	0.5297	23.20	0.3090	15.95	8.28	0.1748	0.0607	100.01
14307,48#64	43.61	1.1073	6.88	0.5180	22.98	0.3070	16.17	8.15	0.2007	0.0769	100.00
14307,48#66	43.61	0.9270	6.77	0.5292	23.11	0.3040	16.36	8.15	0.1748	0.0619	100.00
14307,48#73	43.20	1.9712	7.51	0.5139	23.13	0.2940	14.53	8.47	0.2698	0.1111	100.00
14307,48#76	43.55	0.9339	6.72	0.5354	23.18	0.2920	16.47	8.09	0.1733	0.0648	100.00
14307,48#77	43.47	2.0739	7.59	0.5111	22.73	0.3040	14.44	8.48	0.2830	0.1287	100.01
1430748#93	43.47	1.2858	7.05	0.5205	23.04	0.3020	15.75	8.27	0.2279	0.0878	100.00
14307,49#2	43.53	1.2327	7.09	0.5179	22.95	0.3210	15.80	8.26	0.2187	0.0875	100.01
14307,49#32	43.53	2.0241	7.62	0.4968	22.69	0.2980	14.45	8.49	0.2920	0.1154	100.01
14307,49#34	43.64	0.8356	6.88	0.5486	23.35	0.3100	15.80	8.39	0.2026	0.0544	100.01
14307,49#50	43.53	2.1562	7.82	0.5054	22.78	0.3080	13.79	8.68	0.3050	0.1272	100.00
14307,49#63	43.56	1.5238	7.23	0.5151	22.92	0.2960	15.29	8.33	0.2320	0.0944	99.99
14307,49#91	43.59	1.8696	7.55	0.5059	22.72	0.2980	14.62	8.46	0.2837	0.1126	100.01

Appendix A (cont.)

Electron microprobe analyses results for Apollo 14 volcanic green glasses group B. All data are in weight percent (wt%). See Chapter V for Minimum Detection Limit and Standard Deviation. Data obtained by J.W. Delano and V.A. Fernandes (1998).

Glass ID	SiO_2	TiO_2	Al_2O_3	Cr_2O_3	FeO	MnO	MgO	CaO	Na_2O	K_2O	Total
14307,45 #18	45.09	0.4497	7.26	0.4936	19.05	0.2611	18.94	8.26	0.1544	0.0335	100.00
14307,45 #40	45.41	0.7082	7.55	0.4965	19.18	0.2676	17.47	8.70	0.1792	0.0443	100.00
14307,45 #45	46.11	0.7726	8.46	0.4538	18.75	0.2589	15.67	9.17	0.2576	0.0916	100.00
14307,48 #20	45.60	0.7360	8.43	0.4478	18.87	0.2557	16.25	9.07	0.2537	0.0837	100.00
14307,48 #32	45.87	0.7982	8.69	0.4523	18.78	0.2496	15.50	9.29	0.2637	0.0960	100.00
14307,48 #52	45.06	0.5339	7.31	0.4967	19.15	0.2622	18.60	8.38	0.1684	0.0390	100.00
14307,48 #71	45.07	0.4159	7.11	0.4914	19.12	0.2631	19.12	8.22	0.1523	0.0395	100.00
14307,48 #75	45.31	0.6923	7.59	0.4964	19.22	0.2682	17.51	8.68	0.1800	0.0438	100.00
14307,49 #9	45.27	0.7076	7.64	0.4908	19.34	0.2559	17.40	8.67	0.1855	0.0411	100.00
14307,49 #38	45.12	0.7246	7.65	0.4968	19.46	0.2669	17.38	8.68	0.1860	0.0367	100.00
14307,49 #42AAA	44.96	0.4152	7.07	0.4931	19.31	0.2593	19.09	8.22	0.1557	0.0351	100.01
14307,49 #43	45.23	0.6044	7.37	0.4895	19.25	0.2624	18.17	8.39	0.1894	0.0377	100.00
14307,49 #48	45.08	0.5882	7.30	0.4866	19.27	0.2514	18.43	8.38	0.1701	0.0351	100.00
14307,49 #49	45.14	0.7329	7.67	0.5040	19.34	0.2668	17.33	8.78	0.2013	0.0426	100.00
14307,49 #56	45.12	0.6662	7.52	0.5013	19.25	0.2643	17.90	8.57	0.1763	0.0419	100.00
14307,49 #59	45.02	0.5163	7.25	0.4935	19.30	0.2632	18.59	8.36	0.1648	0.0368	100.00
14307,49 #77	45.21	0.3947	7.16	0.4849	19.16	0.2597	18.78	8.31	0.1963	0.0476	100.00
14307,49 #80	45.07	0.3842	7.18	0.4905	19.33	0.2524	18.83	8.28	0.1467	0.0410	100.00
14307,49 #88	45.43	0.7139	8.02	0.4491	19.06	0.2487	17.01	8.77	0.2356	0.0634	100.00

Appendix A (cont.)

Electron microprobe analyses results for Apollo 14 volcanic green glasses group B. All data are in weight percent (wt%). See Chapter V for Minimum Detection Limit and Standard Deviation. Data obtained by J.W. Delano and V.A. Fernandes (1998).

Glass ID	SiO_2	TiO_2	Al_2O_3	Cr_2O_3	FeO	MnO	MgO	CaO	Na_2O	K_2O	Total
14307,36 #12	45.63	0.7453	8.43	0.4439	19.02	0.2417	16.17	8.99	0.2459	0.0831	100.00
14307,36 #19	45.20	0.7300	7.64	0.4938	19.32	0.2613	17.37	8.74	0.1948	0.0397	100.00
14307,36 #32	45.39	0.7657	8.29	0.4472	18.95	0.2404	16.68	8.94	0.2254	0.0611	100.00
14307,36 #85	45.13	0.7434	7.72	0.4943	19.49	0.2565	17.02	8.80	0.2924	0.0529	100.00
14307,36 #92	46.22	0.6506	8.17	0.5225	19.30	0.2541	15.46	9.17	0.1838	0.0567	100.00
14307,36 #102	45.14	0.7655	8.09	0.4888	19.33	0.2527	16.85	8.83	0.2097	0.0400	100.00
14313,41 #15	45.22	0.7024	7.42	0.4887	19.35	0.2623	17.64	8.66	0.2082	0.0437	100.00
14313,41 #41	45.22	0.6954	7.84	0.4386	19.20	0.2542	17.29	8.77	0.2305	0.0600	100.00
14313,41 #50	45.34	0.8335	7.87	0.4867	19.53	0.2665	16.29	9.15	0.1874	0.0445	100.00
14313,41 #58	45.20	0.7131	7.49	0.4796	19.38	0.2688	17.54	8.72	0.1754	0.0389	100.00
14313,41 #110	45.26	0.7464	7.57	0.4846	19.48	0.2654	17.16	8.82	0.1786	0.0401	100.00
14313,41 #137	44.87	0.6565	7.30	0.4802	19.21	0.2593	18.65	8.36	0.1787	0.0401	100.00

Appendix B

Apollo 14 volcanic green glasses A and B

dynamic partial melting model equations

Dynamic partial melting model equations

The model shown below was calculated with the aid of the computer software Maple V™.

Parameter G was first calculated by simple input of values already known: ρ_f = 2.882 g/cm^3, ρs = 3.3 g/cm3, ϕ = 0.01 or 0.05 depending on the porosity being tested; and D (distribution coefficient) value desired for the run (see Table 5.1.1 for details).

$$G = \frac{\rho_f.\phi+\rho_s.(1-\phi)}{\rho_f.\phi+\rho_s.(1-\phi).D}$$

To calculate X2 (the High-MgO MFEM), the initial X1 (the Lower-MgO MFEM) was given a reasonable value starting at 0.025, increasing in steps of 0.025 up to 0.30 (a total of twelve value obtained for X2). C_L^1 is the highest TiO_2 or corresponding Al_2O_3, CaO, K_2O or Na_2O, and C_L^2 is the lowest TiO_2 or corresponding Al_2O_3, CaO, K_2O or Na_2O

$$\frac{C_L^1}{C_L^2} = \frac{X2[1-(1-X1)^{G(1-D)+1}]}{X1[1-(1-X2)^{G(1-D)+1}]}$$

To calculate DPM the equations belo were used. As it can be observed, to calculate f1 (the lowest-DPM) was not much difficulty, however the calculation f2 was dependent upon the result from the equation above.

$$f1 = \frac{X1.\rho_s.(1-\phi)}{\rho_f.\phi+\rho_s.(1-\phi)} + \frac{\rho_f.\phi}{\rho_f.\phi+\rho_s.(1-\phi)}$$

and

$$f2 = \frac{X2.\rho_s.(1-\phi)}{\rho_f.\phi+\rho_s.(1-\phi)} + \frac{\rho_f.\phi}{\rho_f.\phi+\rho_s.(1-\phi)}$$

Finally, the source initial composition can be estimated by using the equation below. Because the glasses used for this set of calculations belong to the same group, the source composition must be the same (Appendix C).

$$C_o^{\,1} = \frac{C_L^{\,1}.X1[G(1-D)+1]}{G\left[1-(1-X1)^{G(1-D)+1}\right]}$$

and

$$C_o^{\,2} = \frac{C_L^{\,2}.X2[G(1-D)+1]}{G\left[1-(1-X2)^{G(1-D)+1}\right]}$$

Appendix C

Apollo 14 volcanic green glasses A and B

dynamic melting model results

Appendix C

Appendix C-1 Dynamic melting model results for Apollo 14 green glasses A: TiO_2/TiO_2 = 2.9153 ϕ = 0.01, and D = 0.02.

X1	X2	f1	f2	Co1%	Co2%	G
0.0250	0.1221	0.0335	0.1298	0.1039	0.1039	35.0023
0.0500	0.1741	0.0583	0.1813	0.1469	0.1469	35.0023
0.0750	0.2335	0.0831	0.2402	0.1968	0.1968	35.0023
0.1000	0.2988	0.1079	0.3049	0.2518	0.2518	35.0023
0.1250	0.3677	0.1327	0.3732	0.3099	0.3099	35.0023
0.1500	0.4387	0.1574	0.4436	0.3697	0.3697	35.0023
0.1750	0.5108	0.1822	0.5150	0.4304	0.4304	35.0023
0.2000	0.5833	0.2070	0.5869	0.4916	0.4916	35.0023
0.2250	0.6560	0.2318	0.6590	0.5529	0.5529	35.0023
0.2500	0.7289	0.2566	0.7312	0.6142	0.6142	35.0023
0.2750	0.8017	0.2813	0.8035	0.6757	0.6757	35.0023
0.3000	0.8746	0.3061	0.8757	0.7371	0.7371	35.0023

Appendix C-2 Dynamic melting model results for Apollo 14 green glasses A: TiO_2/TiO_2 = 2.9153 ϕ = 0.01, and D = 0.05.

X1	X2	f1	f2	Co1%	Co2%	G
0.0250	0.2013	0.0335	0.2083	0.1732	0.1732	17.1505
0.0500	0.2460	0.0583	0.2526	0.2088	0.2088	17.1505
0.0750	0.2946	0.0831	0.3008	0.2488	0.2488	17.1505
0.1000	0.3475	0.1079	0.3533	0.2930	0.2930	17.1505
0.1250	0.4046	0.1327	0.4098	0.3409	0.3409	17.1505
0.1500	0.4653	0.1574	0.4700	0.3920	0.3920	17.1505
0.1750	0.5292	0.1822	0.5333	0.4459	0.4459	17.1505
0.2000	0.5956	0.2070	0.5992	0.5018	0.5018	17.1505
0.2250	0.6640	0.2318	0.6670	0.5595	0.5595	17.1505
0.2500	0.7339	0.2566	0.7362	0.6183	0.6183	17.1505
0.2750	0.8048	0.2813	0.8065	0.6802	0.6781	17.1505
0.3000	0.8764	0.3061	0.8775	0.7397	0.7384	17.1505

Appendix C (cont.)

Appendix C-3 Dynamic melting model results for Apollo 14 green glasses A: TiO_2/TiO_2 = 2.9153 ϕ = 0.01, and D = 0.10.

X1	X2	f1	f2	Co1%	Co2%	G
0.0250	0.3387	0.0335	0.3445	0.2914	0.2914	9.2704
0.0500	0.3783	0.0558	0.3838	0.3224	0.3224	9.2704
0.0750	0.4200	0.0831	0.4251	0.3559	0.3559	9.2704
0.1000	0.4641	0.1079	0.4688	0.3920	0.3920	9.2704
0.1250	0.5106	0.1327	0.5149	0.4305	0.4305	9.2704
0.1500	0.5597	0.1574	0.5635	0.4716	0.4716	9.2704
0.1750	0.6114	0.1822	0.6148	0.5150	0.5150	9.2704
0.2000	0.6658	0.2070	0.6687	0.5607	0.5608	9.2704
0.2250	0.7228	0.2318	0.7251	0.6087	0.6087	9.2704
0.2500	0.7820	0.2566	0.7839	0.6586	0.6586	9.2704
0.2750	0.8435	0.2813	0.8449	0.7245	0.7104	9.2704
0.3000	0.9070	0.3061	0.9078	0.7750	0.7683	9.2704

Appendix C-4 Dynamic melting model results for Apollo 14 green glasses A: Al_2O_3 / Al_2O_3 = 1.0961, ϕ = 0.01, and D = 0.05.

X1	X2	f1	f2	Co1%	Co2%	G
0.0250	0.0411	0.0335	0.0495	0.5524	0.5524	17.1505
0.0500	0.0672	0.0583	0.0753	0.6661	0.6661	17.1505
0.0750	0.0934	0.0831	0.1014	0.7937	0.7938	17.1505
0.1000	0.1199	0.1079	0.1276	0.9346	0.9346	17.1505
0.1250	0.1467	0.1327	0.1541	1.0873	1.0874	17.1505
0.1500	0.1736	0.1574	0.1808	1.2504	1.2505	17.1505
0.1750	0.2008	0.1822	0.2077	1.4221	1.4222	17.1505
0.2000	0.2281	0.2070	0.2349	1.6007	1.6007	17.1505
0.2250	0.2557	0.2318	0.2622	1.7845	1.7846	17.1505
0.2500	0.2834	0.2566	0.2897	1.9723	1.9723	17.1505
0.2750	0.3113	0.2813	0.3173	2.1695	2.1629	17.1505
0.3000	0.3393	0.3061	0.3450	2.3594	2.3554	17.1505

Appendix C (cont.)

Appendix C-5 Dynamic melting model results for Apollo 14 green glasses A: Al_2O_3 / Al_2O_3 = 1.0961, ϕ = 0.01, and D = 0.10.

X1	X2	f1	f2	Co1%	Co2%	G
0.0250	0.0551	0.0335	0.0634	0.9294	0.9294	9.2704
0.0500	0.0808	0.0583	0.0889	1.0284	1.0284	9.2704
0.0750	0.1067	0.0831	0.1145	1.1353	1.1354	9.2704
0.1000	0.1326	0.1079	0.1402	1.2503	1.2503	9.2704
0.1250	0.1586	0.1327	0.1660	1.3733	1.3733	9.2704
0.1500	0.1848	0.1574	0.1919	1.5041	1.5042	9.2704
0.1750	0.2110	0.1822	0.2179	1.6427	1.6427	9.2704
0.2000	0.2375	0.2070	0.2441	1.7886	1.7886	9.2704
0.2250	0.2640	0.2318	0.2705	1.9414	1.9415	9.2704
0.2500	0.2907	0.2566	0.2969	2.1007	2.1008	9.2704
0.2750	0.3176	0.2813	0.3235	2.3107	2.2659	9.2704
0.3000	0.3446	0.3061	0.3503	2.4718	2.4364	9.2704

Appendix C-6 Dynamic melting model results for Apollo 14 green glasses A: Al_2O_3 / Al_2O_3 = 1.0961, ϕ = 0.01, and D = 0.15.

X1	X2	f1	f2	Co1%	Co2%	G
0.0250	0.0707	0.0335	0.0788	1.3084	1.3084	6.3519
0.0500	0.0961	0.0583	0.1040	1.3988	1.3988	6.3519
0.0750	0.1215	0.0831	0.1292	1.4946	1.4947	6.3519
0.1000	0.1471	0.1079	0.1545	1.5961	1.5961	6.3519
0.1250	0.1727	0.1327	0.1799	1.7032	1.7032	6.3519
0.1500	0.1984	0.1574	0.2054	1.8161	1.8161	6.3519
0.1750	0.2241	0.1822	0.2309	1.9348	1.9349	6.3519
0.2000	0.2500	0.2070	0.2565	2.0594	0.0206	6.3519
0.2250	0.2759	0.2318	0.2823	2.1898	2.1899	6.3519
0.2500	0.3020	0.2566	0.3081	2.3260	2.3261	6.3519
0.2750	0.3281	0.2813	0.3340	2.5586	2.4679	6.3519
0.3000	0.3544	0.3061	0.3600	2.6922	2.6153	6.3519

Appendix C (cont.)

Appendix C-7 Dynamic melting model results for Apollo 14 green glasses A: Al_2O_3 / Al_2O_3 = 1.0961, ϕ = 0.01, and D = 0.20.

X1	X2	f1	f2	Co1%	Co2%	G
0.0250	0.0880	0.0335	0.0960	1.6880	1.6880	4.8310
0.0500	0.1131	0.0583	0.1208	1.7715	1.7716	4.8310
0.0750	0.1382	0.0831	0.1457	1.8592	1.8592	4.8310
0.1000	0.1634	0.1079	0.1707	1.9510	1.9511	4.8310
0.1250	0.1886	0.1327	0.1957	2.0472	2.0473	4.8310
0.1500	0.2139	0.1574	0.2207	2.1478	2.1479	4.8310
0.1750	0.2392	0.1822	0.2458	2.2530	2.2531	4.8310
0.2000	0.2646	0.2070	0.2710	2.3628	2.3629	4.8310
0.2250	0.2900	0.2318	0.2962	2.4774	2.4775	4.8310
0.2500	0.3156	0.2566	0.3216	2.5967	2.5968	4.8310
0.2750	0.3412	0.2813	0.3469	2.8564	2.7210	4.8310
0.3000	0.3669	0.3061	0.3724	2.9683	2.8501	4.8310

Appendix C-8 Dynamic melting model results for Apollo 14 green glasses A: Al_2O_3 / Al_2O_3 = 1.0961, ϕ = 0.01, and D = 0.40.

X1	X2	f1	f2	Co1%	Co2%	G
0.0250	0.1823	0.0335	0.1894	3.2079	3.2080	2.4676
0.0500	0.2057	0.0583	0.2126	3.2688	3.2689	2.4676
0.0750	0.2290	0.0831	0.2358	3.3315	3.3316	2.4676
0.1000	0.2524	0.1079	0.2590	3.3961	3.3962	2.4676
0.1250	0.2759	0.1327	0.2822	3.4627	3.4628	2.4676
0.1500	0.2993	0.1574	0.3054	3.5313	3.5314	2.4676
0.1750	0.3227	0.1822	0.3287	3.6020	3.6021	2.4676
0.2000	0.3462	0.2070	0.3519	3.6750	3.6751	2.4676
0.2250	0.3697	0.2318	0.3752	3.7502	3.7503	2.4676
0.2500	0.3932	0.2566	0.3985	3.8278	3.8280	2.4676
0.2750	0.4167	0.2813	0.4218	4.2106	3.9081	2.4676
0.3000	0.4402	0.3061	0.4451	4.2632	3.9907	2.4676

Appendix C (cont.)

Appendix C-9 Dynamic melting model results for Apollo 14 green glasses A: CaO / CaO = 1.0238, ϕ = 0.01, and D = 0.02.

X1	X2	f1	f2	Co1%	Co2%	G
0.0250	0.0266	0.0335	0.0351	0.3665	0.3665	35.0023
0.0500	0.0519	0.0583	0.0601	0.5179	0.5178	35.0023
0.0750	0.0772	0.0831	0.0853	0.6940	0.6940	35.0023
0.1000	0.1026	0.1079	0.1105	0.8879	0.8879	35.0023
0.1250	0.1281	0.1327	0.1357	1.0928	1.0927	35.0023
0.1500	0.1536	0.1574	0.1610	1.3037	1.3037	35.0023
0.1750	0.1792	0.1822	0.1864	1.5178	1.5178	35.0023
0.2000	0.2048	0.2070	0.2117	1.7334	1.7333	35.0023
0.2250	0.2304	0.2318	0.2371	1.9496	1.9495	35.0023
0.2500	0.2560	0.2566	0.2625	2.1660	2.1659	35.0023
0.2750	0.2815	0.2813	0.2878	2.3826	2.3824	35.0023
0.3000	0.3071	0.3061	0.3132	2.5991	2.5990	35.0023

Appendix C-10 Dynamic melting model results for Apollo 14 green glasses A: CaO / CaO = 1.0238, ϕ = 0.01, and D = 0.05.

X1	X2	f1	f2	Co1%	Co2%	G
0.0250	0.0281	0.0335	0.0366	0.6107	0.6107	17.1505
0.0500	0.0533	0.0583	0.0615	0.7364	0.7363	17.1505
0.0750	0.0785	0.0831	0.0865	0.8775	0.8775	17.1505
0.1000	0.1038	0.1079	0.1116	1.0332	1.0332	17.1505
0.1250	0.1291	0.1327	0.1367	1.2021	1.2020	17.1505
0.1500	0.1544	0.1574	0.1618	1.3824	1.3823	17.1505
0.1750	0.1798	0.1822	0.1870	1.5722	1.5721	17.1505
0.2000	0.2052	0.2070	0.2122	1.7696	1.7695	17.1505
0.2250	0.2307	0.2318	0.2374	1.9728	1.9728	17.1505
0.2500	0.2562	0.2566	0.2627	2.1804	2.1803	17.1505
0.2750	0.2817	0.2813	0.2880	2.3984	2.3910	17.1505
0.3000	0.3072	0.3061	0.3133	2.6084	2.6038	17.1505

Appendix C (cont.)

Appendix C-11 Dynamic melting model results for Apollo 14 green glasses A: CaO / CaO = 1.0238, ϕ = 0.01, and D = 0.10.

X1	X2	f1	f2	Co1%	Co2%	G
0.0250	0.0308	0.0335	0.0392	1.0275	1.0274	9.2704
0.0500	0.0559	0.0583	0.0641	1.1369	1.1369	9.2704
0.0750	0.0810	0.0831	0.0891	1.2551	1.2551	9.2704
0.1000	0.1062	0.1079	0.1140	1.3822	1.3822	9.2704
0.1250	0.1314	0.1327	0.1390	1.5182	1.5181	9.2704
0.1500	0.1566	0.1574	0.1640	1.6629	1.6628	9.2704
0.1750	0.1818	0.1822	0.1890	1.8161	1.8160	9.2704
0.2000	0.2071	0.2070	0.2140	1.9773	1.9773	9.2704
0.2250	0.2324	0.2318	0.2391	2.1463	2.1462	9.2704
0.2500	0.2577	0.2566	0.2641	2.3224	2.3223	9.2704
0.2750	0.2830	0.2813	0.2893	2.5546	2.5049	9.2704
0.3000	0.3083	0.3061	0.3144	2.732699	2.6933	9.2704

Appendix C-12 Dynamic melting model results for Apollo 14 green glasses A: CaO / CaO = 1.0238, ϕ = 0.01, and D = 0.20.

X1	X2	f1	f2	Co1%	Co2%	G
0.0250	0.0372	0.0335	0.0456	1.8661	1.8660	4.8310
0.0500	0.0622	0.0583	0.0704	1.9585	1.9584	4.8310
0.0750	0.0872	0.0831	0.0952	2.0554	2.0553	4.8310
0.1000	0.1122	0.1079	0.1200	2.1569	2.1568	4.8310
0.1250	0.1372	0.1327	0.1448	2.2632	2.2632	4.8310
0.1500	0.1623	0.1574	0.1696	2.3745	2.3744	4.8310
0.1750	0.1873	0.1822	0.1944	2.4908	2.4907	4.8310
0.2000	0.2124	0.2070	0.2193	2.6122	2.6121	4.8310
0.2250	0.2375	0.2318	0.2441	2.7388	2.7387	4.8310
0.2500	0.2626	0.2566	0.2690	2.8708	2.8707	4.8310
0.2750	0.2877	0.2813	0.2939	3.1579	3.0080	4.8310
0.3000	0.3128	0.3061	0.3188	3.2815	3.1506	4.8310

Appendix C (cont.)

Appendix C-13 Dynamic melting model results for Apollo 14 green glasses A: CaO / CaO = 1.0238, ϕ = 0.01, and D = 0.40.

X1	X2	f1	f2	Co1%	Co2%	G
0.0250	0.0562	0.0335	0.0645	3.5464	3.5463	2.4676
0.0500	0.0809	0.0583	0.0889	3.6138	3.6136	2.4676
0.0750	0.1056	0.0831	0.1134	3.6831	3.6829	2.4676
0.1000	0.1303	0.1079	0.1379	3.7545	3.7544	2.4676
0.1250	0.1549	0.1327	0.1623	3.8281	3.8280	2.4676
0.1500	0.1796	0.1574	0.1868	3.9039	3.9038	2.4676
0.1750	0.2043	0.1822	0.2113	3.9821	3.9820	2.4676
0.2000	0.2290	0.2070	0.2357	4.0628	4.0626	2.4676
0.2250	0.2547	0.2318	0.2602	4.1460	4.1458	2.4676
0.2500	0.2784	0.2566	0.2847	4.2318	4.2316	2.4676
0.2750	0.3031	0.2813	0.3092	4.6550	4.3202	2.4676
0.3000	0.3278	0.3061	0.3336	4.7131	4.4116	2.4676

Appendix C-14 Dynamic melting model results for Apollo 14 green glasses A: Na_2O / Na_2O = 1.5731, ϕ = 0.01, and D = 0.0001.

X1	X2	f1	f2	Co1%	Co2%	G
0.0250	0.0413	0.0335	0.0497	0.0085	0.0085	113.0770
0.0500	0.0789	0.0584	0.0869	0.0161	0.0161	113.0770
0.0750	0.1180	0.0831	0.1257	0.0241	0.0241	113.0770
0.1000	0.1573	0.1079	0.1647	0.0321	0.0321	113.0770
0.1250	0.1966	0.1327	0.2037	0.0402	0.0402	113.0770
0.1500	0.2360	0.1574	0.2426	0.0482	0.0482	113.0770
0.1750	0.2753	0.1822	0.2816	0.0563	0.0563	113.0770
0.2000	0.3146	0.2070	0.3206	0.0643	0.0643	113.0770
0.2250	0.3539	0.2318	0.3596	0.0723	0.0723	113.0770
0.2500	0.3933	0.2566	0.3986	0.0804	0.0804	113.0770
0.2750	0.4326	0.2813	0.4376	0.0884	0.0884	113.0770
0.3000	0.4719	0.3061	0.4765	0.0964	0.0964	113.0770

Appendix C (cont.)

Appendix C-15 Dynamic melting model results for Apollo 14 green glasses A: Na_2O / Na_2O = 1.5731, ϕ = 0.01, and D = 0.001.

X1	X2	f1	f2	Co1%	Co2%	G
0.0250	0.0493	0.0335	0.0576	0.0108	0.0108	53.5993
0.0500	0.0831	0.0583	0.0911	0.0171	0.0171	53.5993
0.0750	0.1196	0.0831	0.1273	0.0245	0.0245	53.5993
0.1000	0.1578	0.1079	0.1652	0.0323	0.0323	53.5993
0.1250	0.1968	0.1327	0.2038	0.0402	0.0402	53.5993
0.1500	0.2360	0.1574	0.2427	0.0482	0.0482	53.5993
0.1750	0.2753	0.1822	0.2816	0.0563	0.0563	53.5993
0.2000	0.3146	0.2070	0.3206	0.0643	0.0643	53.5993
0.2250	0.3539	0.2318	0.3596	0.0723	0.0723	53.5993
0.2500	0.3923	0.2566	0.3986	0.0804	0.0804	53.5993
0.2750	0.4326	0.2813	0.4328	0.0884	0.0884	53.5993
0.3000	0.4719	0.3061	0.4765	0.0964	0.0964	53.5993

Appendix C-16 Dynamic melting model results for Apollo 14 green glasses A: Na_2O / Na_2O = 1.5731, ϕ = 0.01, and D = 0.005.

X1	X2	f1	f2	Co1%	Co2%	G
0.0250	0.0450	0.0335	0.0533	0.0095	0.0095	72.9890
0.0500	0.0803	0.0583	0.0884	0.0165	0.0165	72.9890
0.0750	0.1184	0.0831	0.1261	0.0242	0.0242	72.9890
0.1000	0.1574	0.1079	0.1647	0.0322	0.0322	72.9890
0.1250	0.1966	0.1327	0.2037	0.0402	0.0402	72.9890
0.1500	0.2360	0.1574	0.2426	0.0482	0.0482	72.9890
0.1750	0.2753	0.1822	0.2816	0.0563	0.0563	72.9890
0.2000	0.3146	0.2070	0.3206	0.0643	0.0643	72.9890
0.2250	0.3539	0.2318	0.3596	0.0723	0.0723	72.9890
0.2500	0.3933	0.2566	0.3986	0.0804	0.0804	72.9890
0.2750	0.4326	0.2813	0.4376	0.0884	0.0884	72.9890
0.3000	0.4719	0.3061	0.4765	0.0964	0.0964	72.9890

Appendix C (cont.)

Appendix C-17 Dynamic melting model results for Apollo 14 green glasses A: Na_2O / Na_2O = 1.5731, ϕ = 0.01, and D = 0.01.

X1	X2	f1	f2	Co1%	Co2%	G
0.0250	0.0419	0.0335	0.0503	0.0087	0.0087	102.7151
0.0500	0.0790	0.0583	0.0871	0.0162	0.0162	102.7151
0.0750	0.1180	0.0831	0.1257	0.0241	0.0241	102.7151
0.1000	0.1573	0.1079	0.1647	0.0321	0.0322	102.7151
0.1250	0.1966	0.1327	0.2037	0.0402	0.0402	102.7151
0.1500	0.2360	0.1574	0.2426	0.0482	0.0482	102.7151
0.1750	0.2753	0.1822	0.2816	0.0563	0.0563	102.7151
0.2000	0.3146	0.2070	0.3206	0.0643	0.0643	102.7151
0.2250	0.3539	0.2318	0.3596	0.0723	0.0723	102.7151
0.2500	0.3933	0.2566	0.3986	0.0804	0.0804	102.7151
0.2750	0.4326	0.2813	0.4376	0.0884	0.0884	102.7151
0.3000	0.4719	0.3061	0.4765	0.0964	0.0964	102.7151

Appendix C-18 Dynamic melting model results for Apollo 14 green glasses A: K_2O / K_2O = 2.5809, ϕ = 0.01, and D = 0.0001.

X1	X2	f1	f2	Co1%	Co2%	G
0.0250	0.0683	0.0335	0.0765	0.0037	0.0037	113.0770
0.0500	0.1294	0.0583	0.1370	0.0071	0.0071	113.0770
0.0750	0.1936	0.0831	0.2006	0.0106	0.0106	113.0770
0.1000	0.2581	0.1079	0.2646	0.0142	0.0142	113.0770
0.1250	0.3226	0.1327	0.3285	0.0177	0.0177	113.0770
0.1500	0.3871	0.1574	0.3925	0.0212	0.0212	113.0770
0.1750	0.4517	0.1822	0.4565	0.0248	0.0248	113.0770
0.2000	0.5162	0.2070	0.5204	0.0283	0.0283	113.0770
0.2250	0.5807	0.2318	0.5844	0.0319	0.0319	113.0770
0.2500	0.6452	0.2566	0.6483	0.0354	0.0354	113.0770
0.2750	0.7097	0.2813	0.7123	0.0389	0.0389	113.0770
0.3000	0.7743	0.3061	0.7762	0.0425	0.0425	113.0770

Appendix C (cont.)

Appendix C-19 Dynamic melting model results for Apollo 14 green glasses A: K_2O / K_2O = 2.5809, ϕ = 0.01, and D = 0.001.

X1	X2	f1	f2	Co1%	Co2%	G
0.0250	0.0695	0.0335	0.0777	0.0038	0.0038	102.7151
0.0500	0.1297	0.0583	0.1373	0.0071	0.0071	102.7151
0.0750	0.1936	0.0831	0.2007	0.0106	0.0106	102.7151
0.1000	0.2581	0.1079	0.2646	0.0142	0.0142	102.7151
0.1250	0.3226	0.1327	0.3285	0.0177	0.0177	102.7151
0.1500	0.3871	0.1574	0.3925	0.0212	0.0212	102.7151
0.1750	0.4517	0.1822	0.4565	0.0248	0.0248	102.7151
0.2000	0.5162	0.2070	0.5204	0.0283	0.0283	102.7151
0.2250	0.5807	0.2318	0.5844	0.0319	0.0319	102.7151
0.2500	0.6452	0.2566	0.6483	0.0354	0.0354	102.7151
0.2750	0.7097	0.2813	0.7123	0.0389	0.0389	102.7151
0.3000	0.7743	0.3061	0.7762	0.0425	0.0425	102.7151

Appendix C-20 Dynamic melting model results for Apollo 14 green glasses A: K_2O / K_2O = 2.5809, ϕ = 0.01, and D = 0.005.

X1	X2	f1	f2	Co1%	Co2%	G
0.0250	0.0761	0.0335	0.0842	0.0042	0.0042	72.9890
0.0500	0.1321	0.0583	0.1397	0.0072	0.0072	72.9890
0.0750	0.1942	0.0831	0.2012	0.0107	0.0107	72.9890
0.1000	0.2582	0.1079	0.2647	0.0142	0.0142	72.9890
0.1250	0.3226	0.1327	0.3286	0.0177	0.0177	72.9890
0.1500	0.3871	0.1574	0.3925	0.0212	0.0212	72.9890
0.1750	0.4517	0.1822	0.4565	0.0248	0.0248	72.9890
0.2000	0.5162	0.2070	0.5204	0.0283	0.0283	72.9890
0.2250	0.5807	0.2318	0.5844	0.0319	0.0319	72.9890
0.2500	0.6452	0.2566	0.6483	0.0354	0.0354	72.9890
0.2750	0.7097	0.2813	0.7123	0.0389	0.0389	72.9890
0.3000	0.7743	0.3061	0.7762	0.0425	0.0425	72.9890

Appendix C (cont.)

Appendix C-21 Dynamic melting model results for Apollo 14 green glasses A: K_2O / K_2O = 2.5809, ϕ = 0.01, and D = 0.01.

X1	X2	f1	f2	Co1%	Co2%	G
0.0250	0.0859	0.0335	0.0939	0.0047	0.0047	53.5993
0.0500	0.1376	0.0583	0.1451	0.0076	0.0076	53.5993
0.0750	0.1965	0.0831	0.2035	0.0108	0.0108	53.5993
0.1000	0.2590	0.1079	0.2654	0.0142	0.0142	53.5993
0.1250	0.3228	0.1327	0.3288	0.0177	0.0177	53.5993
0.1500	0.3872	0.1574	0.3926	0.0212	0.0212	53.5993
0.1750	0.4517	0.1822	0.4565	0.0248	0.0248	53.5993
0.2000	0.5168	0.2070	0.5204	0.0283	0.0283	53.5993
0.2250	0.5807	0.2318	0.5844	0.0319	0.0319	53.5993
0.2500	0.6452	0.2566	0.6483	0.0354	0.0354	53.5993
0.2750	0.7091	0.2813	0.7123	0.0389	0.0389	53.5993
0.3000	0.7743	0.3061	0.7762	0.0425	0.0425	53.5993

Appendix C-22 Dynamic melting model results for Apollo 14 green glasses A: TiO_2 / TiO_2 = 2.9153, ϕ = 0.05, and D = 0.02.

X1	X2	f1	f2	Co1%	Co2%	G
0.0250	0.2086	0.0678	0.2434	0.1857	0.1857	15.8564
0.0500	0.2528	0.0917	0.2857	0.2222	0.2222	15.8564
0.0750	0.3010	0.1156	0.3317	0.2630	0.2630	15.8564
0.1000	0.3531	0.1396	0.3816	0.3080	0.3080	15.8564
0.1250	0.4093	0.1635	0.4353	0.3568	0.3568	15.8564
0.1500	0.4692	0.1874	0.4925	0.4090	0.4090	15.8564
0.1750	0.5323	0.2113	0.5528	0.4639	0.4639	15.8564
0.2000	0.5980	0.2352	0.6156	0.5212	0.5212	15.8564
0.2250	0.6658	0.2591	0.6805	0.5803	0.5803	15.8564
0.2500	0.7351	0.2830	0.7468	0.6407	0.6407	15.8564
0.2750	0.8057	0.3069	0.8142	0.7048	0.7022	15.8564
0.3000	0.8770	0.3308	0.8824	0.7660	0.7644	15.8564

Appendix C (cont.)

Appendix C-23 Dynamic melting model results for Apollo 14 green glasses A: TiO_2 / TiO_2 = 2.9153, ϕ = 0.05, and D = 0.05.

X1	X2	f1	f2	Co1%	Co2%	G
0.0250	0.2853	0.0678	0.3167	0.2539	0.2539	10.8995
0.0500	0.3265	0.0917	0.3561	0.2874	0.2874	10.8995
0.0750	0.3703	0.1156	0.3980	0.3240	0.3240	10.8995
0.1000	0.4169	0.1396	0.4426	0.3637	0.3637	10.8995
0.1250	0.4666	0.1635	0.4900	0.4064	0.4065	10.8995
0.1500	0.5192	0.1874	0.5403	0.4521	0.4521	10.8995
0.1750	0.5749	0.2113	0.5935	0.5004	0.5004	10.8995
0.2000	0.6333	0.2352	0.6494	0.5513	0.5513	10.8995
0.2250	0.6944	0.2591	0.7078	0.6044	0.6044	10.8995
0.2500	0.7577	0.2830	0.7684	0.6596	0.6596	10.8995
0.2750	0.8231	0.3069	0.8308	0.7255	0.7165	10.8995
0.3000	0.8901	0.3308	0.8949	0.7816	0.7748	10.8995

Appendix C-24 Dynamic melting model results for Apollo 14 green glasses A: TiO_2 / TiO_2 = 2.9153, ϕ = 0.05, and D = 0.10.

X1	X2	f1	f2	Co1%	Co2%	G
0.0250	0.4163	0.0678	0.4420	0.3683	0.3683	7.1659
0.0500	0.4539	0.0917	0.4779	0.3987	0.3987	7.1659
0.0750	0.4932	0.1156	0.5155	0.4311	0.4311	7.1659
0.1000	0.5343	0.1396	0.5547	0.4657	0.4657	7.1659
0.1250	0.5773	0.1635	0.5959	0.5023	0.5023	7.1659
0.1500	0.6225	0.1874	0.6391	0.5411	0.5411	7.1659
0.1750	0.6699	0.2113	0.6844	0.5820	0.5820	7.1659
0.2000	0.7195	0.2352	0.7318	0.6250	0.6251	7.1659
0.2250	0.7715	0.2591	0.7815	0.6701	0.6701	7.1659
0.2500	0.8257	0.2830	0.8333	0.7172	0.7172	7.1659
0.2750	0.8821	0.3069	0.8873	0.7889	0.7662	7.1659
0.3000	0.9406	0.3308	0.9432	0.8359	0.8170	7.1659

Appendix C (cont.)

Appendix C-25 Dynamic melting model results for Apollo 14 green glasses A: Al_2O_3 / Al_2O_3 = 1.1294, ϕ = 0.05, and D = 0.05.

X1	X2	f1	f2	Co1%	Co2%	G
0.0250	0.0495	0.0678	0.0913	0.8100	0.8100	10.8995
0.0500	0.0754	0.0917	0.1160	0.9168	0.9168	10.8995
0.0750	0.1014	0.1156	0.1408	1.0335	1.0336	10.8995
0.1000	0.1275	0.1396	0.1658	1.1602	1.1602	10.8995
0.1250	0.1537	0.1635	0.1909	1.2964	1.2965	10.8995
0.1500	0.1801	0.1874	0.2161	1.4419	1.4420	10.8995
0.1750	0.2066	0.2113	0.2415	1.5962	1.5962	10.8995
0.2000	0.2333	0.2352	0.2670	1.7584	1.7585	10.8995
0.2250	0.2602	0.2591	0.2927	1.9279	1.9280	10.8995
0.2500	0.2873	0.2830	0.3186	2.1038	2.1039	10.8995
0.2750	0.3145	0.3069	0.3446	2.3142	2.2853	10.8995
0.3000	0.3418	0.3308	0.3708	2.4930	2.4715	10.8995

Appendix C-26 Dynamic melting model results for Apollo 14 green glasses A: Al_2O_3 / Al_2O_3 = 1.1294, ϕ = 0.05, and D = 0.10.

X1	X2	f1	f2	Co1%	Co2%	G
0.0250	0.0635	0.0678	0.1047	1.1748	1.1749	7.1659
0.0500	0.0891	0.0917	0.1291	1.2717	1.2718	7.1659
0.0750	0.1147	0.1156	0.1536	1.3752	1.3752	7.1659
0.1000	0.1404	0.1396	0.1782	1.4853	1.4854	7.1659
0.1250	0.1662	0.1635	0.2028	1.6022	1.6023	7.1659
0.1500	0.1920	0.1874	0.2275	1.7259	1.7260	7.1659
0.1750	0.2180	0.2113	0.2524	1.8564	1.8565	7.1659
0.2000	0.2441	0.2352	0.2773	1.9937	1.9938	7.1659
0.2250	0.2703	0.2591	0.3024	2.1349	2.1376	7.1659
0.2500	0.2966	0.2830	0.3275	2.2877	2.2877	7.1659
0.2750	0.3230	0.3069	0.3528	2.5164	2.4440	7.1659
0.3000	0.3496	0.3308	0.3782	2.6661	2.6061	7.1659

Appendix C (cont.)

Appendix C-27 Dynamic melting model results for Apollo 14 green glasses A: Al_2O_3 / Al_2O_3 = 1.1294, ϕ = 0.05, and D = 0.15.

X1	X2	f1	f2	Co1%	Co2%	G
0.0250	0.0790	0.0678	0.1195	1.5406	1.5406	5.3375
0.0500	0.1042	0.0917	0.1436	1.6301	1.6301	5.3375
0.0750	0.1295	0.1156	0.1678	1.7244	1.7244	5.3375
0.1000	0.1549	0.1396	0.1920	1.8236	1.8237	5.3375
0.1250	0.1803	0.1635	0.2163	1.9280	1.9281	5.3375
0.1500	0.2058	0.1874	0.2407	2.0376	2.0376	5.3375
0.1750	0.2313	0.2113	0.2651	2.1524	2.1525	5.3375
0.2000	0.2569	0.2352	0.2896	2.2727	2.2728	5.3375
0.2250	0.2826	0.2591	0.3142	2.3983	2.3984	5.3375
0.2500	0.3084	0.2830	0.3388	2.5294	2.5295	5.3375
0.2750	0.3343	0.3069	0.3635	2.7823	2.6660	5.3375
0.3000	0.3602	0.3308	0.3884	2.9082	2.8078	5.3375

Appendix C-28 Dynamic melting model results for Apollo 14 green glasses A: Al_2O_3 / Al_2O_3 = 1.1294, ϕ = 0.05, and D = 0.20.

X1	X2	f1	f2	Co1%	Co2%	G
0.0250	0.0962	0.0678	0.1359	1.9066	1.9067	4.2525
0.0500	0.1211	0.0917	0.1598	1.9897	1.9889	4.2525
0.0750	0.1461	0.1156	0.1836	2.0766	2.0767	4.2525
0.1000	0.1711	0.1396	0.2075	2.1673	2.1674	4.2525
0.1250	0.1962	0.1635	0.2315	2.2621	2.2622	4.2525
0.1500	0.2213	0.1874	0.2555	2.3610	2.3611	4.2525
0.1750	0.2464	0.2113	0.2795	2.4641	2.4642	4.2525
0.2000	0.2716	0.2352	0.3036	2.5716	2.5717	4.2525
0.2250	0.2969	0.2591	0.3278	2.6835	2.6836	4.2525
0.2500	0.3222	0.2830	0.3520	2.8000	2.8001	4.2525
0.2750	0.3476	0.3069	0.3762	3.0800	2.9211	4.2525
0.3000	0.3730	0.3308	0.4006	3.1866	3.0469	4.2525

Appendix C (cont.)

Appendix C-29 Dynamic melting model results for Apollo 14 green glasses A: Al_2O_3 / Al_2O_3 = 1.1294, ϕ = 0.05, and D = 0.40.

X1	X2	f1	f2	Co1%	Co2%	G
0.0250	0.1899	0.0678	0.2255	3.3720	3.3721	2.3454
0.0500	0.2132	0.0917	0.2478	3.4328	3.4329	2.3454
0.0750	0.2364	0.1156	0.2700	3.4954	3.4956	2.3454
0.1000	0.2597	0.1396	0.2922	3.5599	3.5600	2.3454
0.1250	0.2830	0.1635	0.3145	3.6263	3.6264	2.3454
0.1500	0.3063	0.1874	0.3367	3.6947	3.6948	2.3454
0.1750	0.3296	0.2113	0.3590	3.7652	3.7653	2.3454
0.2000	0.3529	0.2352	0.3813	3.8378	3.8380	2.3454
0.2250	0.3762	0.2591	0.4036	3.9127	3.9128	2.3454
0.2500	0.3995	0.2830	0.4259	3.9899	3.9901	2.3454
0.2750	0.4229	0.3069	0.4482	4.3889	4.0698	2.3454
0.3000	0.4463	0.330761	0.4706	4.4396	4.1520	2.3454

Appendix C-30 Dynamic melting model results for Apollo 14 green glasses A: CaO / CaO = 1.1294, ϕ = 0.05, and D = 0.02.

X1	X2	f1	f2	Co1%	Co2%	G
0.0250	0.0282	0.0678	0.0709	0.6547	0.6547	15.8564
0.0500	0.0534	0.0917	0.0950	0.7834	0.7833	15.8564
0.0750	0.0786	0.1156	0.1191	0.9274	0.9274	15.8564
0.1000	0.1039	0.1396	0.1433	1.0861	1.0861	15.8564
0.1250	0.1292	0.1635	0.1674	1.2582	1.2582	15.8564
0.1500	0.1545	0.1874	0.1917	1.4421	1.4420	15.8564
0.1750	0.1799	0.2113	0.2159	1.6359	1.6358	15.8564
0.2000	0.2053	0.2352	0.2402	1.8379	1.8378	15.8564
0.2250	0.2308	0.2591	0.2646	2.0462	2.0461	15.8564
0.2500	0.2562	0.2830	0.2889	2.2594	2.2593	15.8564
0.2750	0.2817	0.3069	0.3133	2.4853	2.4760	15.8564
0.3000	0.3073	0.3308	0.3377	2.7012	2.6953	15.8564

Appendix C (cont.)

Appendix C-31 Dynamic melting model results for Apollo 14 green glasses A: CaO / CaO = 1.1294, ϕ = 0.05, and D = 0.05.

X1	X2	f1	f2	Co1%	Co2%	G
0.0250	0.0297	0.0678	0.0723	0.8954	0.8954	10.8995
0.0500	0.0548	0.0917	0.0964	1.0136	1.0135	10.8995
0.0750	0.0800	0.1156	0.0800	0.1204	1.1426	10.8995
0.1000	0.1052	0.1396	0.1445	1.2826	1.2826	10.8995
0.1250	0.1304	0.1635	0.1686	1.4332	1.4332	10.8995
0.1500	0.1557	0.187353	0.1928	1.5941	1.5941	10.8995
0.1750	0.1810	0.2113	0.2170	1.7646	1.7646	10.8995
0.2000	0.2063	0.2352	0.2411	1.9440	1.9439	10.8995
0.2250	0.2316	0.2591	0.2654	2.1314	2.1313	10.8995
0.2500	0.2567	0.2830	0.2896	2.3259	2.3258	10.8995
0.2750	0.2824	0.3069	0.3139	2.5584	2.5263	10.8995
0.3000	0.3078	0.330615	0.3382	2.7561	2.7321	10.8995

Appendix C-32 Dynamic melting model results for Apollo 14 green glasses A: CaO / CaO = 1.1294, ϕ = 0.05, and D = 0.10.

X1	X2	f1	f2	Co1%	Co2%	G
0.0250	0.0324	0.0678	0.0749	1.2988	1.2988	7.1659
0.0500	0.0575	0.0917	0.0989	1.4059	1.4059	7.1659
0.0750	0.0826	0.1156	0.1229	1.5203	1.5202	7.1659
0.1000	0.1077	0.1396	0.1469	1.6421	1.6420	7.1659
0.1250	0.1329	0.1635	0.1710	1.7713	1.7712	7.1659
0.1500	0.1580	0.1874	0.1950	1.9081	1.9080	7.1659
0.1750	0.1832	0.2113	0.2191	2.0524	2.0523	7.1659
0.2000	0.2084	0.2352	0.2432	2.2041	2.2040	7.1659
0.2250	0.2336	0.2591	0.2673	2.3631	2.3630	7.1659
0.2500	0.2588	0.2830	0.2914	2.5291	2.5290	7.1659
0.2750	0.2841	0.3069	0.3155	2.7820	2.7018	7.1659
0.3000	0.3093	0.3308	0.3397	2.9475	2.8810	7.1659

Appendix C (cont.)

Appendix C-33 Dynamic melting model results for Apollo 14 green glasses A: CaO / CaO = 1.1294, ϕ = 0.05, and D = 0.20.

X1	X2	f1	f2	Co1%	Co2%	G
0.0250	0.0388	0.0678	0.0810	2.1078	2.1078	4.2525
0.0500	0.0638	0.0917	0.1049	2.1997	2.1996	4.2525
0.0750	0.0888	0.1156	0.1288	2.2957	2.2957	4.2525
0.1000	0.1137	0.1396	0.1527	2.3961	2.3960	4.2525
0.1250	0.1387	0.1635	0.1766	2.5008	2.5007	4.2525
0.1500	0.1638	0.1874	0.2005	2.6101	2.6100	4.2525
0.1750	0.1888	0.2113	0.2244	2.7241	2.7240	4.2525
0.2000	0.2138	0.2352	0.2483	2.8430	2.8429	4.2525
0.2250	0.2388	0.2591	0.2723	2.9667	2.9666	4.2525
0.2500	0.2639	0.2830	0.2962	3.0955	3.0953	4.2525
0.2750	0.2889	0.3069	0.3202	3.4050	3.2292	4.2525
0.3000	0.3140	0.3308	0.3442	3.5229	3.3682	4.2525

Appendix C-34 Dynamic melting model results for Apollo 14 green glasses A: CaO / CaO = 1.1294, ϕ = 0.05, and D = 0.40.

X1	X2	f1	f2	Co1%	Co2%	G
0.0250	0.0578	0.0678	0.0992	3.7278	3.7277	2.3454
0.0500	0.0825	0.0917	0.1228	3.7951	3.7950	2.3454
0.0750	0.1071	0.1156	0.1464	3.8643	3.8642	2.3454
0.1000	0.1318	0.1396	0.1699	3.9356	3.9354	2.3454
0.1250	0.1564	0.1635	0.1935	4.0090	4.0088	2.3454
0.1500	0.1811	0.1874	0.2171	4.0846	4.0845	2.3454
0.1750	0.2057	0.2113	0.2406	4.1625	4.1624	2.3454
0.2000	0.2304	0.2352	0.2642	4.2428	4.2427	2.3454
0.2250	0.2550	0.2591	0.2878	4.3256	4.3255	2.3454
0.2500	0.2797	0.2830	0.3114	4.4110	4.4109	2.3454
0.2750	0.3044	0.3069	0.3349	4.8521	4.4989	2.3454
0.3000	0.3290	0.3308	0.3585	4.9081	4.5898	2.3454

Appendix C (cont.)

Appendix C-35 Dynamic melting model results for Apollo 14 green glasses A: Na_2O / Na_2O = 1.5731, ϕ = 0.05, and D = 0.0001.

X1	X2	f1	f2	Co1%	Co2%	G
0.0250	0.0725	0.0678	0.1133	0.0184	0.0184	22.7063
0.0500	0.1034	0.0917	0.1428	0.0236	0.0236	22.7063
0.0750	0.1356	0.1156	0.1736	0.0296	0.0296	22.7063
0.1000	0.1693	0.1396	0.2058	0.0363	0.0363	22.7063
0.1250	0.2044	0.1635	0.2394	0.0434	0.0434	22.7063
0.1500	0.2407	0.1874	0.2741	0.0510	0.0510	22.7063
0.1750	0.2781	0.2113	0.3098	0.0588	0.0588	22.7063
0.2000	0.3162	0.2352	0.3462	0.0669	0.0669	22.7063
0.2250	0.3548	0.2591	0.3831	0.0750	0.0750	22.7063
0.2500	0.3937	0.2830	0.4203	0.0833	0.0833	22.7063
0.2750	0.4328	0.3069	0.4577	0.0916	0.0915	22.7063
0.3000	0.4720	0.3308	0.4952	0.0999	0.0998	22.7063

Appendix C-36 Dynamic melting model results for Apollo 14 green glasses A: Na_2O / Na_2O = 1.5731, ϕ = 0.05, and D = 0.001.

X1	X2	f1	f2	Co1%	Co2%	G
0.0250	0.0734	0.0678	0.1141	0.0187	0.0187	22.2712
0.0500	0.1042	0.0917	0.1435	0.0239	0.0239	22.2712
0.0750	0.1363	0.1156	0.1743	0.0298	0.0298	22.2712
0.1000	0.1699	0.1396	0.2064	0.0364	0.0364	22.2712
0.1250	0.2049	0.1635	0.2398	0.0435	0.0435	22.2712
0.1500	0.2411	0.1874	0.2744	0.0511	0.0511	22.2712
0.1750	0.2783	0.2113	0.3100	0.0589	0.0589	22.2712
0.2000	0.3163	0.2352	0.3464	0.0669	0.0669	22.2712
0.2250	0.3549	0.2591	0.3832	0.0751	0.0751	22.2712
0.2500	0.3938	0.2830	0.4204	0.0833	0.0833	22.2712
0.2750	0.4328	0.3069	0.4578	0.0916	0.0915	22.2712
0.3000	0.4720	0.3308	0.4952	0.0999	0.0998	22.2712

Appendix C (cont.)

Appendix C-37 Dynamic melting model results for Apollo 14 green glasses A: Na_2O / Na_2O = 1.5731, ϕ = 0.05, and D = 0.005.

X1	X2	f1	f2	Co1%	Co2%	G
0.0250	0.0771	0.0678	0.1177	0.0199	0.0199	20.5232
0.0500	0.1077	0.0917	0.1469	0.0249	0.0249	20.5232
0.0750	0.1395	0.1156	0.1773	0.0307	0.0307	20.5232
0.1000	0.1727	0.1396	0.2090	0.0372	0.0372	20.5232
0.1250	0.2071	0.1635	0.2420	0.0441	0.0441	20.5232
0.1500	0.2428	0.1874	0.2761	0.0515	0.0515	20.5232
0.1750	0.2796	0.2112	0.3112	0.0592	0.0592	20.5232
0.2000	0.3172	0.2352	0.3472	0.0671	0.0671	20.5232
0.2250	0.3554	0.2591	0.3838	0.0752	0.0752	20.5232
0.2500	0.3941	0.2830	0.4207	0.0833	0.0833	20.5232
0.2750	0.4330	0.3069	0.4580	0.0917	0.0916	20.5232
0.3000	0.4722	0.3308	0.4954	0.0999	0.0998	20.5232

Appendix C-38 Dynamic melting model results for Apollo 14 green glasses A: Na_2O / Na_2O = 1.5731, ϕ = 0.05, and D = 0.01.

X1	X2	f1	f2	Co1%	Co2%	G
0.0250	0.0818	0.0678	0.1222	0.0213	0.0213	18.6897
0.0500	0.1122	0.0917	0.1512	0.0263	0.0263	18.6897
0.0750	0.1437	0.1156	0.1813	0.0319	0.0319	18.6897
0.1000	0.1763	0.1396	0.2125	0.0381	0.0381	18.6897
0.1250	0.2102	0.1635	0.2449	0.0449	0.0449	18.6897
0.1500	0.2453	0.1874	0.2791	0.0521	0.0522	18.6897
0.1750	0.2815	0.2113	0.3130	0.0596	0.0596	18.6897
0.2000	0.3185	0.2352	0.3485	0.0674	0.0674	18.6897
0.2250	0.3564	0.2591	0.3846	0.0753	0.0754	18.6897
0.2500	0.3947	0.2830	0.4213	0.0834	0.0834	18.6897
0.2750	0.4334	0.3069	0.4583	0.0918	0.0916	18.6897
0.3000	0.4724	0.3308	0.4956	0.1000	0.0999	18.6897

Appendix C (cont.)

Appendix C-39 Dynamic melting model results for Apollo 14 green glasses A: K_2O / K_2O = 2.5809, ϕ = 0.05, and D = 0.0001.

X1	X2	f1	f2	Co1%	Co2%	G
0.0250	0.1388	0.0678	0.1767	0.0081	0.0081	22.7063
0.0500	0.1818	0.0917	0.2178	0.0104	0.0104	22.7063
0.0750	0.2293	0.1156	0.2632	0.0130	0.0130	22.7063
0.1000	0.2811	0.1396	0.3127	0.0160	0.0160	22.7063
0.1250	0.3368	0.1635	0.3660	0.0191	0.0191	22.7063
0.1500	0.3955	0.1874	0.4221	0.0225	0.0225	22.7063
0.1750	0.4564	0.2113	0.4803	0.0259	0.0259	22.7063
0.2000	0.5188	0.2352	0.5399	0.0295	0.0295	22.7063
0.2250	0.5821	0.2591	0.6005	0.0331	0.0331	22.7063
0.2500	0.6459	0.2830	0.6615	0.0367	0.0367	22.7063
0.2750	0.7101	0.3069	0.7228	0.0404	0.0403	22.7063
0.3000	0.7744	0.3308	0.7843	0.0440	0.0440	22.7063

Appendix C-40 Dynamic melting model results for Apollo 14 green glasses A: K_2O / K_2O = 2.5809, ϕ = 0.05, and D = 0.001.

X1	X2	f1	f2	Co1%	Co2%	G
0.0250	0.1408	0.0678	0.1785	0.0082	0.0082	22.2712
0.0500	0.1836	0.0917	0.2195	0.0105	0.0152	22.2712
0.0750	0.2308	0.1156	0.2646	0.0131	0.0131	22.2712
0.1000	0.2824	0.1396	0.3139	0.0160	0.0160	22.2712
0.1250	0.3377	0.1635	0.3668	0.0192	0.0192	22.2712
0.1500	0.3962	0.1874	0.4227	0.0225	0.0225	22.2712
0.1750	0.4569	0.2113	0.4807	0.0259	0.0259	22.2712
0.2000	0.5191	0.2352	0.5402	0.0295	0.0295	22.2712
0.2250	0.5823	0.2591	0.6006	0.0331	0.0331	22.2712
0.2500	0.6460	0.2830	0.6616	0.0367	0.0367	22.2712
0.2750	0.7101	0.3069	0.7229	0.0404	0.0403	22.2712
0.3000	0.7745	0.3308	0.7844	0.0440	0.0440	22.2712

Appendix C (cont.)

Appendix C-41 Dynamic melting model results for Apollo 14 green glasses A: K_2O / K_2O = 2.5809, ϕ = 0.05, and D = 0.005.

X1	X2	f1	f2	Co1%	Co2%	G
0.0250	0.1493	0.0678	0.1867	0.0088	0.0088	20.5232
0.0500	0.1915	0.0917	0.2270	0.0110	0.0110	20.5232
0.0750	0.2377	0.1156	0.2712	0.0135	0.0135	20.5232
0.1000	0.2881	0.1396	0.3194	0.0164	0.0164	20.5232
0.1250	0.3422	0.1635	0.3711	0.0194	0.0194	20.5232
0.1500	0.3994	0.1874	0.4258	0.0227	0.0227	20.5232
0.1750	0.4591	0.2113	0.4829	0.0261	0.0261	20.5232
0.2000	0.5206	0.2352	0.5416	0.0296	0.0296	20.5232
0.2250	0.5832	0.2591	0.6015	0.0331	0.0331	20.5232
0.2500	0.6466	0.2830	0.6621	0.0367	0.0367	20.5232
0.2750	0.7105	0.3069	0.7232	0.0404	0.0403	20.5232
0.3000	0.7746	0.3308	0.7845	0.0440	0.0440	20.5232

Appendix C-42 Dynamic melting model results for Apollo 14 green glasses A: K_2O / K_2O = 2.5809, ϕ = 0.05, and D = 0.01.

X1	X2	f1	f2	Co1%	Co2%	G
0.0250	0.1601	0.0678	0.1970	0.0094	0.0094	18.6897
0.0500	0.2016	0.0917	0.2367	0.0116	0.0116	18.6897
0.0750	0.2467	0.1156	0.2798	0.0141	0.0141	18.6897
0.1000	0.2957	0.1396	0.3266	0.0168	0.0168	18.6897
0.1250	0.3483	0.1635	0.3769	0.0198	0.0198	18.6897
0.1500	0.4041	0.1874	0.4303	0.0229	0.0229	18.6897
0.1750	0.4625	0.2113	0.4861	0.0263	0.0263	18.6897
0.2000	0.5229	0.2352	0.5439	0.0297	0.0297	18.6897
0.2250	0.5848	0.2591	0.6030	0.0332	0.0332	18.6897
0.2500	0.6476	0.2830	0.6631	0.0368	0.0368	18.6897
0.2750	0.7111	0.3069	0.7238	0.0404	0.0404	18.6897
0.3000	0.7750	0.3308	0.7849	0.0440	0.0440	18.6897

Appendix C (cont.)

Appendix C-43 Dynamic melting model results for Apollo 14 green glasses B: TiO_2 / TiO_2 = 2.1690, ϕ = 0.01, and D = 0.02.

X1	X2	f1	f2	Co1%	Co2%	G
0.0250	0.0883	0.0335	0.0962	0.0356	0.0356	35.0023
0.0500	0.1286	0.0583	0.1363	0.0502	0.0502	35.0023
0.0750	0.1736	0.0831	0.1808	0.0673	0.0673	35.0023
0.1000	0.2223	0.1079	0.2291	0.0862	0.0861	35.0023
0.1250	0.2736	0.1327	0.2799	0.1060	0.1060	35.0023
0.1500	0.3264	0.1574	0.3323	0.1265	0.1265	35.0023
0.1750	0.3800	0.1822	0.3854	0.1473	0.1472	35.0023
0.2000	0.4340	0.2070	0.4389	0.1682	0.1682	35.0023
0.2250	0.4881	0.2318	0.4926	0.1892	0.1891	35.0023
0.2500	0.5423	0.2566	0.5463	0.2039	0.2101	35.0023
0.2750	0.5965	0.2813	0.6000	0.2312	0.2311	35.0023
0.3000	0.6507	0.3061	0.6538	0.2522	0.2521	35.0023

Appendix C-44 Dynamic melting model results for Apollo 14 green glasses B: TiO_2 / TiO_2 = 2.1690, ϕ = 0.01, and D = 0.05.

X1	X2	f1	f2	Co1%	Co2%	G
0.0250	0.1421	0.0335	0.1496	0.0593	0.0592	17.1505
0.0500	0.1782	0.0583	0.1854	0.0715	0.0714	17.1505
0.0750	0.2165	0.0831	0.2234	0.0851	0.0851	17.1505
0.1000	0.2572	0.1079	0.2637	0.1003	0.1002	17.1505
0.1250	0.3004	0.1327	0.3065	0.1166	0.1166	17.1505
0.1500	0.3460	0.1574	0.3517	0.1341	0.1341	17.1505
0.1750	0.3936	0.1822	0.3989	0.1526	0.1525	17.1505
0.2000	0.4431	0.2070	0.4480	0.1717	0.1717	17.1505
0.2250	0.4940	0.2318	0.4985	0.1914	0.1914	17.1505
0.2500	0.5460	0.2566	0.5500	0.2116	0.2115	17.1505
0.2750	0.5988	0.2813	0.6023	0.2327	0.2320	17.1505
0.3000	0.6521	0.3061	0.6551	0.2531	0.2526	17.1505

Appendix C (cont.)

Appendix C-45 Dynamic melting model results for Apollo 14 green glasses B: TiO_2 / TiO_2 = 2.1690, ϕ = 0.01, and D = 0.10.

X1	X2	f1	f2	Co1%	Co2%	G
0.0250	0.2368	0.0335	0.2435	0.0997	0.0997	9.2704
0.0500	0.2697	0.0583	0.2761	0.1103	0.1103	9.2704
0.0750	0.3038	0.0831	0.3099	0.1218	0.1218	9.2704
0.1000	0.3391	0.1079	0.3448	0.1341	0.1341	9.2704
0.1250	0.3757	0.1327	0.3812	0.1473	0.1473	9.2704
0.1500	0.4138	0.1574	0.4189	0.1614	0.1613	9.2704
0.1750	0.4534	0.1822	0.4581	0.1762	0.1762	9.2704
0.2000	0.4945	0.2070	0.4990	0.1919	0.1918	9.2704
0.2250	0.5373	0.2318	0.5414	0.2083	0.2082	9.2704
0.2500	0.5817	0.2566	0.5853	0.2253	0.2253	9.2704
0.2750	0.6275	0.2813	0.6308	0.2479	0.2430	9.2704
0.3000	0.6748	0.3061	0.6776	0.2652	0.2613	9.2704

Appendix C-46 Dynamic melting model results for Apollo 14 green glasses B: Al_2O_3 / Al_2O_3 = 1.0961, ϕ = 0.01, and D = 0.05.

X1	X2	f1	f2	Co1%	Co2%	G
0.0250	0.0371	0.0335	0.0455	0.5595	0.5595	17.1505
0.0500	0.0629	0.0583	0.0711	0.6746	0.6746	17.1505
0.0750	0.0888	0.0888	0.0968	0.8039	0.8039	17.1505
0.1000	0.1149	0.1079	0.1227	0.9466	0.9466	17.1505
0.1250	0.1412	0.1327	0.1487	1.1013	1.1013	17.1505
0.1500	0.1676	0.1574	0.1749	1.2665	1.2665	17.1505
0.1750	0.1942	0.1822	0.2013	1.4404	1.4404	17.1505
0.2000	0.2210	0.2070	0.2278	1.6213	1.6213	17.1505
0.2250	0.2479	0.2318	0.2544	1.8075	1.8075	17.1505
0.2500	0.2749	0.2566	0.2812	1.9976	1.9976	17.1505
0.2750	0.3020	0.2813	0.3081	2.1974	2.1906	17.1505
0.3000	0.3292	0.3061	0.3351	0.2390	2.3856	17.1505

Appendix C (cont.)

Appendix C-47 Dynamic melting model results for Apollo 14 green glasses B: Al_2O_3 / Al_2O_3 = 1.0961, ϕ = 0.01, and D = 0.10.

X1	X2	f1	f2	Co1%	Co2%	G
0.0250	0.0476	0.0335	0.0560	0.9413	0.9413	9.2704
0.0500	0.0732	0.0732	0.0813	1.0416	1.0416	9.2704
0.0750	0.0988	0.0831	0.1066	1.1499	1.1499	9.2704
0.1000	0.1244	0.1079	0.1321	1.2664	1.2664	9.2704
0.1250	0.1502	0.1327	0.1576	1.3909	1.3909	9.2704
0.1500	0.1761	0.1574	0.1833	1.5235	1.5235	9.2704
0.1750	0.2020	0.1822	0.2020	1.6638	1.6638	9.2704
0.2000	0.2280	0.2070	0.2280	1.8116	1.8116	9.2704
0.2250	0.2542	0.2318	0.2542	1.9664	1.9664	9.2704
0.2500	0.2804	0.2566	0.2804	2.1277	2.1277	9.2704
0.2750	0.3068	0.2813	0.3068	2.3405	2.2950	9.2704
0.3000	0.3333	0.3061	0.3333	2.5036	2.4677	9.2704

Appendix C-48 Dynamic melting model results for Apollo 14 green glasses B: Al_2O_3 / Al_2O_3 = 1.0961, ϕ = 0.01, and D = 0.15.

X1	X2	f1	f2	Co1%	Co2%	G
0.0250	0.0594	0.0335	0.0676	1.3252	1.3252	6.3519
0.0500	0.0847	0.0583	0.0927	1.4168	1.4168	6.3519
0.0750	0.1100	0.0831	0.1178	1.5139	1.5139	6.3519
0.1000	0.1354	0.1079	0.1430	1.6166	1.6166	6.3519
0.1250	0.1608	0.1327	0.1682	1.7251	1.7251	6.3519
0.1500	0.1863	0.1574	0.1935	1.8394	1.8394	6.3519
0.1750	0.2119	0.1822	0.2188	1.9597	1.9597	6.3519
0.2000	0.2375	0.2070	0.2442	2.0859	2.0859	6.3519
0.2250	0.2632	0.2318	0.2697	2.2180	2.2180	6.3519
0.2500	0.2890	0.2566	0.2952	2.3559	2.3559	6.3519
0.2750	0.3148	0.2813	0.3208	2.5915	2.4996	6.3519
0.3000	0.3407	0.3061	0.3465	2.7268	2.6488	6.3519

Appendix C (cont.)

Appendix C-49 Dynamic melting model results for Apollo 14 green glasses B: Al_2O_3 / Al_2O_3 = 1.0961, ϕ = 0.01, and D = 0.20.

X1	X2	f1	f2	Co1%	Co2%	G
0.0250	0.0704	0.0335	0.0785	1.7097	1.7027	4.8310
0.0500	0.0975	0.0583	0.1054	1.7943	1.7943	4.8310
0.0750	0.1226	0.0831	0.1303	1.8831	1.8831	4.8310
0.1000	0.1477	0.1079	0.1552	1.9761	1.9761	4.8310
0.1250	0.1729	0.1327	0.1801	2.0735	2.0735	4.8310
0.1500	0.1981	0.1574	0.2051	2.1755	2.1755	4.8310
0.1750	0.2233	0.1822	0.2301	2.2820	2.2820	4.8310
0.2000	0.2486	0.2070	0.2552	2.3932	2.3932	4.8310
0.2250	0.2739	0.2318	0.2803	2.5093	2.5093	4.8310
0.2500	0.2993	0.2566	0.3054	2.6302	2.6302	4.8310
0.2750	0.3247	0.2813	0.3306	2.8932	2.7559	4.8310
0.3000	0.3502	0.3061	0.3559	3.0065	2.8866	4.8310

Appendix C-50 Dynamic melting model results for Apollo 14 green glasses B: Al_2O_3 / Al_2O_3 = 1.0961, ϕ = 0.01, and D = 0.40.

X1	X2	f1	f2	Co1%	Co2%	G
0.0250	0.1393	0.0335	0.1469	3.2492	3.2358	2.4676
0.0500	0.1683	0.0583	0.1756	3.3109	3.3109	2.4676
0.0750	0.1921	0.0831	0.1992	3.3744	3.3744	2.4676
0.1000	0.2159	0.1079	0.2227	3.4398	3.4398	2.4676
0.1250	0.2397	0.1327	0.2463	3.5072	3.5072	2.4676
0.1500	0.2635	0.1574	0.2699	3.5767	3.5767	2.4676
0.1750	0.2873	0.1822	0.2935	3.6484	3.6484	2.4676
0.2000	0.3111	0.2070	0.3171	3.7223	3.7223	2.4676
0.2250	0.3349	0.2318	0.3407	3.7985	3.7985	2.4676
0.2500	0.3588	0.2566	0.3644	3.8771	3.8771	2.4676
0.2750	0.3826	0.2813	0.3880	4.2648	3.9582	2.4676
0.3000	0.4065	0.3061	0.4117	4.3181	4.0420	2.4676

Appendix C (cont.)

Appendix C-51 Dynamic melting model results for Apollo 14 green glasses B: CaO / CaO = 1.1051, ϕ = 0.01, and D = 0.02.

X1	X2	f1	f2	Co1%	Co2%	G
0.0250	0.0318	0.0335	0.0403	0.3044	0.3905	35.0023
0.0500	0.0581	0.0583	0.0663	0.5516	0.5516	35.0023
0.0750	0.0846	0.0831	0.0926	0.7393	0.7393	35.0023
0.1000	0.1115	0.1079	0.1193	0.9458	0.9458	35.0023
0.1250	0.1387	0.1327	0.1462	1.1640	1.1640	35.0023
0.1500	0.1660	0.1574	0.1733	1.3887	1.3888	35.0023
0.1750	0.1935	0.1822	0.2006	1.6168	1.6168	35.0023
0.2000	0.2211	0.2070	0.2279	1.8464	1.8464	35.0023
0.2250	0.2487	0.2318	0.2552	2.0766	2.0767	35.0023
0.2500	0.2763	0.2566	0.2826	2.3072	2.3072	35.0023
0.2750	0.3039	0.2813	0.3100	2.5379	2.5379	35.0023
0.3000	0.3315	0.3061	0.3374	2.7686	2.7686	35.0023

Appendix C-52 Dynamic melting model results for Apollo 14 green glasses B: CaO / CaO = 1.1051, ϕ = 0.01, and D = 0.05.

X1	X2	f1	f2	Co1%	Co2%	G
0.0250	0.0382	0.0335	0.0466	0.6505	0.6505	17.1505
0.0500	0.0640	0.0583	0.0722	0.7844	0.7844	17.1505
0.0750	0.0901	0.0831	0.0980	0.9803	0.9347	17.1505
0.1000	0.1163	0.1079	0.1240	1.1006	1.1006	17.1505
0.1250	0.1427	0.1327	0.1502	1.2805	1.2805	17.1505
0.1500	0.1692	0.1574	0.1765	1.4725	1.4726	17.1505
0.1750	0.1960	0.1822	0.2030	1.6747	1.6747	17.1505
0.2000	0.2229	0.2070	0.2297	1.8850	1.8850	17.1505
0.2250	0.2500	0.2318	0.2565	2.1015	2.1015	17.1505
0.2500	0.2772	0.2566	0.2835	2.3225	2.3226	17.1505
0.2750	0.3045	0.2813	0.3106	2.5548	2.5470	17.1505
0.3000	0.3319	0.3061	0.3378	2.7785	2.7737	17.1505

Appendix C (cont.)

Appendix C-53 Dynamic melting model results for Apollo 14 green glasses B: CaO / CaO = 1.1051, ϕ = 0.01, and D = 0.10.

X1	X2	f1	f2	Co1%	Co2%	G
0.0250	0.0497	0.0335	0.0580	1.0944	1.0945	9.2704
0.0500	0.0753	0.0583	0.0833	1.2110	1.2110	9.2704
0.0750	0.1009	0.0831	0.1088	1.3370	1.3370	9.2704
0.1000	0.1267	0.1079	0.1343	1.4724	1.4724	9.2704
0.1250	0.1525	0.1327	0.1599	1.6172	1.6172	9.2704
0.1500	0.1784	0.1574	0.1856	1.7713	1.7713	9.2704
0.1750	0.2045	0.1822	0.2114	1.9344	1.9345	9.2704
0.2000	0.2306	0.2070	0.2373	2.1062	2.1063	9.2704
0.2250	0.2569	0.2318	0.2634	2.2862	2.2863	9.2704
0.2500	0.2832	0.2566	0.2895	2.4738	2.4738	9.2704
0.2750	0.3097	0.2813	0.3158	2.7212	2.6683	9.2704
0.3000	0.3363	0.3061	0.3421	2.9108	2.8691	9.2704

Appendix C-54 Dynamic melting model results for Apollo 14 green glasses B: CaO / CaO = 1.1051, ϕ = 0.01, and D = 0.20.

X1	X2	f1	f2	Co1%	Co2%	G
0.0250	0.0767	0.0335	0.0848	1.9878	1.9878	4.8310
0.0500	0.1018	0.0583	0.1096	2.0862	2.0862	4.8310
0.0750	0.1269	0.0831	0.1345	2.1894	2.1894	4.8310
0.1000	0.1520	0.1079	0.1594	2.2975	2.2976	4.8310
0.1250	0.1772	0.1327	0.1844	2.4108	2.4109	4.8310
0.1500	0.2024	0.1574	0.2094	2.5293	2.5294	4.8310
0.1750	0.2276	0.1822	0.2344	2.6532	2.6532	4.8310
0.2000	0.2530	0.2070	0.2595	2.7825	2.7826	4.8310
0.2250	0.2783	0.2318	0.2846	2.9174	2.9175	4.8310
0.2500	0.3037	0.2566	0.3098	3.0579	3.0580	4.8310
0.2750	0.3292	0.2813	0.3351	3.3637	3.2043	4.8310
0.3000	0.3548	0.3061	0.3604	3.4955	3.3562	4.8310

Appendix C (cont.)

Appendix C-55 Dynamic melting model results for Apollo 14 green glasses B: CaO / CaO = 1.1051, ϕ = 0.01, and D = 0.40.

X1	X2	f1	f2	Co1%	Co2%	G
0.0250	0.1549	0.0335	0.1623	3.7776	3.7777	2.4676
0.0500	0.1786	0.0583	0.1858	3.8493	3.8494	2.4676
0.0750	0.2022	0.0831	0.2092	3.9232	3.9233	2.4676
0.1000	0.2259	0.1079	0.2327	3.9993	3.9994	2.4676
0.1250	0.2496	0.1327	0.2562	4.0777	4.0778	2.4676
0.1500	0.2733	0.1574	0.2797	4.1585	4.1559	2.4676
0.1750	0.2970	0.1822	0.3032	4.2418	4.2419	2.4676
0.2000	0.3207	0.2070	0.3267	4.3277	4.3278	2.4676
0.2250	0.3445	0.2318	0.3502	4.4163	4.4164	2.4676
0.2500	0.3682	0.2566	0.3737	4.5077	4.5078	2.4676
0.2750	0.3920	0.2813	0.3973	4.9584	4.6021	2.4676
0.3000	0.4157	0.3061	0.4209	5.0204	4.6995	2.4676

Appendix C-56 Dynamic melting model results for Apollo 14 green glasses B: Na_2O / Na_2O = 1.2774, ϕ = 0.01, and D = 0.0001.

X1	X2	f1	f2	Co1%	Co2%	G
0.0250	0.0331	0.0335	0.0415	0.0050	0.0050	113.0770
0.0500	0.0640	0.0583	0.0722	0.0095	0.0095	113.0770
0.0750	0.0958	0.0831	0.1037	0.0142	0.0142	113.0770
0.1000	0.1277	0.1079	0.1354	0.0189	0.0189	113.0770
0.1250	0.1597	0.1327	0.1670	0.0236	0.0236	113.0770
0.1500	0.1916	0.1574	0.1987	0.0284	0.0284	113.0770
0.1750	0.2235	0.1822	0.2303	0.0331	0.0331	113.0770
0.2000	0.2555	0.2070	0.2620	0.0378	0.0378	113.0770
0.2250	0.2874	0.2318	0.2936	0.0425	0.0425	113.0770
0.2500	0.3194	0.2566	0.3253	0.0473	0.0473	113.0770
0.2750	0.3513	0.2813	0.3570	0.0520	0.0520	113.0770
0.3000	0.3832	0.3061	0.3886	0.0567	0.0567	113.0770

Appendix C (cont.)

Appendix C-57 Dynamic melting model results for Apollo 14 green glasses B: Na_2O / Na_2O = 1.2774, ϕ = 0.01, and D = 0.001.

X1	X2	f1	f2	Co1%	Co2%	G
0.0250	0.0334	0.0335	0.0419	0.0051	0.0051	102.7151
0.0500	0.0641	0.0583	0.0723	0.0095	0.0095	102.7151
0.0750	0.0958	0.0831	0.1037	0.0142	0.0142	102.7151
0.1000	0.1277	0.1079	0.1354	0.0189	0.0189	102.7151
0.1250	0.1597	0.1327	0.1670	0.0236	0.0236	102.7151
0.1500	0.1916	0.1574	0.1987	0.0284	0.0284	102.7151
0.1750	0.2235	0.1822	0.2303	0.0331	0.0331	102.7151
0.2000	0.2555	0.2070	0.2620	0.0378	0.0378	102.7151
0.2250	0.2874	0.2318	0.2936	0.0425	0.0425	102.7151
0.2500	0.3194	0.2566	0.3253	0.0473	0.0473	102.7151
0.2750	0.3513	0.2813	0.3570	0.0520	0.0520	102.7151
0.3000	0.3832	0.3061	0.3886	0.0567	0.0567	102.7151

Appendix C-58 Dynamic melting model results for Apollo 14 green glasses B: Na_2O / Na_2O = 1.2774, ϕ = 0.01, and D = 0.005.

X1	X2	f1	f2	Co1%	Co2%	G
0.0250	0.0351	0.0335	0.0435	0.0056	0.0056	72.9890
0.0500	0.0649	0.0583	0.0731	0.0097	0.0097	72.9890
0.0750	0.0961	0.0831	0.1040	0.0142	0.0142	72.9890
0.1000	0.1278	0.1079	0.1354	0.0189	0.0019	72.9890
0.1250	0.1597	0.1327	0.1670	0.0236	0.0236	72.9890
0.1500	0.1916	0.1574	0.1987	0.0284	0.0284	72.9890
0.1750	0.2235	0.1822	0.2303	0.0331	0.0331	72.9890
0.2000	0.2555	0.2070	0.2620	0.0378	0.0378	72.9890
0.2250	0.2874	0.2318	0.2936	0.0425	0.0425	72.9890
0.2500	0.3194	0.2566	0.3253	0.0473	0.0473	72.9890
0.2750	0.3513	0.2813	0.3570	0.0520	0.0520	72.9890
0.3000	0.3832	0.3061	0.3886	0.0567	0.0567	72.9890

Appendix C (cont.)

Appendix C-59 Dynamic melting model results for Apollo 14 green glasses B: Na_2O / Na_2O = 1.2774, ϕ = 0.01, and D = 0.01.

X1	X2	f1	f2	Co1%	Co2%	G
0.0250	0.0374	0.0335	0.0458	0.0063	0.0063	53.5993
0.0500	0.0665	0.0583	0.0746	0.0101	0.0101	53.5993
0.0750	0.0968	0.0831	0.1047	0.0144	0.0144	53.5993
0.1000	0.1281	0.1079	0.1357	0.0190	0.0190	53.5993
0.1250	0.1598	0.1327	0.1671	0.0236	0.0236	53.5993
0.1500	0.1916	0.1574	0.1987	0.0284	0.0284	53.5993
0.1750	0.2236	0.1822	0.2303	0.0331	0.0331	53.5993
0.2000	0.2555	0.2070	0.2620	0.0378	0.0378	53.5993
0.2250	0.2874	0.2318	0.2936	0.0425	0.0425	53.5993
0.2500	0.3194	0.2566	0.3250	0.0473	0.0473	53.5993
0.2750	0.3513	0.2813	0.3570	0.0520	0.0520	53.5993
0.3000	0.3832	0.3061	0.3886	0.0567	0.0567	53.5993

Appendix C-60 Dynamic melting model results for Apollo 14 green glasses B: K_2O / K_2O = 1.0854, ϕ = 0.01, and D = 0.0001.

X1	X2	f1	f2	Co1%	Co2%	G
0.0250	0.0275	0.0335	0.0361	0.0012	0.0012	113.0770
0.0500	0.0543	0.0583	0.0626	0.0023	0.0023	113.0770
0.0750	0.0814	0.0831	0.0894	0.0034	0.0034	113.0770
0.1000	0.1085	0.1079	0.1163	0.0045	0.0045	113.0770
0.1250	0.1357	0.1327	0.1432	0.0056	0.0056	113.0770
0.1500	0.1628	0.1574	0.1701	0.0067	0.0067	113.0770
0.1750	0.1899	0.1822	0.1970	0.0079	0.0079	113.0770
0.2000	0.2171	0.2070	0.2239	0.0090	0.0090	113.0770
0.2250	0.2442	0.2318	0.2508	0.0101	0.0101	113.0770
0.2500	0.2714	0.2566	0.2777	0.0115	0.0112	113.0770
0.2750	0.2985	0.2813	0.3046	0.0123	0.0123	113.0770
0.3000	0.3256	0.3061	0.3315	0.0135	0.0135	113.0770

Appendix C (cont.)

Appendix C-61 Dynamic melting model results for Apollo 14 green glasses B: K_2O / K_2O = 1.0854, ϕ = 0.01, and D = 0.001.

X1	X2	f1	f2	Co1%	Co2%	G
0.0250	0.0277	0.0335	0.0362	0.0012	0.0012	102.7151
0.0500	0.0544	0.0583	0.0626	0.0023	0.0023	102.7151
0.0750	0.0814	0.0831	0.0895	0.0034	0.0034	102.7151
0.1000	0.1085	0.1079	0.1163	0.0045	0.0045	102.7151
0.1250	0.1357	0.1327	0.1432	0.0056	0.0056	102.7151
0.1500	0.1628	0.1574	0.1701	0.0067	0.0067	102.7151
0.1750	0.1899	0.1822	0.1970	0.0079	0.0079	102.7151
0.2000	0.2171	0.2070	0.2239	0.0090	0.0090	102.7151
0.2250	0.2442	0.2318	0.2508	0.0101	0.0101	102.7151
0.2500	0.2714	0.2566	0.2777	0.0112	0.0112	102.7151
0.2750	0.2985	0.2813	0.3046	0.0123	0.0123	102.7151
0.3000	0.3256	0.3061	0.3315	0.0135	0.0135	102.7151

Appendix C-62 Dynamic melting model results for Apollo 14 green glasses B: K_2O / K_2O = 1.0854, ϕ = 0.01, and D = 0.005.

X1	X2	f1	f2	Co1%	Co2%	G
0.0250	0.0282	0.0335	0.0367	0.0013	0.0013	72.9890
0.0500	0.0547	0.0583	0.0629	0.0023	0.0023	72.9890
0.0750	0.0815	0.0831	0.0895	0.0034	0.0034	72.9890
0.1000	0.1086	0.1079	0.1164	0.0045	0.0045	72.9890
0.1250	0.1357	0.1327	0.1432	0.0056	0.0056	72.9890
0.1500	0.1628	0.1574	0.1701	0.0067	0.0067	72.9890
0.1750	0.1899	0.1822	0.1970	0.0079	0.0079	72.9890
0.2000	0.2171	0.2070	0.2239	0.0090	0.0090	72.9890
0.2250	0.2442	0.2318	0.2508	0.0101	0.0101	72.9890
0.2500	0.2714	0.2566	0.2777	0.0112	0.0112	72.9890
0.2750	0.2985	0.2813	0.3046	0.0123	0.0123	72.9890
0.3000	0.3256	0.3061	0.3315	0.0135	0.0135	72.9890

Appendix C (cont.)

Appendix C-63 Dynamic melting model results for Apollo 14 green glasses B: K_2O / K_2O = 1.0854, ϕ = 0.01, and D = 0.01.

X1	X2	f1	f2	Co1%	Co2%	G
0.0250	0.0290	0.0335	0.0375	0.0015	0.0015	53.5993
0.0500	0.0552	0.0583	0.0635	0.0024	0.0024	53.5993
0.0750	0.0818	0.0831	0.0898	0.0034	0.0034	53.5993
0.1000	0.1087	0.1079	0.1165	0.0045	0.0045	53.5993
0.1250	0.1357	0.1327	0.1433	0.0056	0.0056	53.5993
0.1500	0.1628	0.1574	0.1701	0.0067	0.0067	53.5993
0.1750	0.1899	0.1822	0.1970	0.0079	0.0079	53.5993
0.2000	0.2171	0.2070	0.2239	0.0090	0.0090	53.5993
0.2250	0.2442	0.2318	0.2508	0.0101	0.0101	53.5993
0.2500	0.2714	0.2566	0.2777	0.0112	0.0112	53.5993
0.2750	0.2985	0.2813	0.3046	0.0123	0.0123	53.5993
0.3000	0.3256	0.3061	0.3315	0.0135	0.0135	53.5993

Appendix C-64 Dynamic melting model results for Apollo 14 green glasses B: TiO_2 / TiO_2 = 2.169, ϕ = 0.05, and D = 0.02.

X1	X2	f1	f2	Co1%	Co2%	G
0.0250	0.1471	0.0678	0.1846	0.0635	0.0635	15.8564
0.0500	0.1829	0.0917	0.2188	0.0760	0.0760	15.8564
0.0750	0.2209	0.1156	0.2551	0.0900	0.0900	15.8564
0.1000	0.2612	0.1396	0.2936	0.1054	0.1054	15.8564
0.1250	0.3038	0.1635	0.3344	0.1221	0.1221	15.8564
0.1500	0.3488	0.1874	0.3774	0.1399	0.1399	15.8564
0.1750	0.3959	0.2113	0.4225	0.1587	0.1587	15.8564
0.2000	0.4449	0.2352	0.4693	0.1783	0.1783	15.8564
0.2250	0.4953	0.2591	0.5175	0.1985	0.1985	15.8564
0.2500	0.5469	0.2830	0.5669	0.2192	0.2192	15.8564
0.2750	0.5994	0.3069	0.6170	0.2412	0.2402	15.8564
0.3000	0.6525	0.3308	0.6678	0.2621	0.2615	15.8564

Appendix C (cont.)

Appendix C-65 Dynamic melting model results for Apollo 14 green glasses B: TiO_2 / TiO_2 = 2.169, ϕ = 0.05, and D = 0.05.

X1	X2	f1	f2	Co1%	Co2%	G
0.0250	0.1998	0.0678	0.2349	0.0869	0.0869	10.8995
0.0500	0.2337	0.0917	0.2674	0.0983	0.9835	10.8995
0.0750	0.2691	0.1156	0.3012	0.1109	0.1108	10.8995
0.1000	0.3060	0.1396	0.3365	0.1245	0.1244	10.8995
0.1250	0.3445	0.1635	0.3733	0.1391	0.1390	10.8995
0.1500	0.3848	0.1874	0.4119	0.1547	0.1546	10.8995
0.1750	0.4269	0.2113	0.4521	0.1712	0.1712	10.8995
0.2000	0.4709	0.2352	0.4941	0.1886	0.1886	10.8995
0.2250	0.5165	0.2591	0.5377	0.2068	0.2068	10.8995
0.2500	0.5637	0.2830	0.5829	0.2257	0.2256	10.8995
0.2750	0.6124	0.3069	0.6294	0.2482	0.2451	10.8995
0.3000	0.6622	0.3308	0.6771	0.2674	0.2651	10.8995

Appendix C-66 Dynamic melting model results for Apollo 14 green glasses B: TiO_2 / TiO_2 = 2.169, ϕ = 0.05, and D = 0.10.

X1	X2	f1	f2	Co1%	Co2%	G
0.0250	0.2912	0.0678	0.3223	0.1260	0.1260	7.1659
0.0500	0.3228	0.0917	0.3525	0.1364	0.1364	7.1659
0.0750	0.3552	0.1156	0.3836	0.1475	0.1475	7.1659
0.1000	0.3886	0.1396	0.4155	0.1593	0.1593	7.1659
0.1250	0.4231	0.1635	0.4484	0.1719	0.1718	7.1659
0.1500	0.4587	0.1874	0.4825	0.1851	0.1851	7.1659
0.1750	0.4955	0.2113	0.5176	0.1991	0.1991	7.1659
0.2000	0.5335	0.2352	0.5540	0.2139	0.2138	7.1659
0.2250	0.5730	0.2591	0.5917	0.2293	0.2292	7.1659
0.2500	0.6138	0.2830	0.6308	0.2454	0.2454	7.1659
0.2750	0.6560	0.3069	0.6712	0.2699	0.2621	7.1659
0.3000	0.6997	0.3308	0.7129	0.2860	0.2795	7.1659

Appendix C (cont.)

Appendix C-67 Dynamic melting model results for Apollo 14 green glasses B: Al_2O_3 / Al_2O_3 = 1.0961, ϕ = 0.05, and D = 0.05.

X1	X2	f1	f2	Co1%	Co2%	G
0.0250	0.0434	0.0678	0.0855	0.8204	0.8204	10.8995
0.0500	0.0691	0.0917	0.1100	0.9286	0.9286	10.8995
0.0750	0.0948	0.1156	0.1346	1.0468	1.0468	10.8995
0.1000	0.1206	0.1396	0.1592	1.1751	1.1751	10.8995
0.1250	0.1465	0.1635	0.1840	1.3131	1.3131	10.8995
0.1500	0.1725	0.1874	0.2089	1.4605	1.4605	10.8995
0.1750	0.1987	0.2113	0.2339	1.6167	1.6167	10.8995
0.2000	0.2249	0.2352	0.2590	1.7811	1.7811	10.8995
0.2250	0.2513	0.2591	0.2842	1.9527	1.9527	10.8995
0.2500	0.2778	0.2830	0.3096	2.1309	2.1309	10.8995
0.2750	0.3044	0.3069	0.3350	2.3440	2.3147	10.8995
0.3000	0.3312	0.3308	0.3606	2.5251	2.5032	10.8995

Appendix C-68 Dynamic melting model results for Apollo 14 green glasses B: Al_2O_3 / Al_2O_3 = 1.0961, ϕ = 0.05, and D = 0.10.

X1	X2	f1	f2	Co1%	Co2%	G
0.0250	0.0540	0.0678	0.0955	1.1900	1.1900	7.1659
0.0500	0.0794	0.0917	0.1198	1.2881	1.2881	7.1659
0.0750	0.1048	0.1156	0.1442	1.39287	1.3929	7.1659
0.1000	0.1303	0.1396	0.1686	1.5044	1.5044	7.1659
0.1250	0.1559	0.1635	0.1930	1.6228	1.6228	7.1659
0.1500	0.1816	0.1874	0.2175	1.7481	1.7481	7.1659
0.1750	0.2073	0.2113	0.2421	1.8803	1.8803	7.1659
0.2000	0.2331	0.2352	0.2668	2.0193	2.0193	7.1659
0.2250	0.2589	0.2591	0.2915	2.1650	2.1650	7.1659
0.2500	0.2849	0.2830	0.3163	2.3171	2.3171	7.1659
0.2750	0.3110	0.3069	0.3412	2.5488	2.4754	7.1659
0.3000	0.3308	0.3308	0.3662	2.6396	2.6396	7.1659

Appendix C (cont.)

Appendix C-69 Dynamic melting model results for Apollo 14 green glasses B: Al_2O_3 / Al_2O_3 = 1.0961, ϕ = 0.05, and D = 0.15.

X1	X2	f1	f2	Co1%	Co2%	G
0.0250	0.0657	0.0678	0.1067	1.5604	1.5604	5.3375
0.0500	0.0908	0.0917	0.1308	1.65104	1.6510	5.3375
0.0750	0.1161	0.1156	0.1549	1.7466	1.7466	5.3375
0.1000	0.1413	0.1396	0.1790	1.8471	1.8471	5.3375
0.1250	0.1666	0.1635	0.2032	1.9528	1.9528	5.3375
0.1500	0.1920	0.1874	0.2275	2.0638	2.0638	5.3375
0.1750	0.2173	0.2113	0.2517	2.1801	2.1801	5.3375
0.2000	0.2428	0.2352	0.2761	2.3019	2.3019	5.3375
0.2250	0.2683	0.2591	0.3005	2.4292	2.4292	5.3375
0.2500	0.2939	0.2830	0.3249	2.5619	2.5619	5.3375
0.2750	0.3195	0.3069	0.3494	2.7002	2.7002	5.3375
0.3000	0.3452	0.3308	0.3740	2.8439	2.8439	5.3375

Appendix C-70 Dynamic melting model results for Apollo 14 green glasses B: Al_2O_3 / Al_2O_3 = 1.0961, ϕ = 0.05, and D = 0.20.

X1	X2	f1	f2	Co1%	Co2%	G
0.0250	0.0763	0.0678	0.1169	1.9312	1.9232	4.2525
0.0500	0.1037	0.0917	0.1430	2.0153	2.0153	4.2525
0.0750	0.1286	0.1156	0.1669	2.1033	2.1033	4.2525
0.1000	0.1536	0.1396	0.1908	2.1952	2.1952	4.2525
0.1250	0.1786	0.1635	0.2147	2.2912	2.2912	4.2525
0.1500	0.2037	0.1874	0.2387	2.3914	2.3914	4.2525
0.1750	0.2288	0.2113	0.2627	2.4958	2.4958	4.2525
0.2000	0.2539	0.2352	0.2867	2.6047	2.6047	4.2525
0.2250	0.2791	0.2591	0.3108	2.7180	2.7180	4.2525
0.2500	0.3043	0.2830	0.3349	2.8360	2.8360	4.2525
0.2750	0.3296	0.3069	0.3591	3.1196	2.9586	4.2525
0.3000	0.3549	0.3308	0.3833	3.2276	3.0860	4.2525

Appendix C (cont.)

Appendix C-71 Dynamic melting model results for Apollo 14 green glasses B: Al_2O_3 / Al_2O_3 = 1.0961, ϕ = 0.05, and D = 0.40.

X1	X2	f1	f2	Co1%	Co2%	G
0.0250	0.1450	0.0678	0.1826	3.4154	3.4014	2.3454
0.0500	0.1741	0.0917	0.2104	3.4770	3.4770	2.3454
0.0750	0.1978	0.1156	0.2331	3.5404	3.5404	2.3454
0.1000	0.2215	0.1396	0.2557	3.6057	3.6057	2.3454
0.1250	0.2452	0.1635	0.2783	3.6730	3.6730	2.3454
0.1500	0.2688	0.1874	0.3010	3.7422	3.7422	2.3454
0.1750	0.2925	0.2113	0.3236	3.8136	3.8136	2.3454
0.2000	0.3162	0.2352	0.3463	3.8872	3.8872	2.3454
0.2250	0.3400	0.2591	0.3690	3.9631	3.9631	2.3454
0.2500	0.3637	0.2830	0.3917	4.0413	4.0413	2.3454
0.2750	0.3874	0.3069	0.4143	4.4454	4.1220	2.3454
0.3000	0.4112	0.3308	0.4371	4.4967	4.2052	2.3454

Appendix C-72 Dynamic melting model results for Apollo 14 green glasses B: CaO / CaO = 1.1051, ϕ = 0.05, and D = 0.02.

X1	X2	f1	f2	Co1%	Co2%	G
0.0250	0.0387	0.0678	0.0810	0.6974	0.6974	15.8564
0.0500	0.0646	0.0917	0.1057	0.8344	0.8345	15.8564
0.0750	0.0906	0.1156	0.1306	0.9879	0.9879	15.8564
0.1000	0.1168	0.1396	0.1556	1.1569	1.1570	15.8564
0.1250	0.1431	0.1635	0.1808	1.3403	1.3403	15.8564
0.1500	0.1696	0.1874	0.2061	1.5361	1.5361	15.8564
0.1750	0.1963	0.2113	0.2317	1.7426	1.7426	15.8564
0.2000	0.2232	0.2352	0.2573	1.9577	1.9577	15.8564
0.2250	0.2502	0.2591	0.2832	2.1796	2.1796	15.8564
0.2500	0.2774	0.2830	0.3091	2.4067	2.4067	15.8564
0.2750	0.3046	0.3069	0.3352	2.6473	2.6376	15.8564
0.3000	0.3320	0.3308	0.3614	2.8773	2.8712	15.8564

Appendix C (cont.)

Appendix C-73 Dynamic melting model results for Apollo 14 green glasses B: CaO / CaO = 1.1051, ϕ = 0.05, and D = 0.05.

X1	X2	f1	f2	Co1%	Co2%	G
0.0250	0.0451	0.0678	0.0871	0.9538	0.9538	10.8995
0.0500	0.0708	0.0917	0.1116	1.0796	1.0797	10.8995
0.0750	0.0966	0.1156	0.1363	1.2171	1.2171	10.8995
0.1000	0.1224	0.1396	0.1610	1.3662	1.3662	10.8995
0.1250	0.1485	0.1635	0.1859	1.5267	1.5267	10.8995
0.1500	0.1746	0.1874	0.2108	1.6980	1.6981	10.8995
0.1750	0.2008	0.2113	0.2359	1.8797	1.8797	10.8995
0.2000	0.2272	0.2352	0.2612	2.0707	2.0708	10.8995
0.2250	0.2537	0.2591	0.2865	2.2704	2.2704	10.8995
0.2500	0.2804	0.2830	0.3120	2.4775	2.4776	10.8995
0.2750	0.3072	0.3069	0.3376	2.7252	2.6912	10.8995
0.3000	0.3341	0.3308	0.3633	2.9358	2.9104	10.8995

Appendix C-74 Dynamic melting model results for Apollo 14 green glasses B: CaO / CaO = 1.1051, ϕ = 0.05, and D = 0.10.

X1	X2	f1	f2	Co1%	Co2%	G
0.0250	0.0566	0.0678	0.0980	1.3835	1.3835	7.1659
0.0500	0.0820	0.0917	0.1224	1.4976	1.4976	7.1659
0.0750	0.1075	0.1156	1.4673	1.6194	1.6195	7.1659
0.1000	0.1331	0.1396	0.1712	1.7491	1.7491	7.1659
0.1250	0.1587	0.1635	0.1957	1.8868	1.8868	7.1659
0.1500	0.1844	0.1874	0.2203	2.0325	2.0325	7.1659
0.1750	0.2102	0.2113	0.2449	2.1862	2.1862	7.1659
0.2000	0.2361	0.2352	0.2696	2.3478	2.3478	7.1659
0.2250	0.2620	0.2591	0.2945	2.5171	2.5172	7.1659
0.2500	0.2881	0.2830	0.3194	2.6940	2.6940	7.1659
0.2750	0.3142	0.3069	0.3444	2.9634	2.8781	7.1659
0.3000	0.3405	0.3308	0.3695	3.1397	3.0690	7.1659

Appendix C (cont.)

Appendix C-75 Dynamic melting model results for Apollo 14 green glasses B:
CaO / CaO = 1.1051, ϕ = 0.05, and D = 0.20.

X1	X2	f1	f2	Co1%	Co2%	G
0.0250	0.0835	0.0678	0.1238	2.2453	2.2453	4.2525
0.0500	0.1084	0.0917	0.1476	2.3431	2.3432	4.2525
0.0750	0.1334	0.1156	0.1715	2.4454	2.4455	4.2525
0.1000	0.1584	0.1396	0.1954	2.5523	2.5523	4.2525
0.1250	0.1834	0.1635	0.2193	2.6638	2.6639	4.2525
0.1500	0.2085	0.1874	0.2433	2.7803	2.7804	4.2525
0.1750	0.2336	0.2113	0.2673	2.9017	2.9018	4.2525
0.2000	0.2588	0.2352	0.2913	3.0283	3.0284	4.2525
0.2250	0.2840	0.2591	0.3154	3.1601	3.1602	4.2525
0.2500	0.3092	0.2830	0.3396	3.2973	3.2973	4.2525
0.2750	0.3345	0.3069	0.3637	3.6270	3.4399	4.2525
0.3000	0.3599	0.3308	0.3880	3.7525	3.5880	4.2525

Appendix C-76 Dynamic melting model results for Apollo 14 green glasses B:
CaO / CaO = 1.1051, ϕ = 0.05, and D = 0.40.

X1	X2	f1	f2	Co1%	Co2%	G
0.0250	0.1613	0.0678	0.1982	3.9709	3.9710	2.3454
0.0500	0.1849	0.0917	0.2207	4.0425	4.0426	2.3454
0.0750	0.2084	0.1156	0.2432	4.1162	4.1163	2.3454
0.1000	0.2320	0.1396	0.2657	4.1922	4.1923	2.3454
0.1250	0.2556	0.1635	0.2883	4.2703	4.2705	2.3454
0.1500	0.2791	0.1874	0.3108	4.3509	4.3510	2.3454
0.1750	0.3027	0.2113	0.3334	4.4339	4.4340	2.3454
0.2000	0.3263	0.2352	0.3559	4.5194	4.5195	2.3454
0.2250	0.3499	0.2591	0.3785	4.6076	4.6077	2.3454
0.2500	0.3735	0.2830	0.4011	4.6986	4.6987	2.3454
0.2750	0.3972	0.3069	0.4237	5.1684	4.7925	2.3454
0.3000	0.4208	0.3308	0.4463	5.2281	4.8893	2.3454

Appendix C-77 Dynamic melting model results for Apollo 14 green glasses B: Na_2O / Na_2O = 1.2774, ϕ = 0.05, and D = 0.0001.

X1	X2	f1	f2	Co1%	Co2%	G
0.0250	0.0496	0.0678	0.0913	0.0108	0.0108	22.7063
0.0500	0.0773	0.0092	0.1178	0.0139	0.0139	22.7063
0.0750	0.1057	0.1156	0.1450	0.0174	0.0174	22.7063
0.1000	0.1347	0.1396	0.1727	0.0213	0.0213	22.7063
0.1250	0.1643	0.1635	0.2011	0.0255	0.0255	22.7063
0.1500	0.1946	0.1874	0.2300	0.0300	0.0300	22.7063
0.1750	0.2254	0.2113	0.2594	0.0346	0.0346	22.7063
0.2000	0.2565	0.2352	0.2892	0.0393	0.0393	22.7063
0.2250	0.2880	0.2591	0.3193	0.0441	0.0441	22.7063
0.2500	0.3197	0.2830	0.3496	0.0490	0.0490	22.7063
0.2750	0.3514	0.3069	0.3799	0.0539	0.0538	22.7063
0.3000	0.3833	0.3308	0.4104	0.0587	0.0587	22.7063

Appendix C-78 Dynamic melting model results for Apollo 14 green glasses B: Na_2O / Na_2O = 1.2774, ϕ = 0.05, and D = 0.001.

X1	X2	f1	f2	Co1%	Co2%	G
0.0250	0.0500	0.0678	0.0917	0.0110	0.0110	22.2712
0.0500	0.0777	0.0917	0.1182	0.0140	0.0140	22.2712
0.0750	0.1060	0.1156	0.1453	0.0175	0.0175	22.2712
0.1000	0.1350	0.1396	0.1730	0.0214	0.0214	22.2712
0.1250	0.1646	0.1635	0.2013	0.0256	0.0256	22.2712
0.1500	0.1948	0.1874	0.2302	0.0300	0.0300	22.2712
0.1750	0.2255	0.2113	0.2596	0.0346	0.0346	22.2712
0.2000	0.2567	0.2352	0.2893	0.0393	0.0393	22.2712
0.2250	0.2881	0.2591	0.3194	0.0441	0.0441	22.2712
0.2500	0.3197	0.2830	0.3496	0.0490	0.0490	22.2712
0.2750	0.3515	0.3069	0.3800	0.0539	0.0538	22.2712
0.3000	0.3833	0.3308	0.4104	0.0587	0.0587	22.2712

Appendix C-79 Dynamic melting model results for Apollo 14 green glasses B: Na_2O / Na_2O = 1.2774, ϕ = 0.05, and D = 0.005.

X1	X2	f1	f2	Co1%	Co2%	G
0.0250	0.0520	0.0678	0.0936	0.0117	0.0117	20.5232
0.0500	0.0796	0.0917	0.1200	0.0147	0.0147	20.5232
0.0750	0.1078	0.1156	0.1470	0.0181	0.0181	20.5232
0.1000	0.1365	0.1396	0.1745	0.0218	0.0218	20.5232
0.1250	0.1659	0.1635	0.2025	0.0259	0.0259	20.5232
0.1500	0.1958	0.1874	0.2312	0.0303	0.0303	20.5232
0.1750	0.2263	0.2113	0.2603	0.0348	0.0348	20.5232
0.2000	0.2572	0.2352	0.2898	0.0395	0.0394	20.5232
0.2250	0.2884	0.2591	0.3197	0.0442	0.0442	20.5232
0.2500	0.3199	0.2830	0.3498	0.0490	0.0490	20.5232
0.2750	0.3516	0.3069	0.3801	0.0539	0.0538	20.5232
0.3000	0.3834	0.3308	0.4105	0.0587	0.0587	20.5232

Appendix C-80 Dynamic melting model results for Apollo 14 green glasses B: Na_2O / Na_2O = 1.2774, ϕ = 0.05, and D = 0.01.

X1	X2	f1	f2	Co1%	Co2%	G
0.0250	0.0545	0.0678	0.0960	0.0125	0.0125	18.6897
0.0500	0.0820	0.0917	0.1223	0.0155	0.0155	18.6897
0.0750	0.1100	0.1156	0.1491	0.0188	0.0188	18.6897
0.1000	0.1385	0.1396	0.1764	0.0224	0.0224	18.6897
0.1250	0.1676	0.1635	0.2042	0.0264	0.0264	18.6897
0.1500	0.1973	0.1874	0.2325	0.0306	0.0306	18.6897
0.1750	0.2274	0.2113	0.2614	0.0350	0.0350	18.6897
0.2000	0.2580	0.2352	0.2907	0.0392	0.0396	18.6897
0.2250	0.2890	0.2591	0.3202	0.0443	0.0443	18.6897
0.2500	0.3204	0.2830	0.3502	0.0491	0.0491	18.6897
0.2750	0.3519	0.3069	0.3804	0.0540	0.0539	18.6897
0.3000	0.3836	0.3308	0.4106	0.0588	0.0587	18.6897

Appendix C-81 Dynamic melting model results for Apollo 14 green glasses B: K_2O / K_2O = 1.0854, ϕ = 0.05, and D = 0.0001.

X1	X2	f1	f2	Co1%	Co2%	G
0.0250	0.0330	0.0678	0.0755	0.0026	0.0026	22.7063
0.0500	0.0588	0.0917	0.1002	0.0033	0.0033	22.7063
0.0750	0.0848	0.1156	0.1250	0.0041	0.0041	22.7063
0.1000	0.1110	0.1396	0.1501	0.0051	0.0051	22.7063
0.1250	0.1374	0.1635	0.1753	0.0061	0.0061	22.7063
0.1500	0.1640	0.1874	0.2007	0.0071	0.0071	22.7063
0.1750	0.1907	0.2113	0.2262	0.0082	0.0082	22.7063
0.2000	0.2175	0.2352	0.2519	0.0093	0.0093	22.7063
0.2250	0.2445	0.2591	0.2777	0.0105	0.0105	22.7063
0.2500	0.2715	0.2830	0.3035	0.0119	0.0116	22.7063
0.2750	0.2986	0.3069	0.3294	0.0128	0.0128	22.7063
0.3000	0.3257	0.3308	0.3553	0.0139	0.0139	22.7063

Appendix C-82 Dynamic melting model results for Apollo 14 green glasses B: K_2O / K_2O = 1.0854, ϕ = 0.05, and D = 0.001.

X1	X2	f1	f2	Co1%	Co2%	G
0.0250	0.0331	0.0678	0.0756	0.0026	0.0023	22.2712
0.0500	0.0589	0.0917	0.1003	0.0033	0.0033	22.2712
0.0750	0.0849	0.1156	0.1251	0.0042	0.0042	22.2712
0.1000	0.1111	0.1396	0.1502	0.0051	0.0051	22.2712
0.1250	0.1375	0.1635	0.1754	0.0061	0.0061	22.2712
0.1500	0.1640	0.1874	0.2008	0.0071	0.0071	22.2712
0.1750	0.1907	0.2113	0.2263	0.0082	0.0082	22.2712
0.2000	0.2176	0.2352	0.2520	0.0093	0.0093	22.2712
0.2250	0.2445	0.2591	0.2777	0.0105	0.0105	22.2712
0.2500	0.2715	0.2830	0.3035	0.0116	0.0116	22.2712
0.2750	0.2986	0.3069	0.3294	0.0128	0.0128	22.2712
0.3000	0.3257	0.3308	0.3553	0.0139	0.0139	22.2712

Appendix C-83 Dynamic melting model results for Apollo 14 green glasses B: K_2O / K_2O = 1.0854, ϕ = 0.05, and D = 0.005.

X1	X2	f1	f2	Co1%	Co2%	G
0.0250	0.0338	0.0678	0.0762	0.0028	0.0028	20.5232
0.0500	0.0595	0.0917	0.1009	0.0035	0.0035	20.5232
0.0750	0.0855	0.1156	0.1257	0.0043	0.0043	20.5232
0.1000	0.1116	0.1396	0.1507	0.0052	0.0052	20.5232
0.1250	0.1379	0.1635	0.1758	0.0062	0.0062	20.5232
0.1500	0.1644	0.1874	0.2011	0.0072	0.0072	20.5232
0.1750	0.1910	0.2113	0.2266	0.0083	0.0083	20.5232
0.2000	0.2178	0.2352	0.2522	0.0094	0.0094	20.5232
0.2250	0.2447	0.2591	0.2779	0.0105	0.0105	20.5232
0.2500	0.2716	0.2830	0.3036	0.0116	0.0116	20.5232
0.2750	0.2986	0.3069	0.3295	0.0128	0.0128	20.5232
0.3000	0.3257	0.3308	0.3553	0.0139	0.0139	20.5232

Appendix C-84 Dynamic melting model results for Apollo 14 green glasses B: K_2O / K_2O = 1.0854, ϕ = 0.05, and D = 0.01.

X1	X2	f1	f2	Co1%	Co2%	G
0.0250	0.0346	0.0678	0.0770	0.0030	0.0030	18.6897
0.0500	0.0603	0.0917	0.1016	0.0037	0.0037	18.6897
0.0750	0.0862	0.1156	0.1264	0.0045	0.0045	18.6897
0.1000	0.1123	0.1396	0.1513	0.0053	0.0053	18.6897
0.1250	0.1385	0.1635	0.1764	0.0063	0.0063	18.6897
0.1500	0.1649	0.1874	0.2016	0.0073	0.0073	18.6897
0.1750	0.1914	0.2113	0.2270	0.0083	0.0083	18.6897
0.2000	0.2181	0.2352	0.2525	0.0094	0.0094	18.6897
0.2250	0.2449	0.2591	0.2781	0.0105	0.0105	18.6897
0.2500	0.2718	0.2830	0.3038	0.0117	0.0117	18.6897
0.2750	0.2988	0.3069	0.3296	0.0128	0.0128	18.6897
0.3000	0.3258	0.3308	0.3554	0.0140	0.0139	18.6897

Appendix D

Apollo 14 volcanic green glasses A and B

dynamic melting model plots

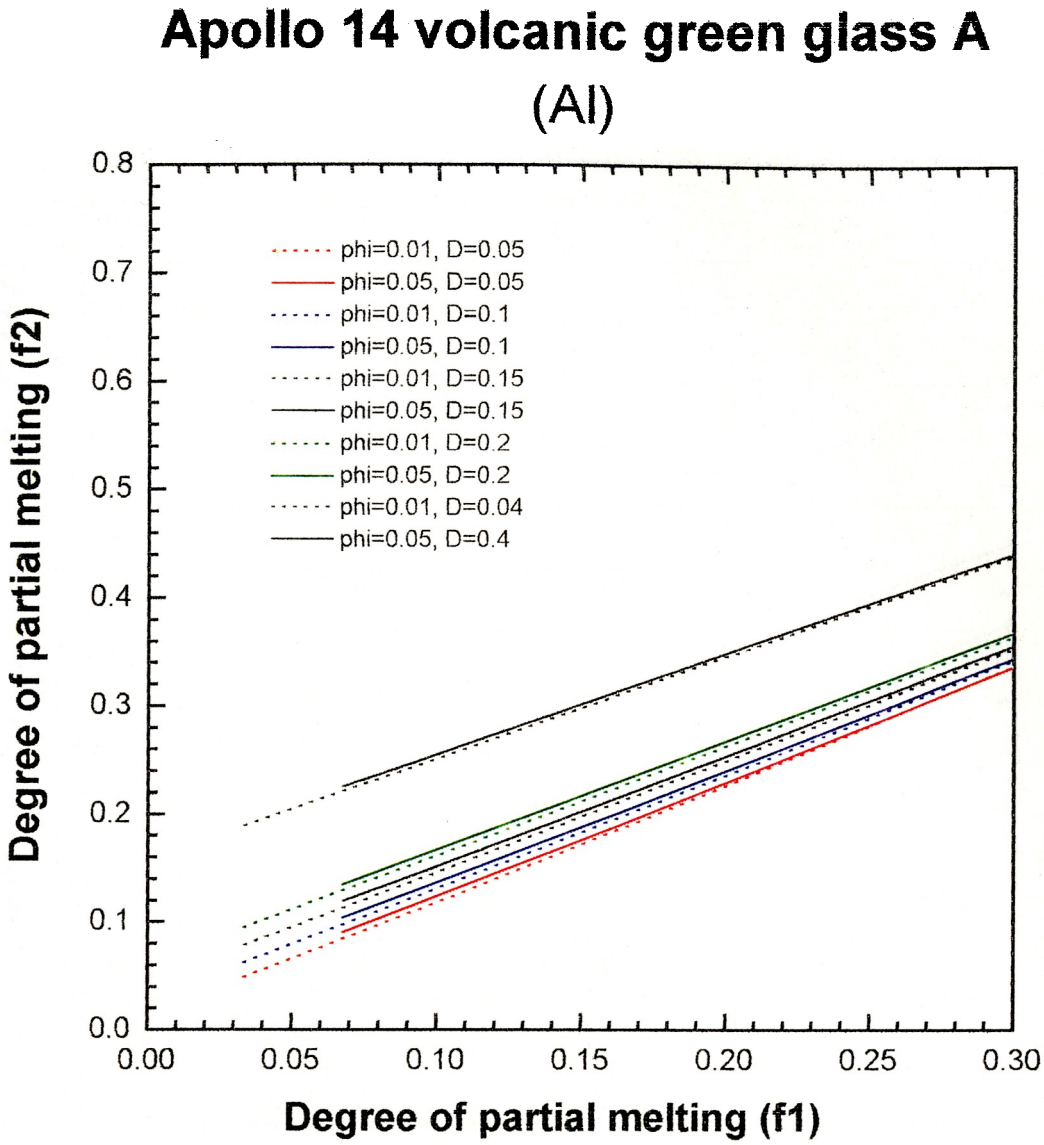

Appendix D-1 Degree of partial melting results for the dynamic melting model applied on Apollo 14 volcanic green glasses A chemical data: Al (see legend for porosity and distribution coefficient details) .

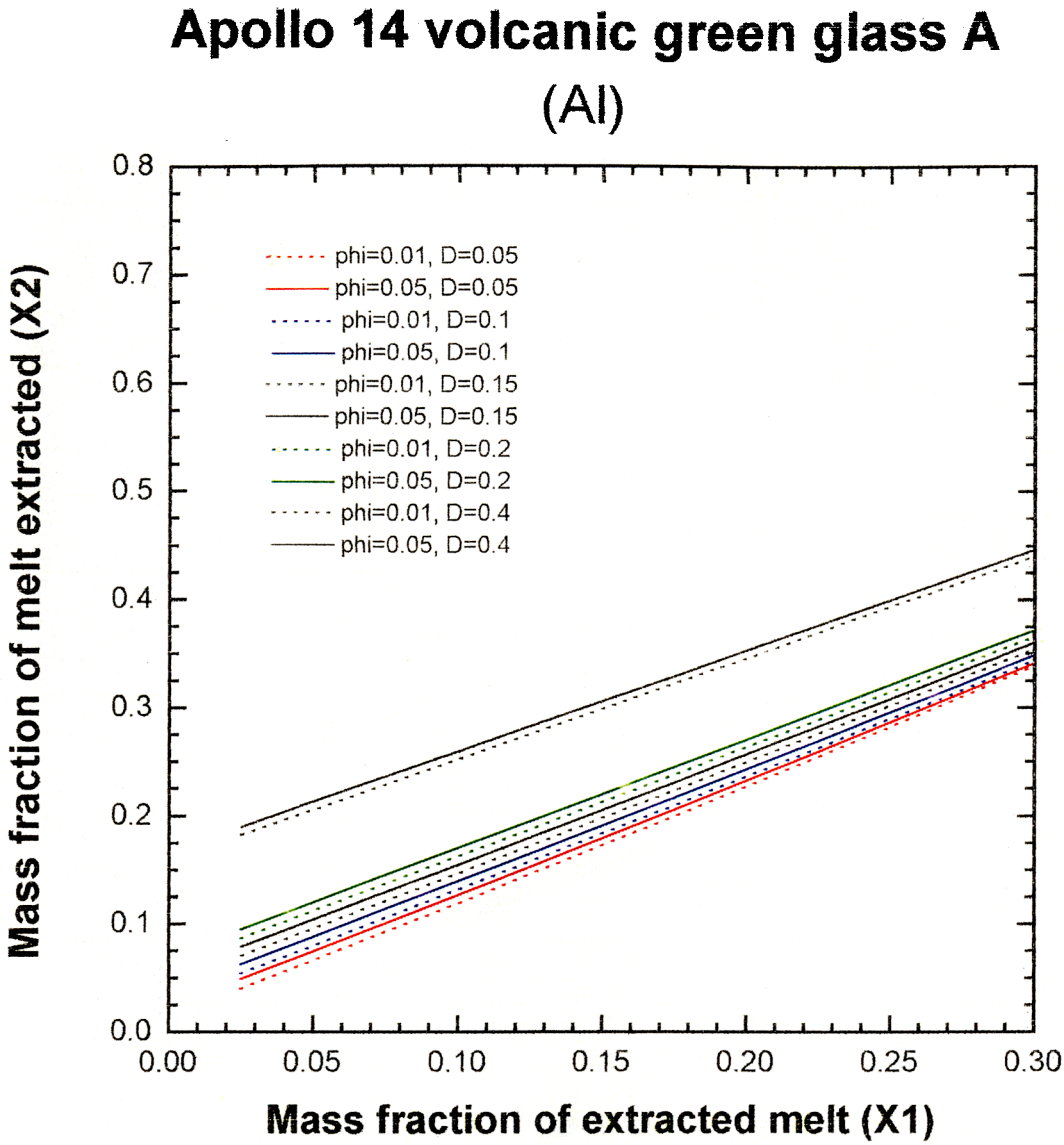

Appendix D-2 Mass of melt extracted results for the dynamic melting model applied on Apollo 14 volcanic green glasses A chemical data: Al (see legend for porosity and distribution coefficient details) .

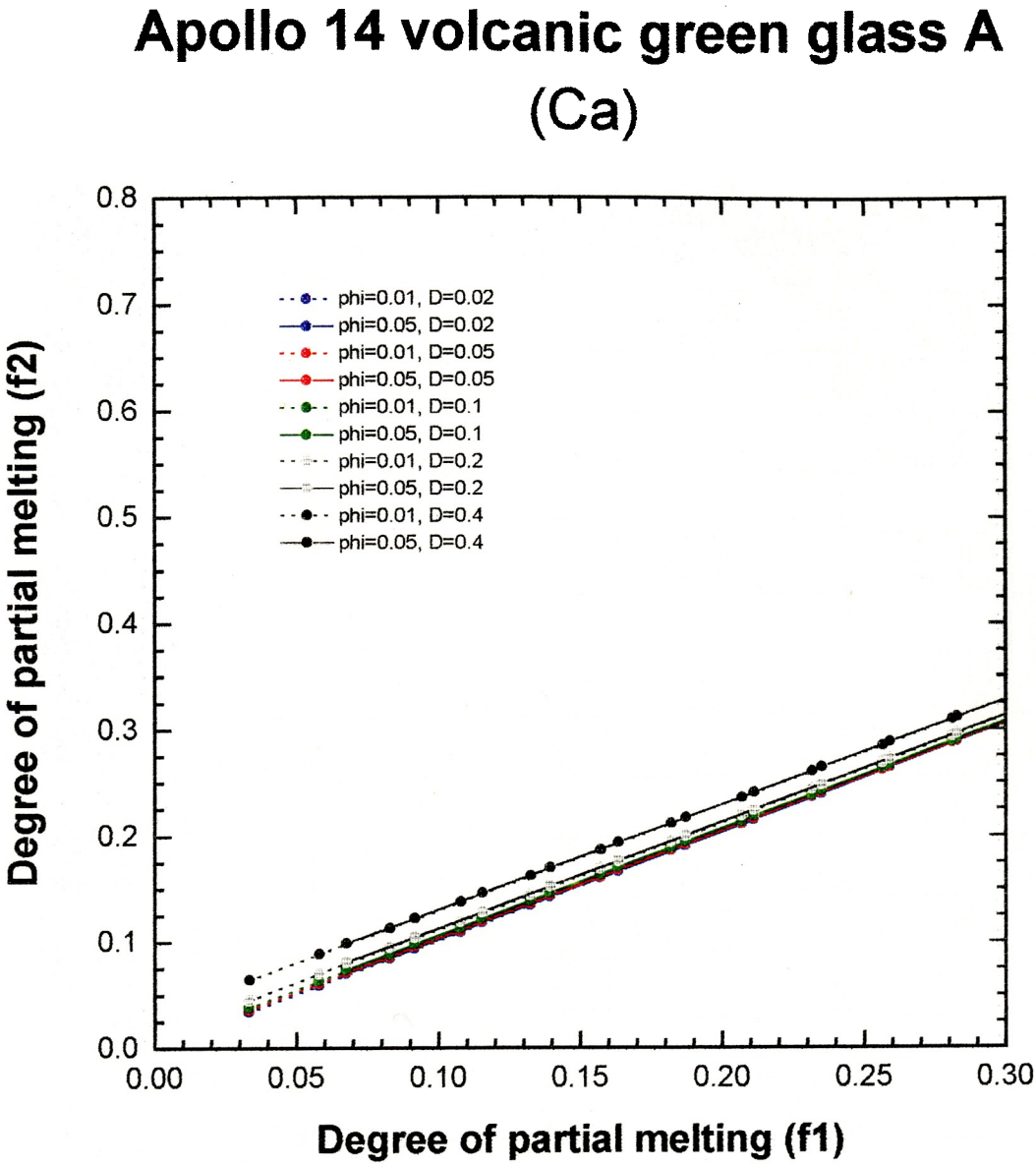

Appendix D-3 Degree of partial melting results for the dynamic melting model applied on Apollo 14 volcanic green glasses A chemical data: Ca (see legend for porosity and distribution coefficient details) .

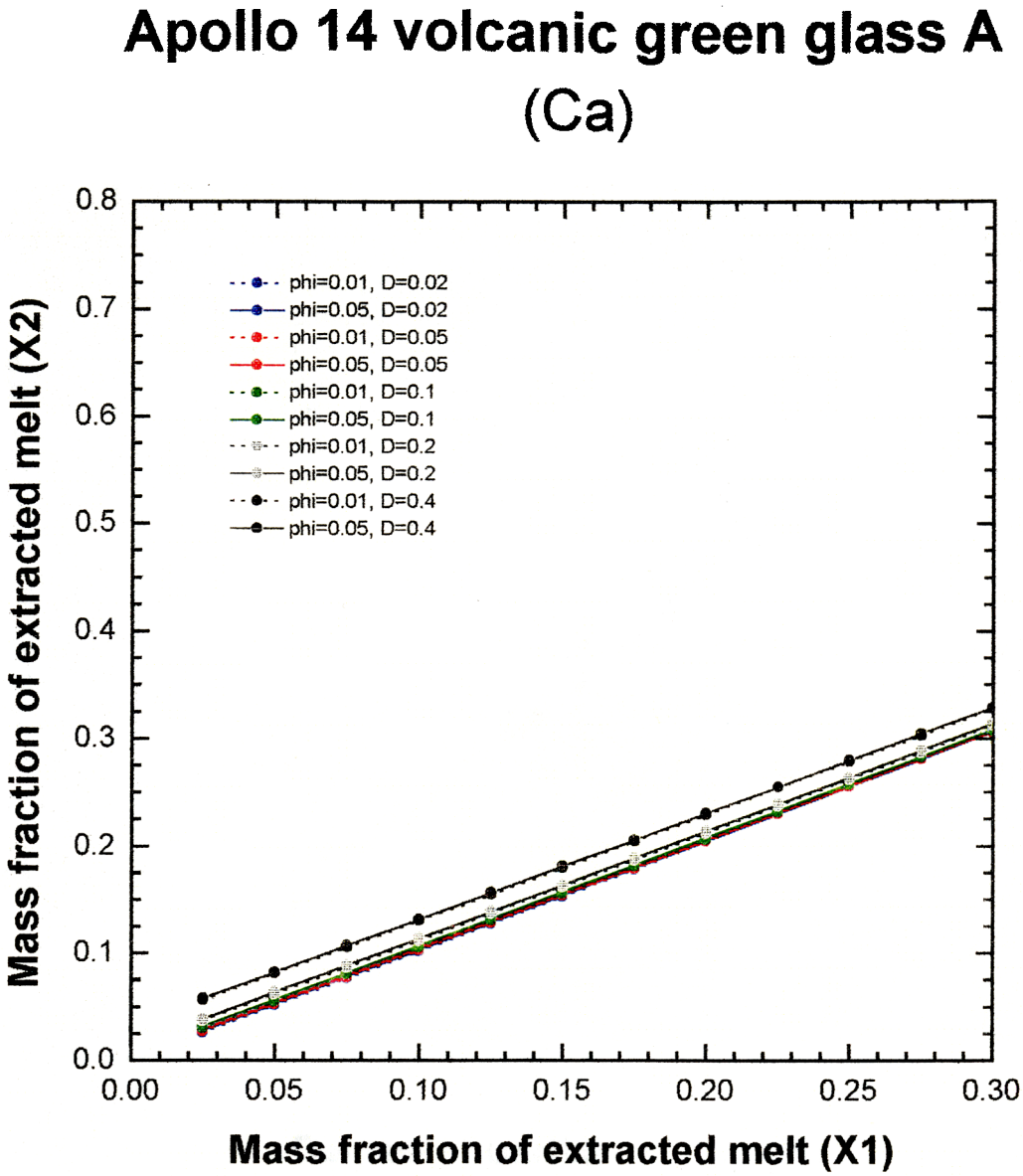

Appendix D-4 Mass of melt extracted results for the dynamic melting model applied on Apollo 14 volcanic green glasses A chemical data: Ca (see legend for porosity and distribution coefficient details) .

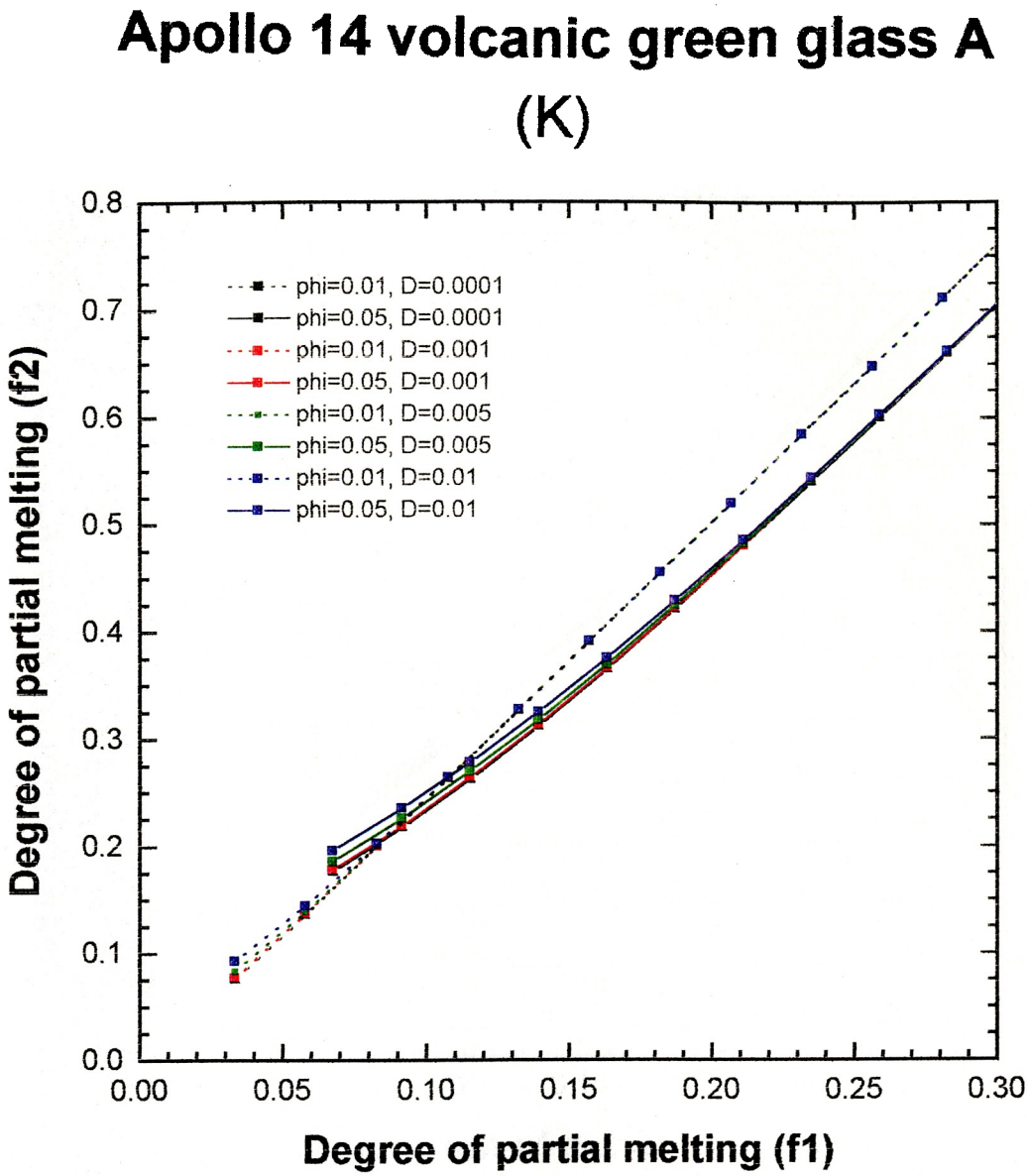

Appendix D-5 Degree of partial melting results for the dynamic melting model applied on Apollo 14 volcanic green glasses A chemical data: K (see legend for porosity and distribution coefficient details) .

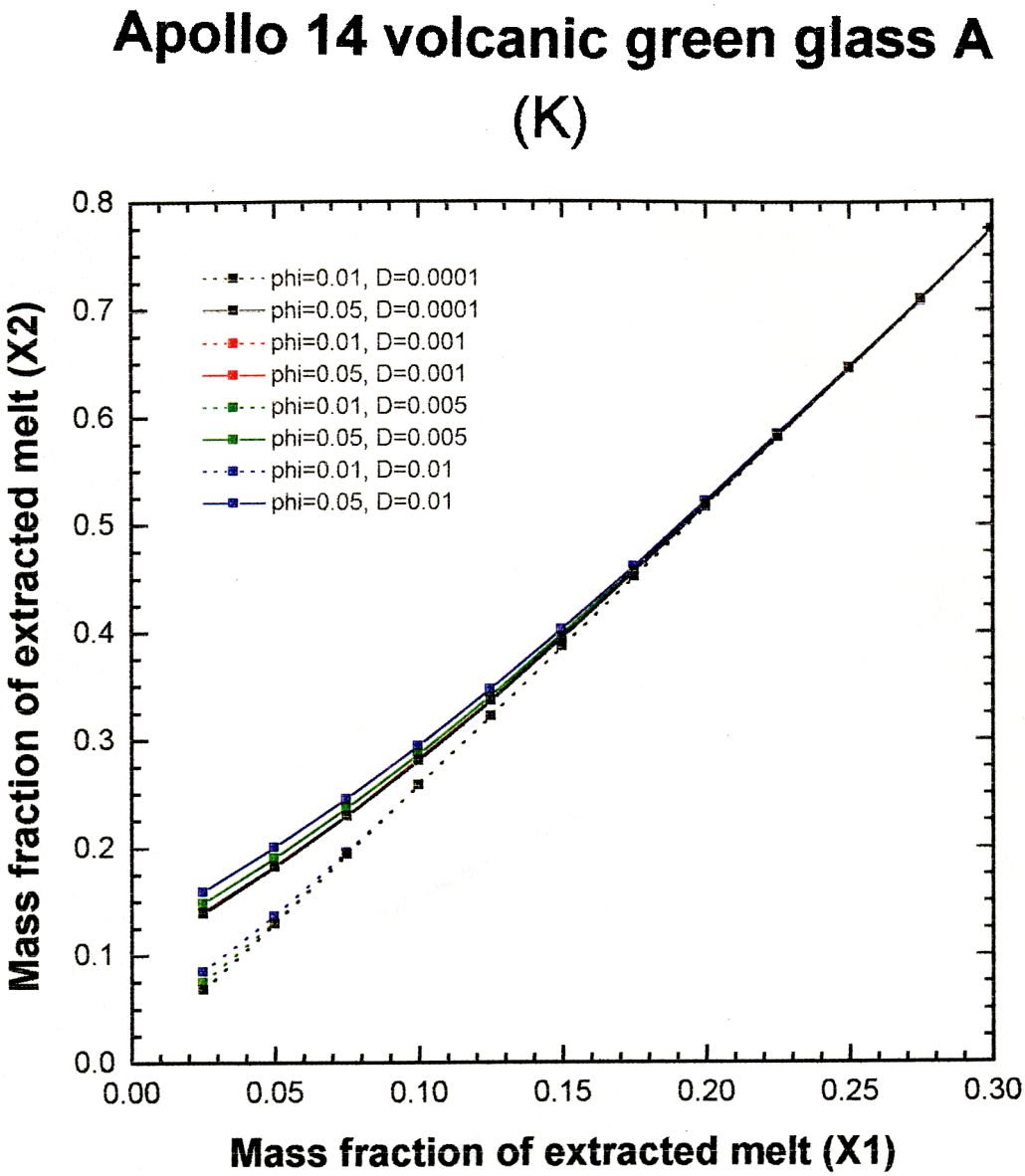

Appendix D-6 Mass fraction of extracted melt results for the dynamic melting model applied on Apollo 14 volcanic green glasses A chemical data: K (see legend for porosity and distribution coefficient details) .

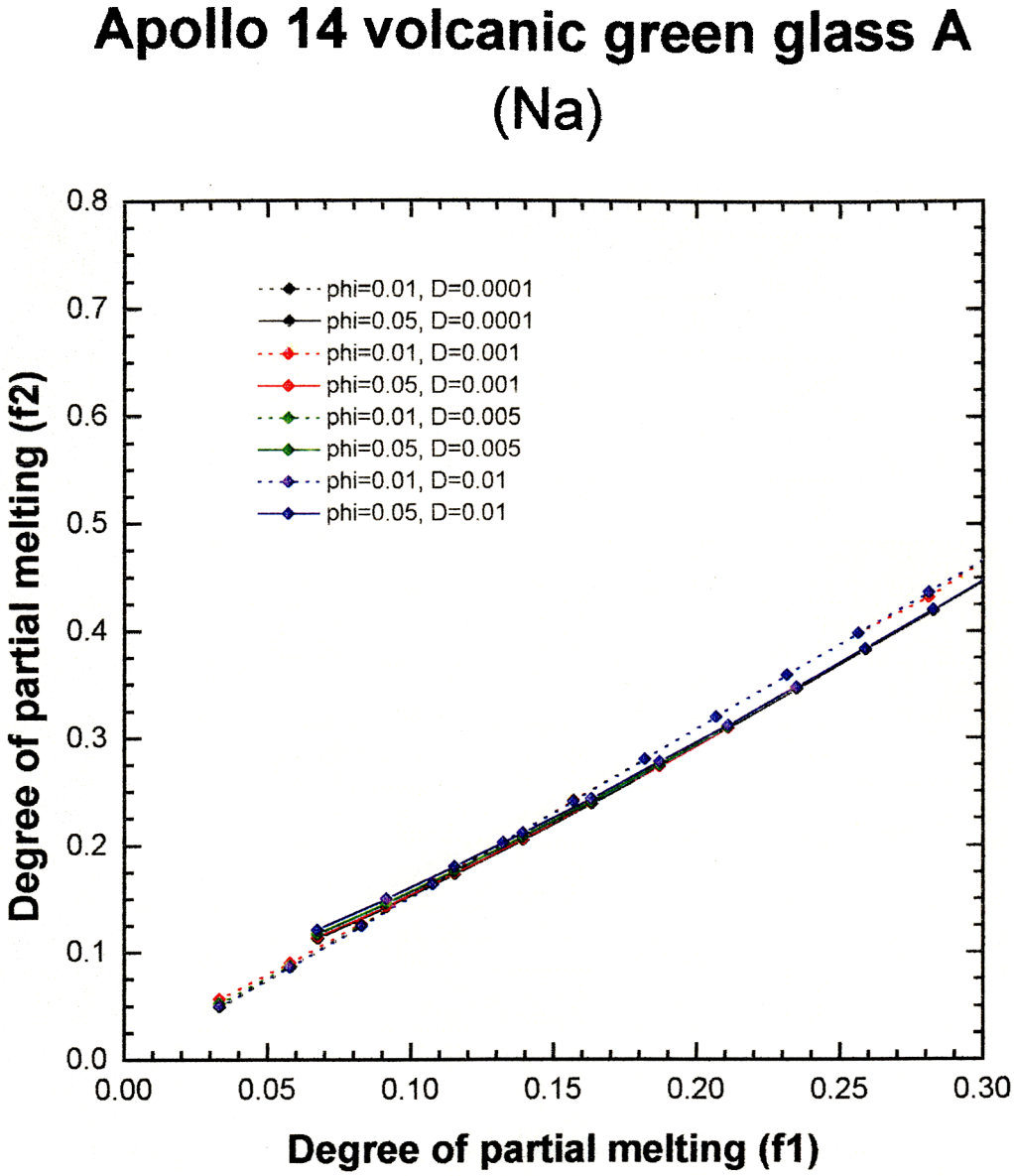

Appendix D-7 Degree of partial melting results for the dynamic melting model applied on Apollo 14 volcanic green glasses A chemical data: Na (see legend for porosity and distribution coefficient details) .

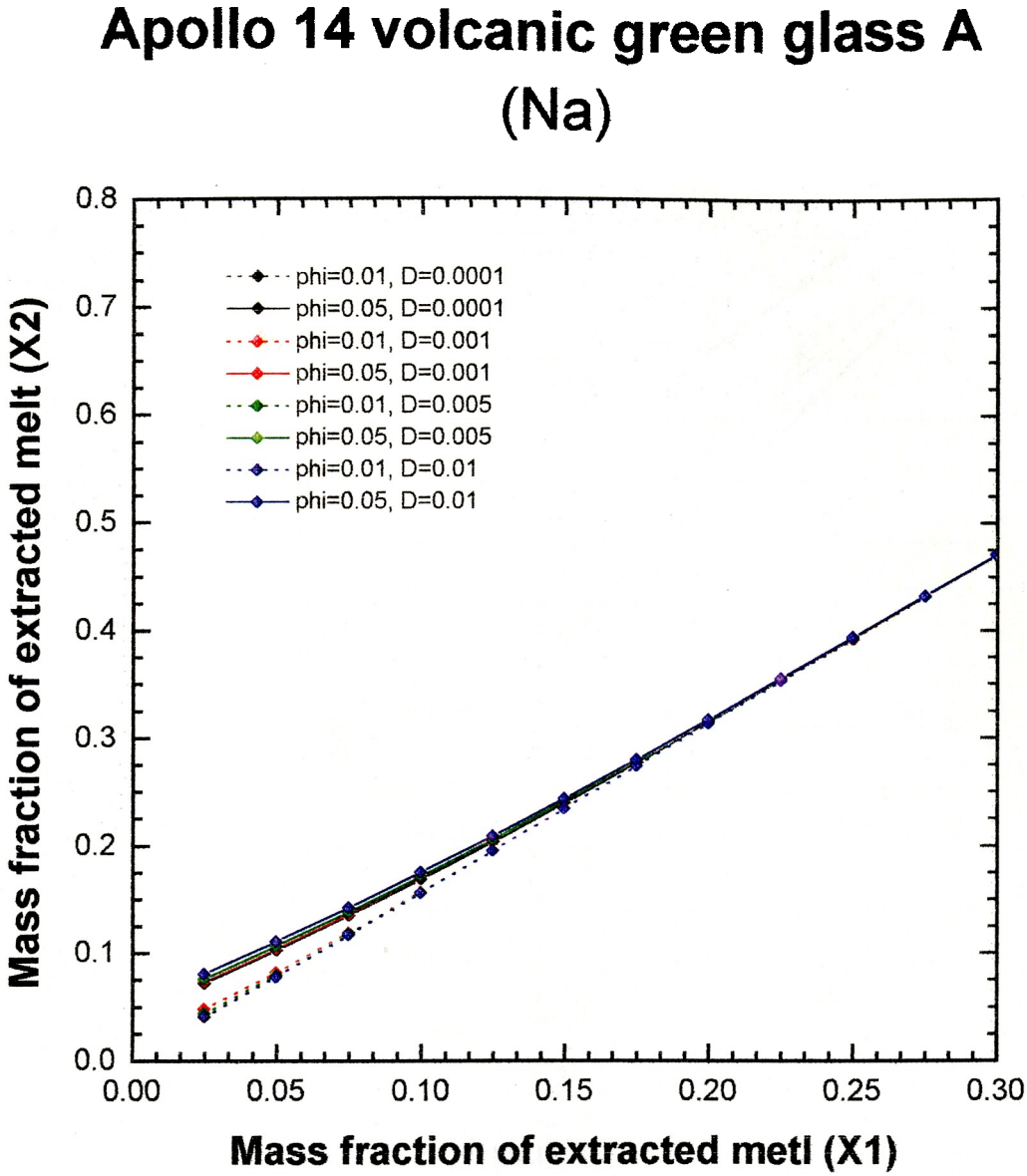

Appendix D-8 Mass fraction of extracted melt results for the dynamic melting model applied on Apollo 14 volcanic green glasses A chemical data: Na (see legend for porosity and distribution coefficient details) .

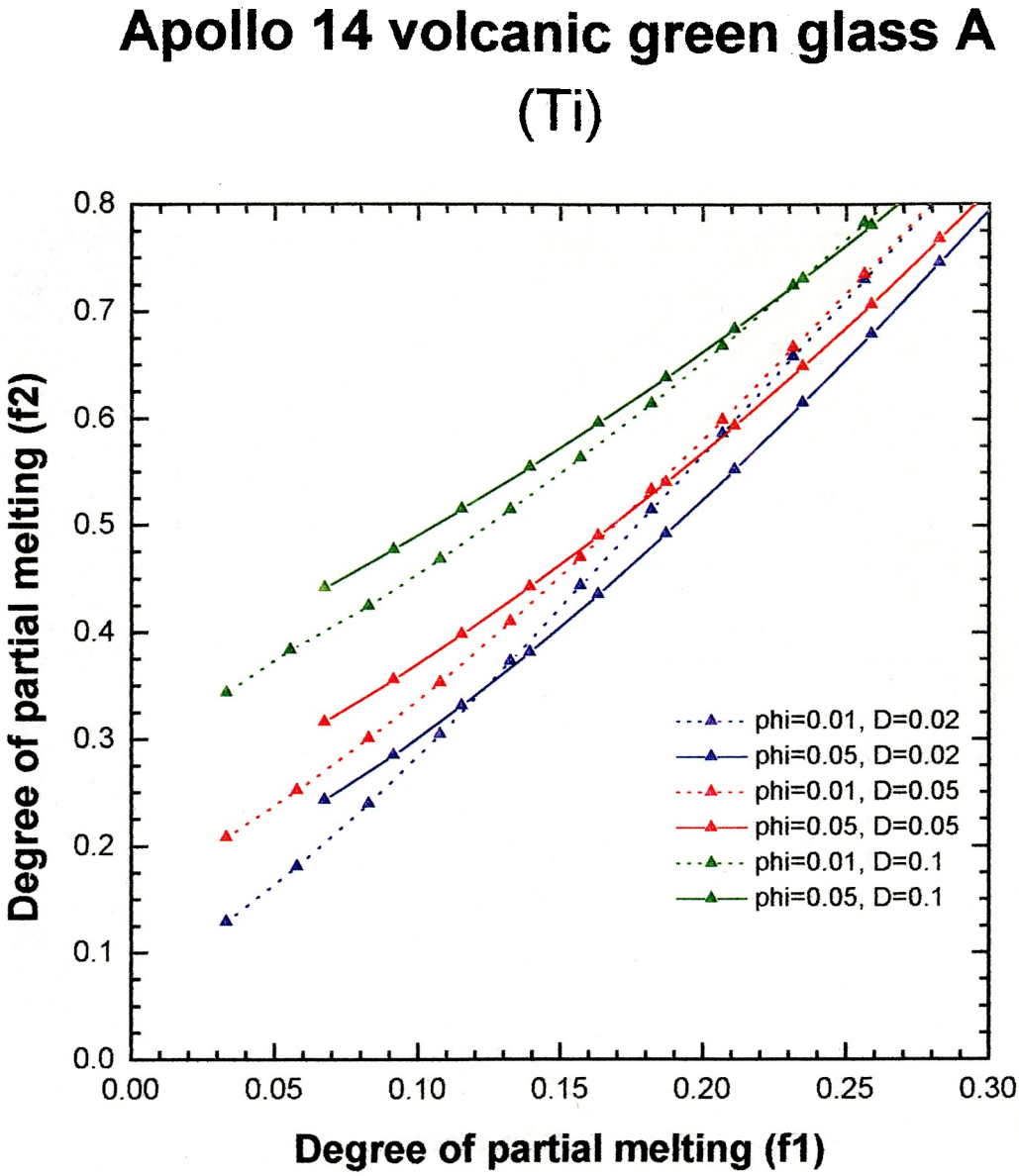

Appendix D-9 Degree of partial melting results for the dynamic melting model applied on Apollo 14 volcanic green glasses A chemical data: Ti (see legend for porosity and distribution coefficient details) .

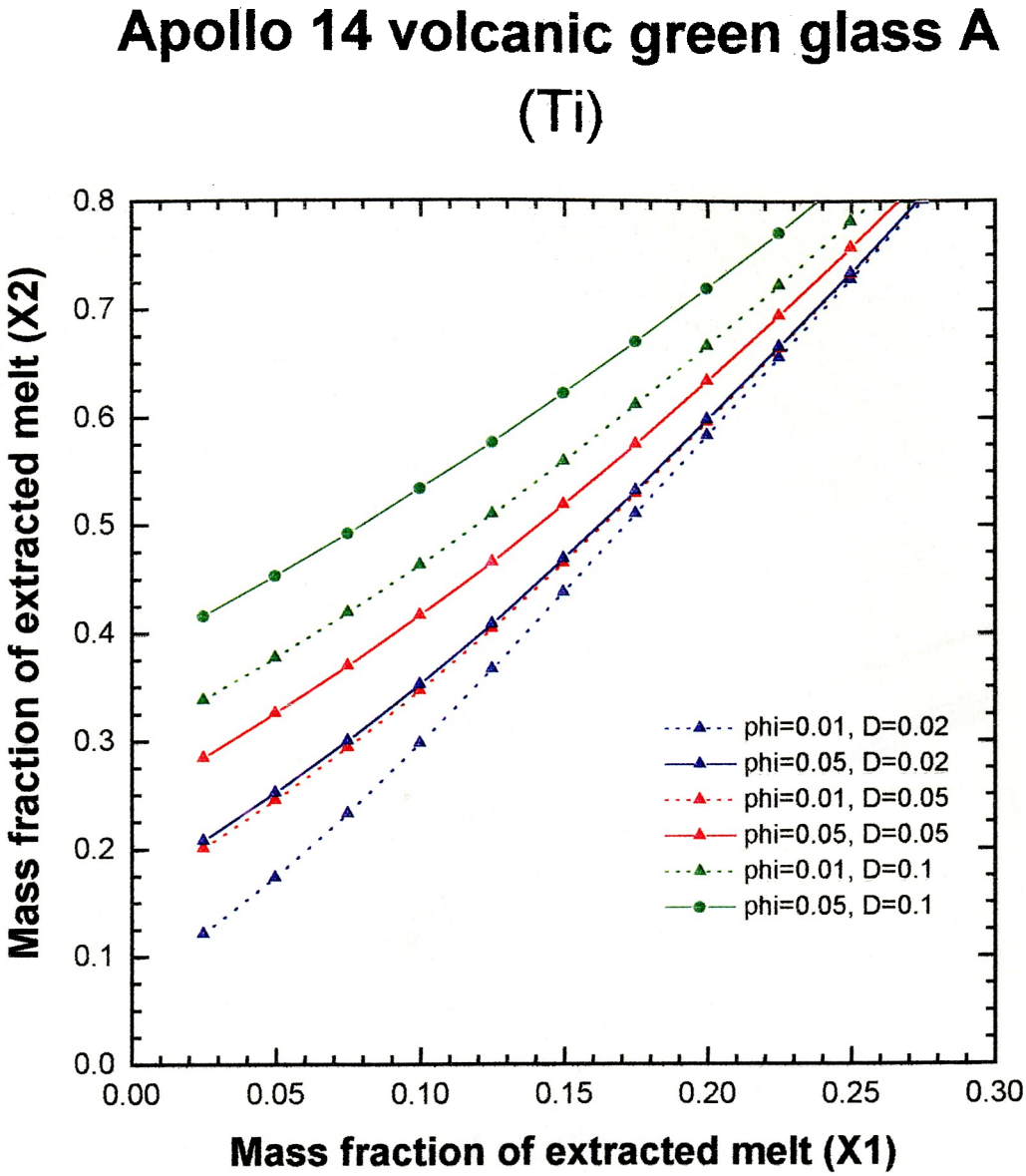

Appendix D-10 Mass of extracted melt results for the dynamic melting model applied on Apollo 14 volcanic green glasses A chemical data: Ti (see legend for porosity and distribution coefficient details) .

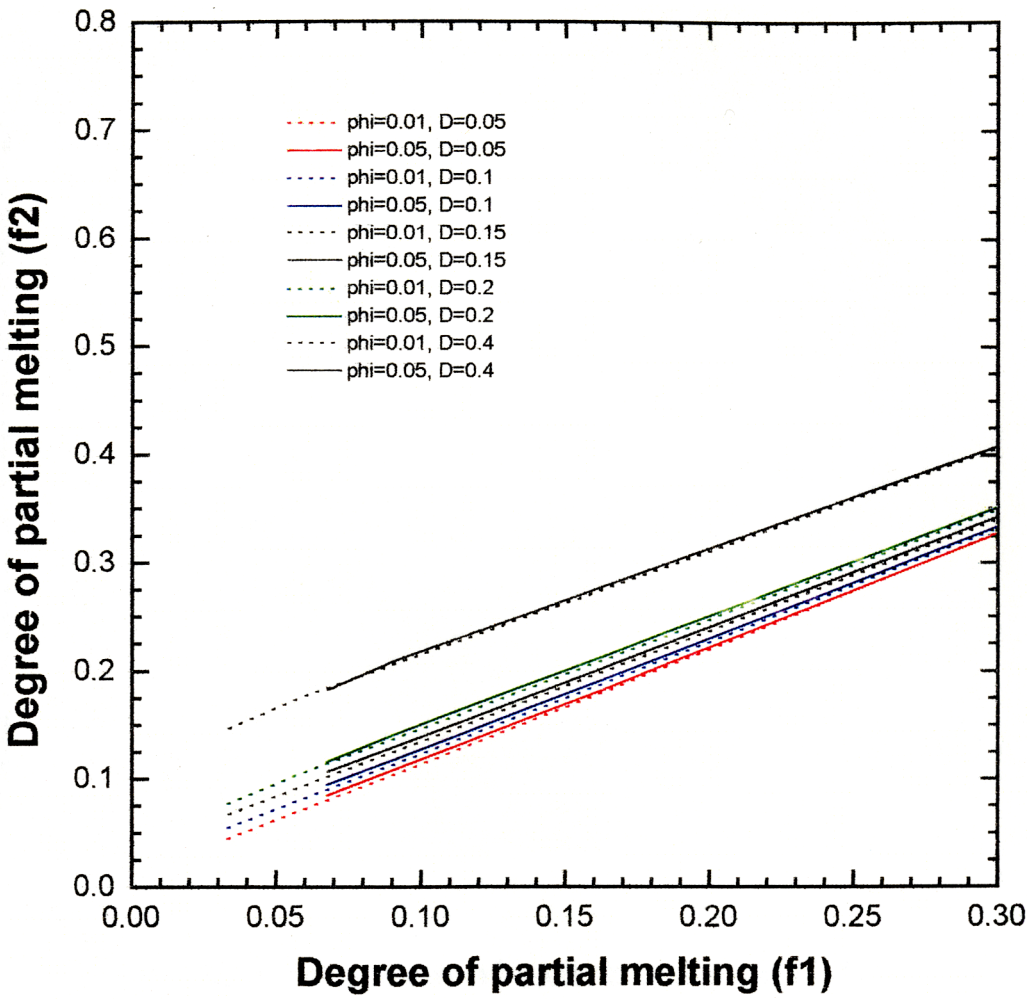

Appendix D-11 Degree of partial melting results for the dynamic melting model applied on Apollo 14 volcanic green glasses B chemical data: Al (see legend for porosity and distribution coefficient details) .

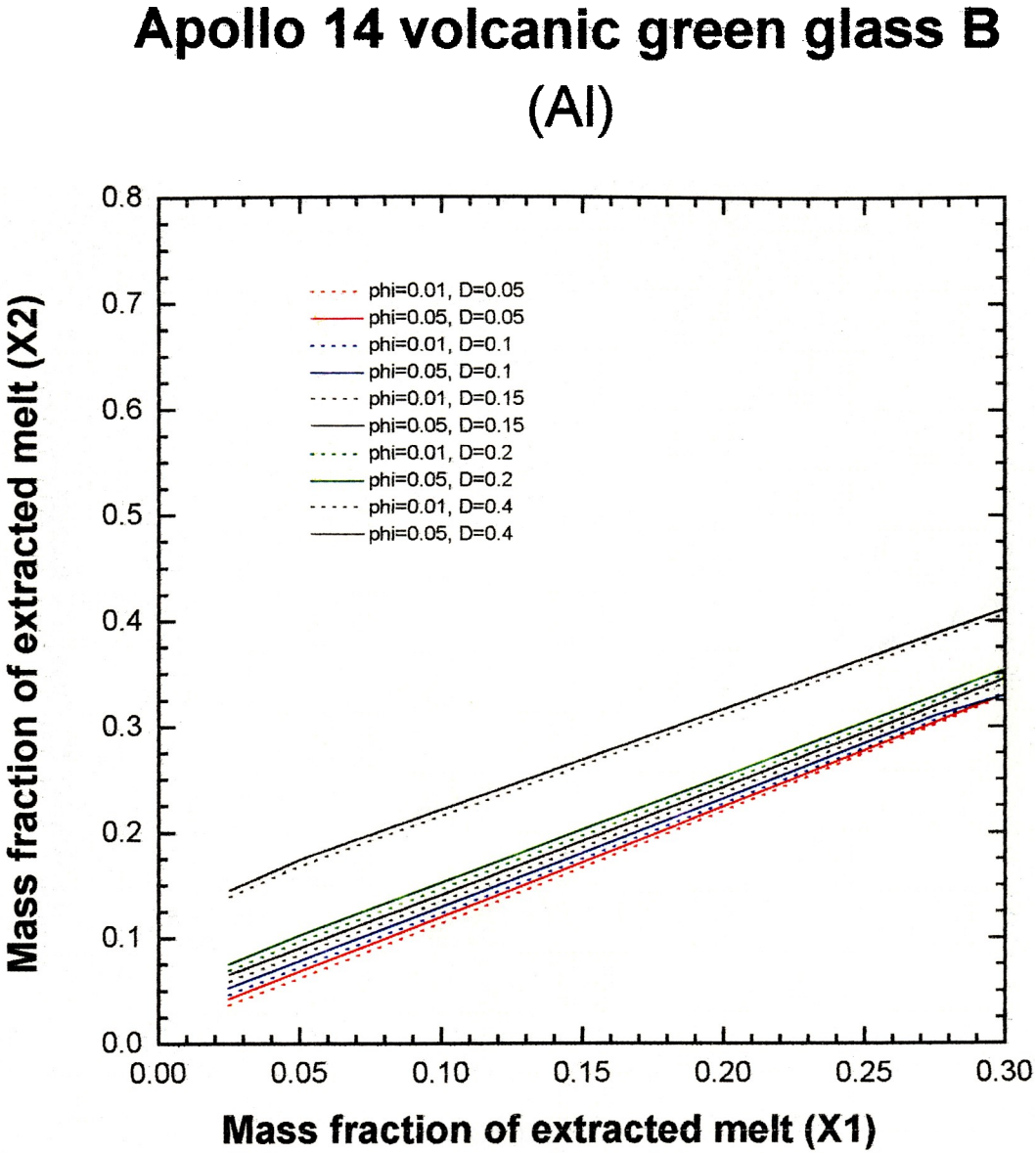

Appendix D-12 Mass of extracted melt results for the dynamic melting model applied on Apollo 14 volcanic green glasses B chemical data: Al (see legend for porosity and distribution coefficient details) .

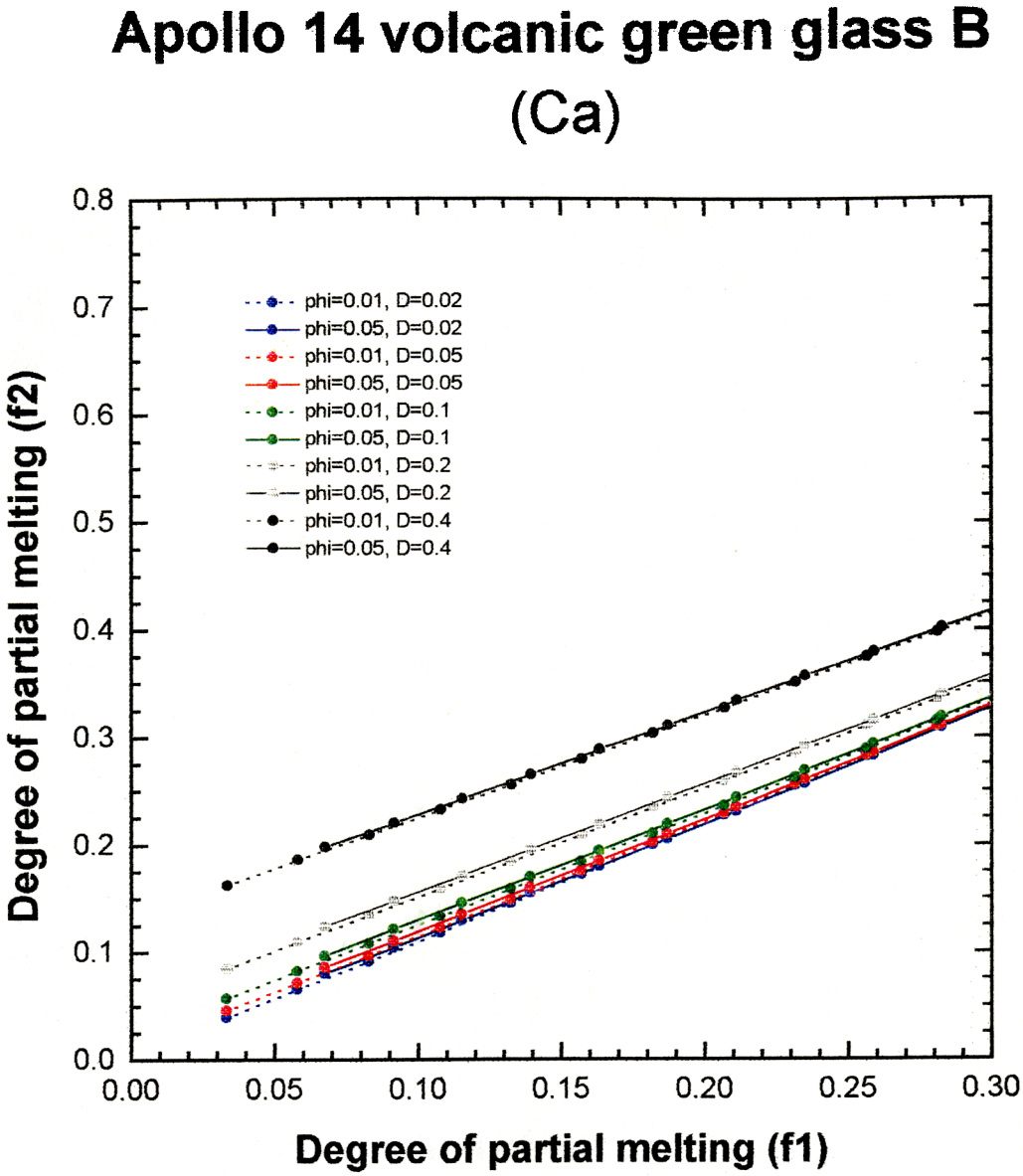

Appendix D-13 Degree of partial melting results for the dynamic melting model applied on Apollo 14 volcanic green glasses B chemical data: Ca (see legend for porosity and distribution coefficient details) .

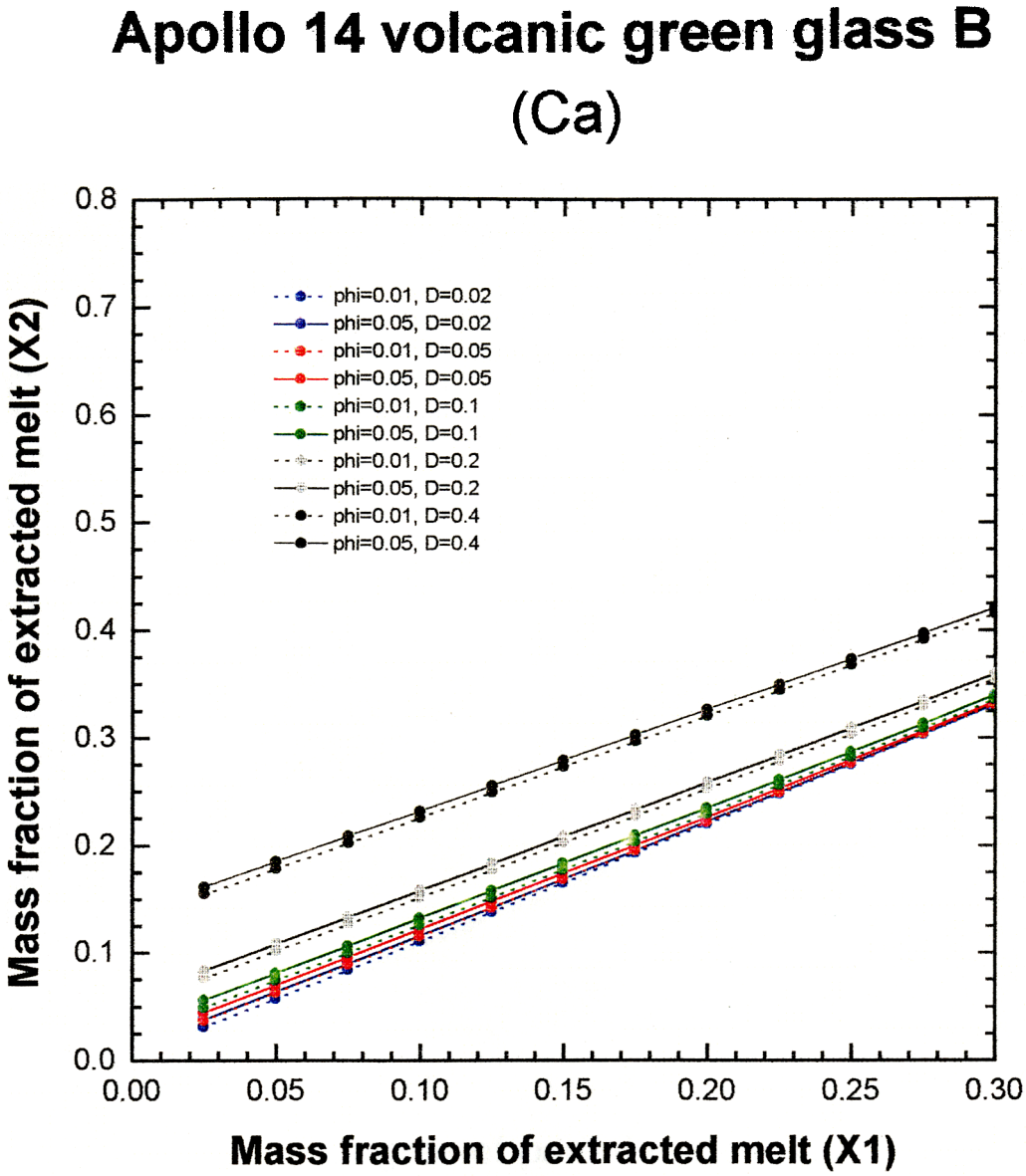

Appendix D-14 Mass of extracted melt results for the dynamic melting model applied on Apollo 14 volcanic green glasses B chemical data: Ca (see legend for porosity and distribution coefficient details) .

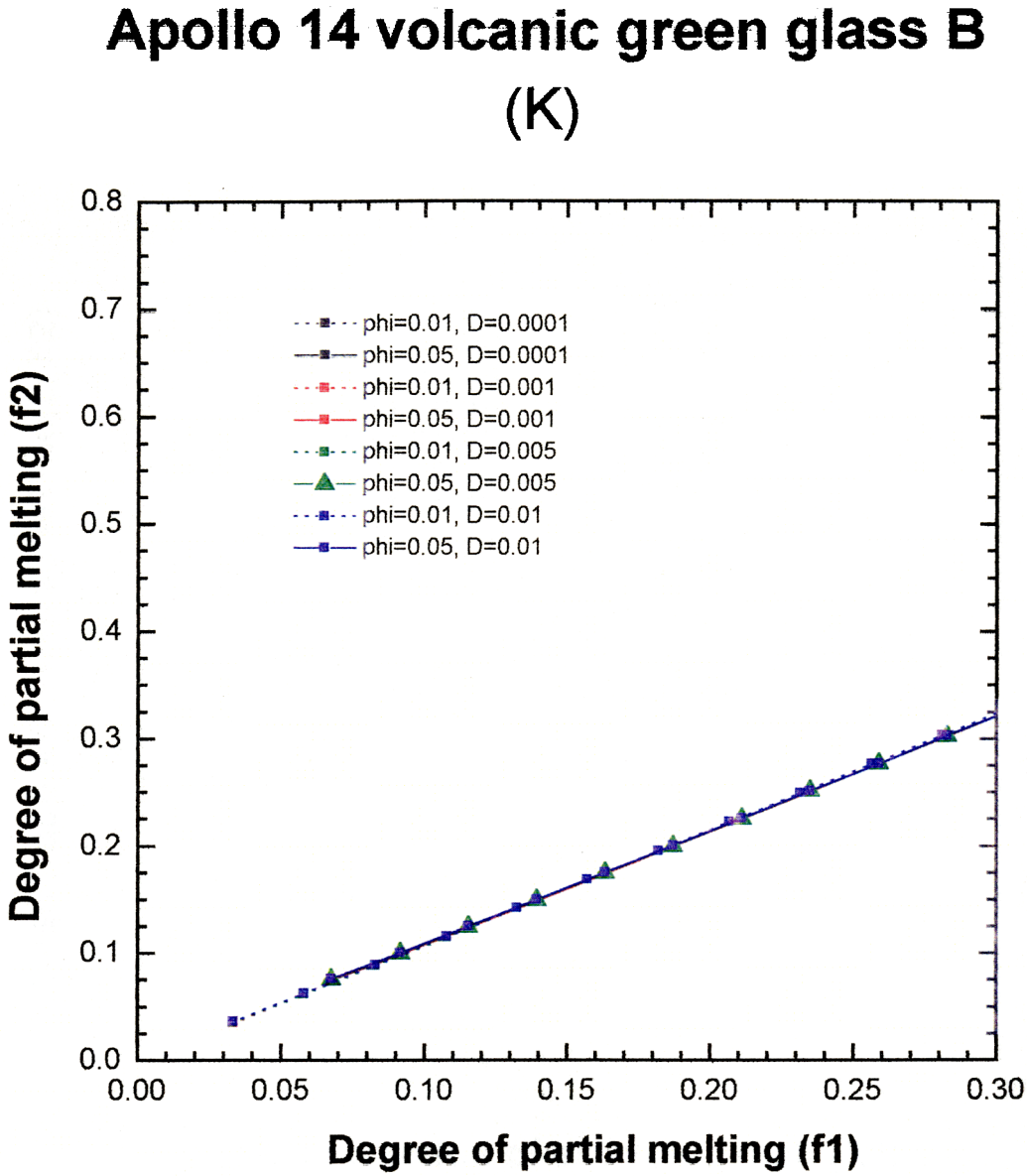

Appendix D-15 Degree of partial melting results for the dynamic melting model applied on Apollo 14 volcanic green glasses B chemical data: K (see legend for porosity and distribution coefficient details) .

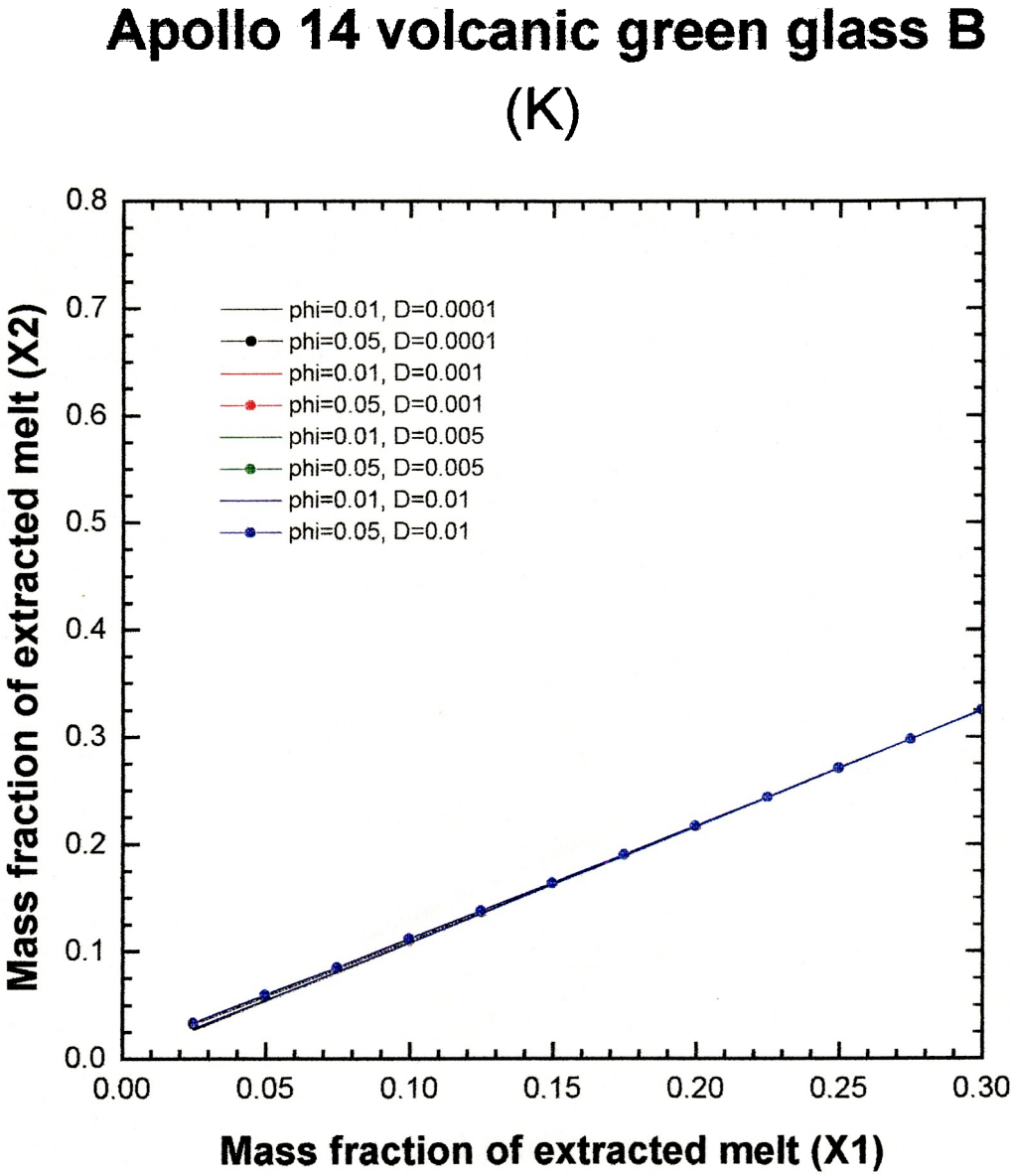

Appendix D-16 Mass fraction of extracted melt results for the dynamic melting model applied on Apollo 14 volcanic green glasses B chemical data: K (see legend for porosity and distribution coefficient details) .

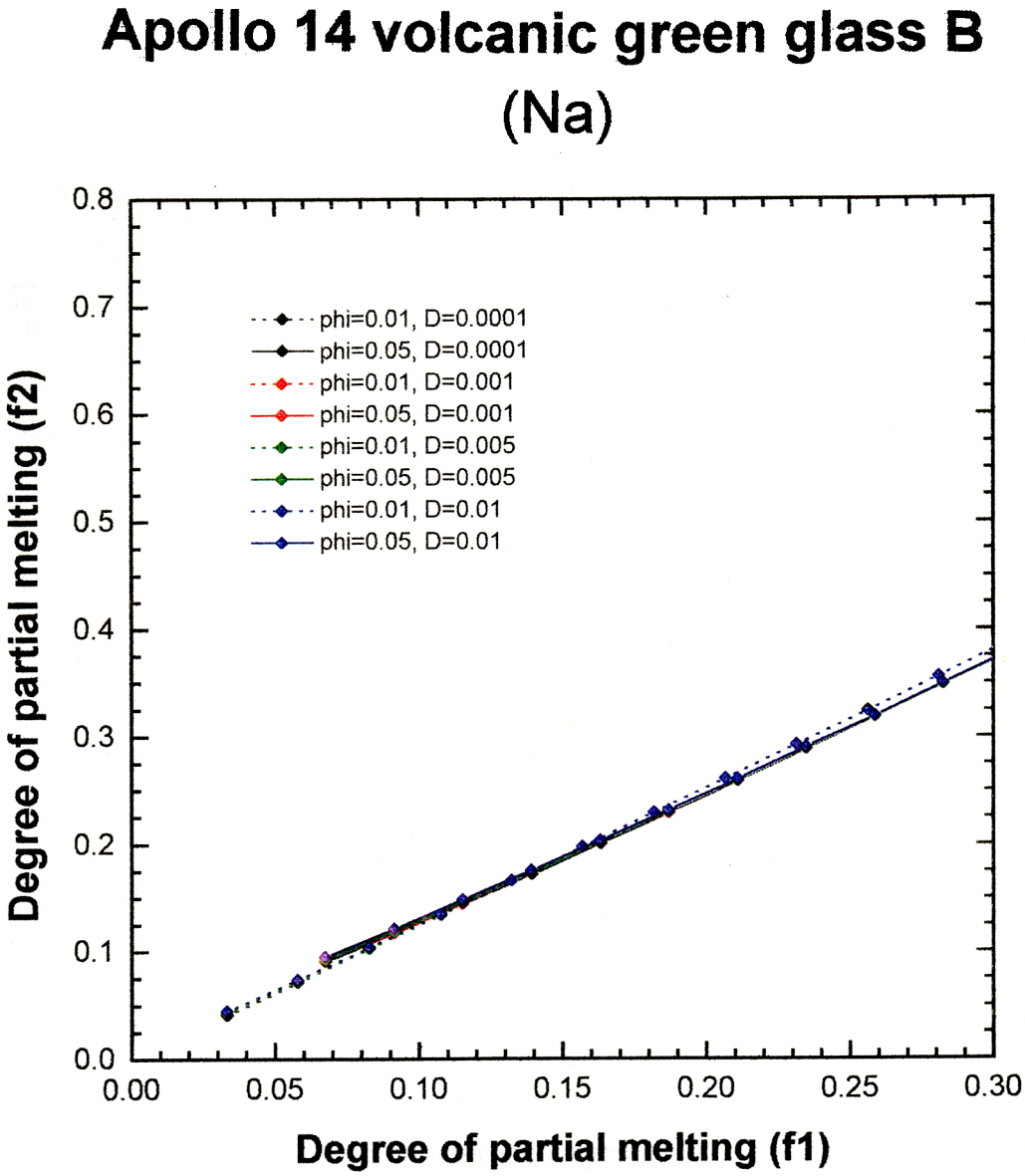

Appendix D-17 Degree of partial melting results for the dynamic melting model applied on Apollo 14 volcanic green glasses B chemical data: Na (see legend for porosity and distribution coefficient details) .

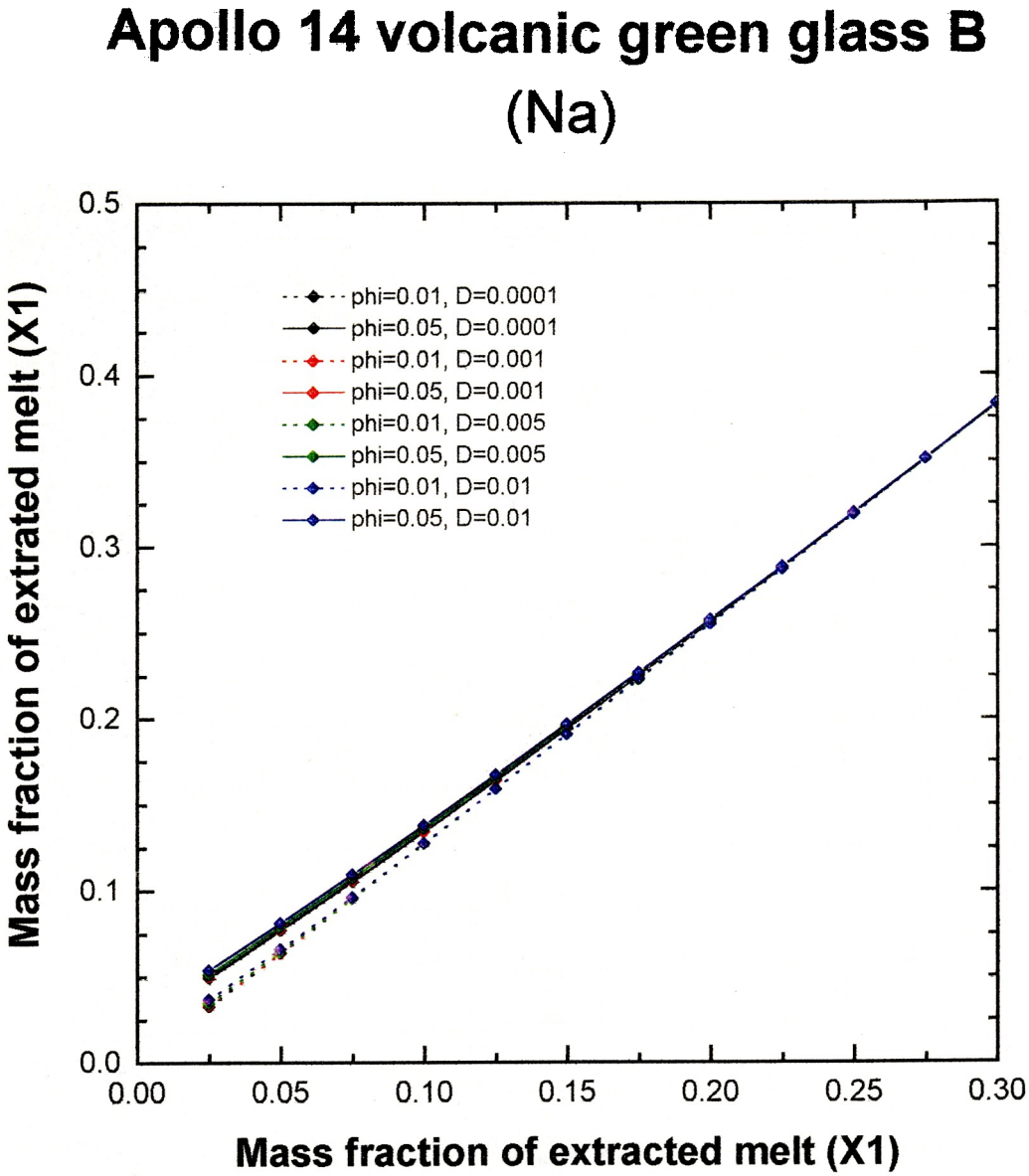

Appendix D-18 Mass fraction of extracted melt results for the dynamic melting model applied on Apollo 14 volcanic green glasses B chemical data: Na (see legend for porosity and distribution coefficient details) .

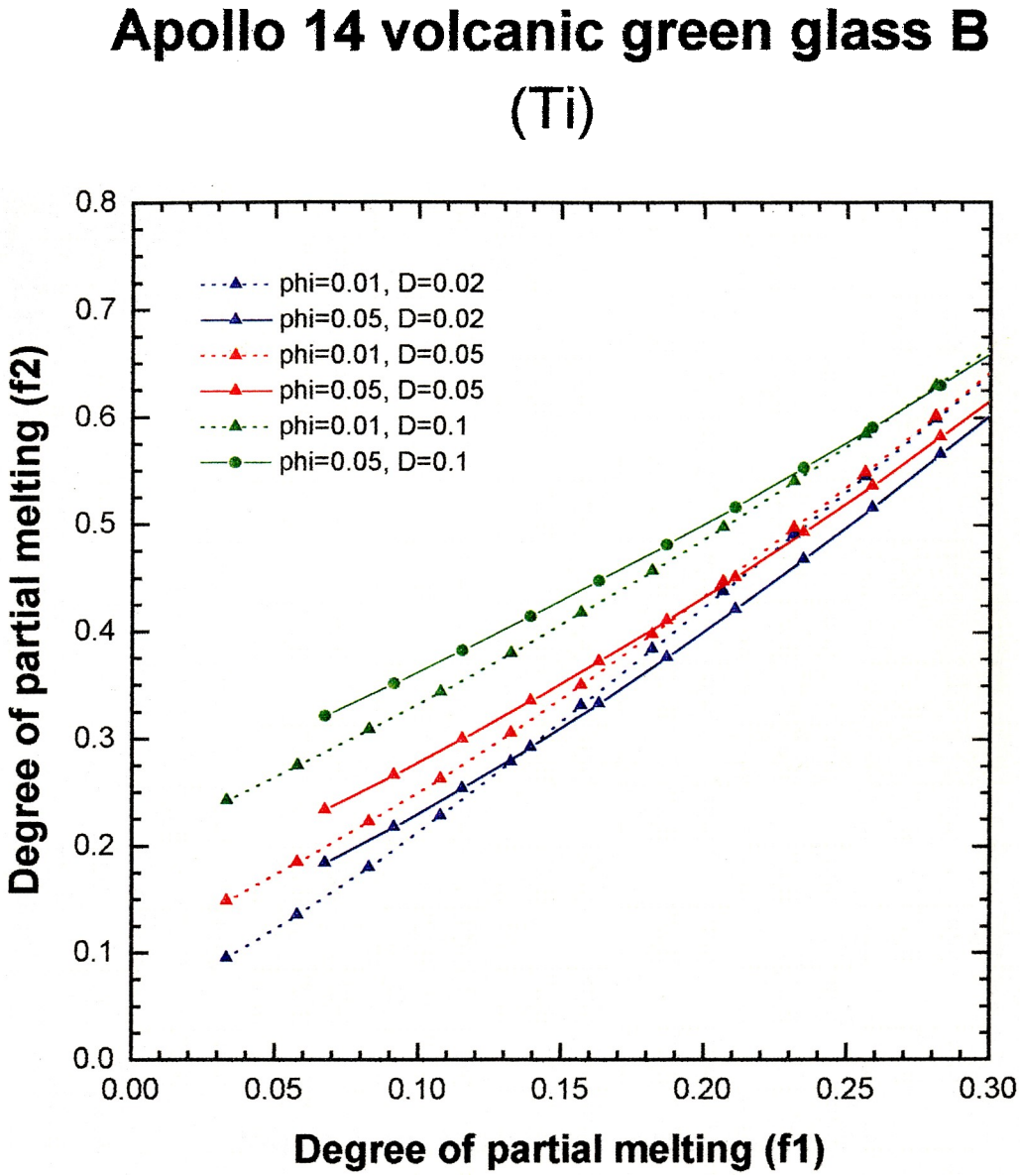

Appendix D-19 Mass fraction of extracted melt results for the dynamic melting model applied on Apollo 14 volcanic green glasses B chemical data: Ti (see legend for porosity and distribution coefficient details) .

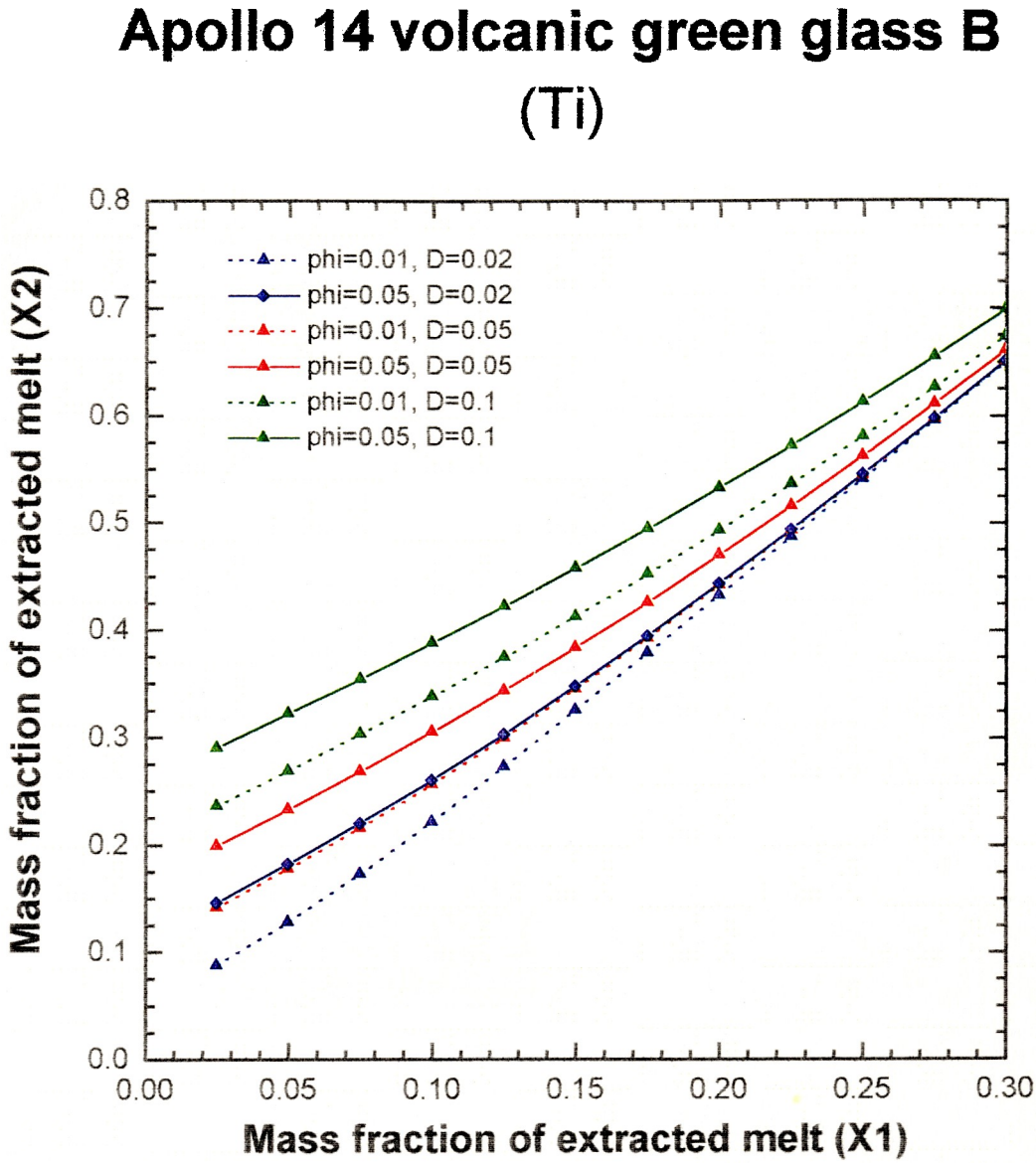

Appendix D-20 Mass fraction of extracted melt results for the dynamic melting model applied on Apollo 14 volcanic green glasses B chemical data: Ti (see legend for porosity and distribution coefficient details) .